

# **An Encoded Microwell Array for Multi-Image Analysis of Cells**

A thesis submitted to Cardiff University in accordance with the  
requirements for the degree of

DOCTOR OF PHILOSOPHY  
BY EXAMINATION AND THESIS

By

**Edward John Sayers**

## **Abstract**

In cell populations there is a great deal of heterogeneity. Cells can be seen to react different to the same stimulus despite being the same cell type and under the same conditions. Single cell analysis of a population is, therefore, crucial to understanding the nature of these differences. Using different technologies to study a single cell can help a researcher gather more data on the nature of these differences.

The first part of this study looked at the development of a microwell array as a technique to allow correlative microscopy of non-adherent cell types. Laser ablation was used to generate microwells in both glass and the silicone polymer, polydimethylsiloxane (PDMS). Different methods were tested to increase quality of the microwells with the use of a sacrificial layer proving successful. Microwells were determined to be suitable for both live cell imaging and scanning electron microscopy imaging with correlative microscopy of non-adherent cells demonstrated. A new microwell design to allow the tracking of a single well through different imaging steps including sectioning was devised.

Surface modification was required to make PDMS more cytophilic and different methods were investigated in the next part of this thesis. More cytocompatible surfaces were produced for PDMS using silanisation of the surface to produce amine moieties proved the most successful.

In the final part of the thesis the cell penetrating peptide (CPP) octaarginine was investigated along with the pro-apoptotic peptides PAD and the Bcl-2 converter peptide. The blebbing effects of the two peptides were analysed using non-adherent cells in microwells and fixed cells on a normal surface. Apoptosis as means of cell death by these peptides was disputed and the necrotic blebbing caused by these peptides investigated.

## **Acknowledgements**

Most importantly of all I would like to thank my three supervisors, in no particular order; Chris Allender for his expertise in surface chemistry; David Barrow for his expertise in engineering and substrates; and Arwyn Jones for his expertise in cell biology and cell penetrating peptides. All three supervisors have provided strong help and guidance throughout the lifetime of this PhD.

I would also like to thank my fellow students in the various laboratories I have used who have provided additional ideas and taught me some of the skills I've needed to undertake this challenge. Catherine Naseriyan (nee Watkins) and Monerah Al-Soraj have been consistent aids in all areas related to cell biology and CPPs. Jenna Bowen and Mark Kelly have provided assistance in surface chemistry. Laser machining would have not been possible without the aid of Neil Sykes in the Engineering department. My former housemate Neil Bennet has also provided invaluable assistance from the Physics department and Electron Microscopy would not have been possible without Guy Pierce and Anthony Hann in Biosciences.

I would also like to thank my family and friends for their emotional help throughout my time at Cardiff along with the occasional beer or two.

## **Table of Contents**

1. General Introduction.....	1
1.1 Introduction.....	1
1.2 Correlative Microscopy.....	1
1.2.1 Limitations and Advances in Light Microscopy.....	1
1.2.2 Limitations and Advances in Electron Microscopy.....	3
1.2.3 Advances in Correlative Microscopy.....	4
1.3 Microwells and Cell Retention.....	8
1.3.1 Microwell Arrays.....	9
1.4 Surface Modification.....	10
1.4.1 Cell Patterning.....	10
1.4.2 Modification of PDMS.....	11
1.4.2.1 Covalent Modification of PDMS.....	12
1.4.2.2 Non-Covalent Modification of PDMS.....	13
1.4.2.3 Interpenetrating Networks in PDMS.....	14
1.5 Endocytosis.....	14
1.5.1 Macropinocytosis.....	14
1.5.2 Other Key Endocytic Pathways.....	15
1.5.2.1 Clathrin dependent endocytosis.....	15
1.5.2.2 Caveolin dependent endocytosis.....	16
1.5.2.3 Phagocytosis.....	17
1.6 Cell Penetrating Peptides.....	18
1.7 Aims of this Thesis.....	21
1.8 References.....	23
2 Materials and Methods.....	35
2.1 Cell Culture.....	35
2.2 PBS Formulation.....	36
2.3 Laser ablation and Surface Treatment.....	37
2.4 Autofluorescence of laser ablated wells.....	38
2.5 Fluorescence imaging of cells in glass and PDMS microwells.....	39
2.6 SEM Imaging of cells.....	39
2.7 Correlative light-SEM.....	40

2.8 Sectioning of PDMS.....	40
2.9 Moulding of arrays.....	41
2.10 Sectioning epoxy.....	42
2.11 Live cell imaging in encoded microwell arrays.....	42
2.12 Silanisation of glass surfaces.....	43
2.13 Contact angle measurements.....	44
2.14 Cell Surface Imaging.....	44
2.15 Succinic anhydride and succinimidyl ester modification of surfaces.....	45
2.16 Hydrosilylation Reaction on PDMS.....	45
2.17 Activation of PDMS by UV/Ozone treatment.....	46
2.18 Silanisation of PDMS.....	46
2.19 Thin layer coating.....	46
2.20 Sol-Gel.....	47
2.21 Swelling of PDMS.....	47
2.22 Sol-gel interpenetrating network in PDMS.....	47
2.23 Sol-Gel Particles in PDMS.....	48
2.24 r8 – Alexa488 and r8-PAD – Alexa488 Uptake in HeLa.....	48
2.25 EGF and Peptide treatment on HeLa cells fixed cell imaging.....	49
2.26 Live cell imaging of transfected cells.....	49
2.27 SEM of peptide treated cells.....	50
2.28 Nucleus volume measurements.....	50
2.29 Live cell imaging of peptide treated cells.....	51
2.30 Pak-1 siRNA treated cells.....	51
2.31 Cytochalasin D and Blebbistatin inhibition in HeLa cells.....	52
2.32 References.....	52
3. Design and Manufacture of Encoded Microwell Arrays.....	53
3.1 Introduction.....	53
3.1.2 Aim.....	55
3.2 Results.....	55
3.2.1 Laser Ablation and Optimisation of Microwell Quality in Glass Surfaces.....	55
3.2.2 Autofluorescence in Glass Microwells.....	58
3.2.3 Autofluorescence in polydimethylsiloxane (PDMS) and Fused Silica.....	59
3.2.4 Development of a Cover Slip Manifold for Live Cell Imaging.....	61

3.2.5 SEM Imaging of Non-Adherent Cells in Microwells.....	64
3.2.6 Correlative Live-SEM Imaging of Non-Adherent Cells in Microwells .....	65
3.2.7 Sectioning PDMS .....	66
3.2.8 Sectioning Epoxy.....	68
3.2.9 Designing an Encoded Array.....	70
3.2.10 Live and Fixed Cell Imaging in the Encoded Array.....	74
3.3 Discussion .....	75
3.3.1 Improving Quality of Laser Ablated Material.....	75
3.3.2 PDMS as an Alternative Material.....	78
3.3.3 Autofluorescence of Glass.....	78
3.3.4 Imaging in Microwells.....	79
3.3.5 Sectioning PDMS and Epoxy .....	80
3.3.6 Encoded Microwells .....	81
3.3.7 Conclusion .....	81
3.4 References .....	82
4. Surface Modification and Cell Surface Interaction .....	86
4.1 Introduction .....	86
4.1.4 Aim .....	87
4.2 Results .....	88
4.2.1 Surface Modification of Glass.....	88
4.2.2 Surface modification of PDMS .....	95
4.2.2.1 Surface Chemistry.....	96
4.2.2.1.1 Modification of PDMS by Catalytic Hydrosilylation .....	96
4.2.2.1.2 Modification of PDMS Surfaces using Silanes.....	101
4.2.2.2 Thin layer coating .....	106
4.2.3 Interpenetrating Network.....	107
4.2.3.1 Sol-Gel .....	108
4.2.3.2 PDMS-Sol-Gel interpenetrating network .....	111
4.3 Discussion .....	115
4.3.1 PDMS .....	115
4.3.2 Hydrosilylation .....	116
4.3.3 Silinisation.....	117
4.3.4 Interpenetrating Network.....	118

4.3.5 Conclusions .....	119
4.4 References .....	120
5. Live Cell Microscopy and Cell Penetrating Peptides .....	123
5.1 Introduction .....	124
5.1.1 Macropinocytosis.....	124
5.1.2 Cell Penetrating Peptides.....	126
5.1.3 Cell Death and Associated Cell Blebbing .....	129
5.1.4 Aims.....	130
5.2 Results .....	131
5.2.1 Uptake of Octaarginine.....	131
5.2.2 Stimulation of Macropinocytosis by EGF and Octaarginine.....	132
5.2.3 Pro-apoptotic peptides and cell blebbing.....	137
5.2.3.1 Plasma Membrane Blebbing .....	137
5.2.2.2 R8-PAD.....	139
5.2.2.3 Bcl-2 targeting peptide.....	149
5.3 Discussion .....	153
5.3.1 Macropinocytosis and uptake of r8 .....	153
5.3.2 Cell dynamics of r8-PAD .....	154
5.3.3 Cell death from fsr-1-r8.....	157
5.3.4 Conclusions .....	157
5.4 References .....	158
6. General Discussion .....	166
7 Appendix.....	143

## Figure Legend

Figure 2.1:	Method for producing a replica mould of wells from glass to epoxy	41
Figure 3.1:	Microwell debris removal after different treatments	55
Figure 3.2:	Autofluorescence of glass microwell arrays	57
Figure 3.3:	Fluorescence properties of ablated fused silica and glass cover slips	59
Figure 3.4:	Live KG1a cells imaged in glass and PDMS microwells	60
Figure 3.5:	Manifold design	62
Figure 3.6:	Bottom plate of manifold	62
Figure 3.7:	Top plate of manifold	63
Figure 3.8:	SEM of KG1a cells in microwells	64
Figure 3.9:	Correlative microscopy of KG1a cells in microwells	64
Figure 3.10:	Crosslinking of PDMS	65
Table 3.11:	Properties of different mixing ratio of dvPDMS, PDMS pre-polymer and curing agent	67
Table 3.12:	Mixing ratios of epoxy 301-2 and the ability of the resultant polymer to be sectioned	68
Figure 3.13:	Microscopy and sectioning of encoded microwells	68
Figure 3.14:	Possible microwell designs	69
Figure 3.15:	Encoded array design	72
Figure 3.17:	Correlative live-fixed imaging of Mcf-7 cells in encoded microwells	73
Figure 4.1:	Silane modification of glass surfaces	87
Figure 4.2:	HeLa cells grown on different surfaces	88
Figure 4.3:	Reaction of primary amine with ester	90
Figure 4.4:	Contact angle of glass surfaces following treatment with different silanising reagents	91
Figure 4.5:	Surfaces incubated with a fluorescent probe to amines	92
Figure 4.6:	HeLa cells grown on different surfaces	93
Figure 4.7:	Vinyl-hydrosilyl reaction	95
Figure 4.8:	FTIR spectrum of Sylgard184 at different mixing ratios	96
Figure 4.9:	PEG hydrosilylation reactions using divinyl PEG and PEG (meth)acrylate	97
Figure 4.10:	Hydrosilylation reaction between different PDMS polymers and PEG (meth)acrylate	98

Figure 4.11:	Hydrosilylation of PDMS with PEG derivatives	99
Figure 4.12:	Contact angle change during UV/O <sub>3</sub> treatment of PDMS	101
Figure 4.13:	Determining reaction length and concentration for modifying activated PDMS with APTES	102
Figure 4.14:	HeLa cells grown on different modified surfaces and albumin coated surfaces	104
Figure 4.15:	HeLa cells grown on gold coated PDMS and glass	106
Figure 4.16:	Hydrolysis and condensation of triethoxysilane forms the siloxane linkage	107
Figure 4.17:	Sol-gel reaction and dried gel	108
Table 4.18:	Formation of sol-gel using TEOS and DMDES	109
Figure 4.19:	Swelling of PDMS in different solvents	111
Figure 4.20:	Water droplets on IPN of TEOS sol-gel in PDMS	112
Figure 4.21:	Effect of silica beads on sol-gel IPN in PDMS and HeLa cells	113
Figure 5.1:	Different uptake pathways used by cells	122
Figure 5.3:	Cellular distribution of Alexa-R8 in HeLa and KG1a cells	129
Figure 5.4:	Actin distribution in HeLa cells after short term incubation with no peptide, GS <sub>4</sub> , EGF or R8	131
Figure 5.5:	GPI-GFP transfected HeLa cells incubated with GS <sub>4</sub> , r8 or EGF	132
Figure 5.6:	Scanning electron micrographs of HeLa cells after short incubation with no peptide, GS <sub>4</sub> , r8 or EGF	133
Figure 5.7:	Apoptotic and necrotic bleb formation in HeLa cells in response to hydrogen peroxide	136
Figure 5.8:	Helical wheel showing layout of the PAD cargo	137
Figure 5.9:	HeLa cells incubated with 10μM r8-Alexa488 or r8-pad-Alexa488	138
Figure 5.10:	HeLa cells after incubation with different concentrations of r8-PAD stained for actin and nucleus	140
Figure 5.11:	HeLa cells transfected with actin-GFP or GPI-GFP expressing plasmid incubated with r8, PAD or r8-PAD	142
Figure 5.12:	HeLa cells treated with Pak-1 siRNA	144
Figure 5.13:	HeLa cells incubated with r8-PAD after inhibition with cytpchalasin D or Blebbistatin	146
Figure 5.14:	Structural details of the Bcl-2 converter peptide and its control	147

Figure 5.15:	Bleb formation and cell death in KG1a, K562 and MCF-7 cells	150
Table 6.1:	How the coded microwell array may be modified for use with alternative microscopes	168

## Abbreviations

AFM	Atomic Force Microscope
APTES	Aminotriethoxysilane
ATP	Adenosine Triphosphate
BARS	Brefeldin-A ADP-ribosylated Substrate
Bcl-2	B-cell Lymphoma 2
cAMP	Cyclic Adenosine Monophosphate
Cdc42	Cell Division Control Protein 42
CH <sub>3</sub>	Methyl
CLEM	Correlative Light-Electron Microscopy
CME	Clathrin Mediated Endocytosis
CPP	Cell Penetrating Peptide
CtBP1	C-terminal Binding Protein 1
DIC	Differential Interference Contrast
DMDES	Dimethyldiethoxysilane
DMEM	Dulbecco's Modified Eagle Medium
DMSO	Dimethyl Sulfoxide
DNA	Deoxyribonucleic Acid
dvPDMS	Divinyl Polydimethylsiloxane
dV-PEG	Divinyl Polyethylene Glycol
EGF	Epidermal Growth Factor
EGFR	Epidermal Growth Factor Receptor
EIPA	5-[ <i>N</i> -ethyl- <i>N</i> -isopropyl] alimoride
EM	Electron Microscopy
FBS	Foetal Bovine Serum
FITC	Fluorescein Isothiocyanate
FTIR	Fourier Transform Infrared
GFP	Green Fluorescent Protein
gp41	Glycoprotein 41
GPI-GFP	Glycophosphatidylinositol Green Fluorescent Protein
GS <sub>4</sub>	(Glycine-Serine) <sub>4</sub> – used as control peptide
GTPase	Guanidine Triphosphatase
GUV	Giant Unilaminar Vesicle
HCl	Hydrochloric Acid
HEPES	4-(2-hydroxyethyl)-1-piperazineethanesulfonic acid
HER-2	Human Epidermal Growth Factor Receptor 2
HIV-1	Human Immunodeficiency Virus 1
ID	Identification
IgG	Immunoglobulin G
IPN	Interpenetrating Network
IU	International Unit
KOH	Potassium Hydroxide
laser	Light Amplification Stimulated Emission Radiation
LCD	Liquid Crystal Display
LED	Light Emitting Diode
LSCM	Laser Scanning Confocal Microscope

NH <sub>2</sub>	Amine
NH <sub>4</sub> OH	Ammonium Hydroxide or Ammonia Water
OH	Hydroxyl
OptiMEM	A reduced serum modified Eagle's medium
PAD	Pro-apoptotic domain
Pak-1	p21-activated Kinase 1
PALM	Photoactivated Localisation Microscopy
PBS	Phosphate Buffer Solution
PDGF	Platelet Derived Growth Factor
PDGFR	Platelet Derived Growth Factor Receptor
PDMS	Polydimethylsiloxane
PEG	Polyethylene Glycol
PEGMA	Polyethylene Glycol (Meth)acrylate
PI	Propidium Iodide
PI(4,5)P <sub>2</sub>	Phosphatidyl 4,5,bisphosphate
PKC $\delta$	Protein Kinase C Delta
PMHS	Polymethylhydrosilane
PTD-5	Protein Transduction Domain 5
pVEC	Peptide Vascular Endothelial-Cadherin
QD	Quantum Dots
R8	Octaarginine
Rac1	Ras-related C3 Botulinum Toxin Substrate 1
RGD	Arginine-Glycine-Aspartic Acid (peptide)
Rho	Ras homologue
RNA	Ribonucleic Acid
ROCK	Rho-associated Protein Kinase
RPMI	Roswell Park Memorial Institute (medium)
SA	Succinic Anhydride
Scar	Suppressor of cAMP Receptor
SEM	Scanning Electron Microscope
siRNA	Small Interfering Ribonucleic Acid
STED	Stimulated Emission Depletion
STORM	Stoichastic Optical Reconstruction Microscope
TEA	Triethylamine
TEM	Transmission Electron Microscope
TEOS	Tetraethoxysilane
THF	Tetrahydrofuran
TIRF	Total Internal Reflection Fluorescence
UV	Ultra-Violet
WASp	Wiskott-Aldrich Syndrome Protein

## **1. General Introduction**

### **1.1 Introduction**

The use of microscopy as a tool for life science research remains essential. The first recognisable microscope was developed in the late 16<sup>th</sup> century and consisted of just two lenses the eyepiece and the objective which is thought to have achieved a 9X magnification (Croft, 2006). Over the intervening years magnification and resolution have increased to and beyond the diffraction limit (Galbraith and Galbraith, 2011) and cells can be imaged in a variety of ways using fluorescence microscopy, electron microscopy (Koster and Klumperman, 2003) and even Raman spectroscopy (Pezacki *et al.*, 2011).

### **1.2 Correlative Microscopy**

#### **1.2.1 Limitations and Advances in Light Microscopy**

Live cell microscopy enables a user to follow a selection of cells over time allowing high quality imaging typically using fluorescent conjugates as probes (Fernandez-Suarez and Ting, 2008). Due to the wavelength and properties of light, structural resolution is typically limited to above 100nm in the xy plane (Mironov and Beznoussenko, 2009) with confocal limited to 200-500nm in the z-axis (Galbraith and Galbraith, 2011). This makes it difficult to resolve ultrastructural cell details which can typically be lower than this. To obtain greater structural detail, different microscopes are needed and high quality light microscopes, such as STED (Stimulated Emission Depletion) microscopy (Hell and Wichmann, 1994), STORM (STochastic Optical Reconstruction

Microscopy) (Rust *et al.*, 2006) and PALM (PhotoActivated Localisation Microscopy) (Betzig *et al.*, 2006), have recently been developed which begin to address this problem.

STED microscopes decrease the effective size of the point spread function (the associated blurring of a single point of light due to diffraction) by reducing the emission of surrounding fluorophores limiting fluorescence to only the fluorophores activated in the centre of the light spot (Hell and Wichmann, 1994). Longer wavelengths of light are emitted around the circumference of the light beam which causes this cancellation reducing the fluorophore to its ground state (Galbraith and Galbraith, 2011). The resolution is reduced to ~70nm allowing for greater detail without sacrificing exposure lengths.

Both PALM and STORM use single molecule activation techniques to generate images from individual fluorophores probability determined position (Galbraith and Galbraith, 2011). For STORM, fluorescence pairs consisting of an activator and fluorescence reporter are used (Huang *et al.*, 2008). Using different wavelengths of light the reporter can be switched from a fluorescence ready state and a dark state. The activator facilitates switching between the dark and fluorescent states and this is used to only activate a small number of the reporter fluorophores at any one time (Rust *et al.*, 2006). This reduces the number of active fluorophores in the light spot allowing a probability map to be created of the position of each fluorophore down to 20nm. PALM uses photoactivatable fluorophores whereby the fluorophore is in a dark state until it is activated by a single wavelength, this makes it able to fluoresce when exposed by a second wavelength (Hess *et al.*, 2006). By switching on these

fluorophores individually the centre of the fluorescence emission can be determined and an image can be built up in much higher resolution, typically 20nm in the xy plane. For both STORM and PALM, the option of high resolution imaging is offset by the long exposure times needed to build up a single image. Imaging takes place over a number of hours, ruling out the use of any live samples.

### 1.2.2 Limitations and Advances in Electron Microscopy

There are two main classes of electron microscope, the scanning electron microscopy (SEM) used for cell surface/topography imaging and transmission electron microscopy (TEM) used for higher ultra-structural detail (Bozzola, 2001). Traditional TEM creates a two dimensional electron density map of the sample, to obtain 3D structure serial sections can be obtained and a 3D reconstruction can be generated. This method limits the z-axis resolution to the thickness of the section which, using ultramicrotomes, can be as low as 30-40nm (Koster *et al.*, 1997). To obtain higher z-axis resolution, electron tomography was developed for single sections. To obtain a 3D image from a single micrograph the sample is imaged from multiple angles by tilting the sample around an axis (Rebled *et al.*, 2011). Computer analysis can subsequently use each individual micrograph to build a 3D model of the single section and thus differentiating between closely localised structures in the micrograph (McIntosh *et al.*, 2005). This single axis tilting does, however, leave an information gap at the pivot point where there is not enough data to properly reconstruct the image. Subsequent development of two-axis tilting

has overcome this problem improving the 3D reconstructions (Penczek *et al.*, 1995).

### 1.2.3 Advances in Correlative Microscopy

Correlative microscopy incorporates the two fields of light microscopy and electron microscopy. Some of the first correlative studies compared light images and electron microscopy images from the same tissue (Burkholder and Bergeron, 1970). Subsequently, alternating semi-thin sections ( $> 0.2 \mu\text{m}$ ) for light microscopy and ultrathin sections ( $< 0.1 \mu\text{m}$ ) for TEM were obtained through the sample (Mironov and Beznoussenko, 2009). Semi-thin sections were stained for proteins and this limited how thin the sections could get before clarity was lost under light microscopy. Fluorescent labelling of ultrathin sections is, however, possible (Nisman *et al.*, 2004) and this has allowed fluorescence microscopy and TEM to be performed on the same sample.

Alternative methods were also explored for fluorescence imaging of cells followed by detailed TEM that is not limited to just one section. Using fixed cells, a target protein was fluorescently labelled, a region of interest was found and the sample was imaged using a confocal microscope (Ren *et al.*, 2003). Using a series of electron microscopy (EM) grids to keep track of the region of interest, the sample was recovered, embedded, sectioned and imaged using a TEM. This technique required the researcher to precisely align EM grids over the region of interest three times before sectioning and although ultimately a successful and inexpensive method would require the researcher to be exact with successive grid placements and difficult to perform with live cell imaging.

Gridded cover slips have also been utilised to locate cells during and after light microscopy (Richter *et al.*, 2005). GFP transfected adherent cells were fixed and fluorescently imaged on a gridded coverslip and a region of interest located. After imaging, the sample was embedded, sectioned and imaged using a TEM. This technique is an improvement over the use of multiple EM grids as the gridded coverslip leaves a location indent in the resin allowing fast localisation when sectioning. Although this technique was performed on fixed cells, with reliable grids and fixation techniques it is possible to extend this technique for live cell imaging before fixation.

More recently, a chip was devised that could image live bacteria under fluorescence microscopy or TEM by encasing the sample in extremely thin layers of glass (Yew *et al.*, 2008). This direct imaging under both light and electron microscopes is not possible for cells, however, due to the thin < 200 nm thickness required for TEM.

To obtain true correlative microscopy, where the same sample is analysed under both light and electron microscopy, the target needs to be dual labelled with both a fluorophore and an electron dense marker. This was originally achieved either by using two secondary antibodies, a fluorescent and an electron dense antibody (Mironov and Beznoussenko, 2009), or by having the secondary antibody dual labelled such as with FluoroNanoGold (Powell *et al.*, 1997) (Powell *et al.*, 1998). Labelling of the required sample remains a key component in correlative microscopy and a variety of solutions of the different

requirements of labels that they can be visible under light and electron beams are outlined below.

The most recently developed labelling technique that has a use in CLEM is quantum dots. Quantum dots (QDs) are small particles of semiconductor alloys that both fluoresce and are electron dense (Giepmans, 2008). This makes them ideal for correlative microscopy as they can be imaged under light and electron microscopy without further modification to the sample. By modifying the size of the dot different fluorescence emission wavelengths can be generated that, along with different shapes, can also be determined under the electron microscope allowing for multiprobe imaging of a sample (Cortese *et al.*, 2009). Other fluorescent probes have also been used, although quite often these require conversion to an electron dense material. FIAsh and ReAsH are biarsenical-tetracysteine labels that bind to a specific cysteine rich peptide sequence and fluoresce (Ellisman *et al.*, 2002). These fluorophores can subsequently be used to photoconvert diaminobenzidine into a polymer which precipitates osmium at the localised site.

With the ability to image the same structure under both conditions, two key steps need to be solved. The first key step is the suitable fixation and embedding of a sample, whilst locating the sample after embedding and/or imaging is also important (Mironov and Beznoussenko, 2009). There are two main types of fixation, chemical fixation and cryofixation. For fixation of cell monocultures, chemical fixation occurs over the course of a few seconds, whilst cryofixation can occur in milliseconds. Time difference in both cases

can be limited by how quickly the user can fix the sample. Verkade *et al.* have developed a rapid transfer cryofixation system which allows a user to move from live video imaging to cryofixation in under ten seconds (Verkade, 2008). Using high pressure freezing samples can be maintained with few artifacts generated, with the use of the technique demonstrated in endosome fusion studies (Brown *et al.*, 2009). Chemical fixation has also been demonstrated to generate artefacts in TEM imaging (Koster and Klumperman, 2003). This is because fixation using aldehyde cross-link between proteins causing the cell to shrink and because aldehydes do not react with lipids and carbohydrates further fixation is required.

Locating your sample after sectioning is a critical step. It would be impossible to undertake correlative microscopy on the same cell if that cell cannot be subsequently re-located. Different methods have been employed here although some techniques remain simple (Ren *et al.*, 2003). The difficulty involved is often due to the size of the sample; a typical adherent cell is between 40  $\mu\text{m}$  and 100  $\mu\text{m}$  across but can often be less than 8  $\mu\text{m}$  deep. Use of a grid has been devised, where the grid is patterned onto the top side of the glass cover slip, this pattern can be transferred into the embedding matrix where the approximate cell position can be marked (Richter *et al.*, 2005). By comparing the fluorescence profile with the TEM profile correlative sections can be found (Mironov *et al.*, 2000). A good method that allows quick and simple location of the sample without having to transfer cells away from a surface would, therefore, be a useful tool.

### **1.3 Microwells and Cell Retention**

During live-cell imaging, cells need to be retained whilst different reagents flow around them. Adherent cells are easier to image in this respect as they are adhered to the surface during the experiment, whilst non-adherent cells are liable to move around during the experiment. A method for retaining cells is therefore required to allow live cell imaging to take place.

Different cell retention technologies have been devised using physical structures like microwell traps (Taylor and Walt, 2000), energy dependent mechanisms like dielectrophoresis (Hunt *et al.*, 2008) or optical tweezers (Luo *et al.*, 2007), or using chemical patterning to determine cell localisation.

Dielectrophoresis involves the implementation of a non-uniform AC current across a particle. This induces polarisation of the particle allowing the particle or cell to become trapped or manoeuvred around a surface (Fatoyinbo *et al.*, 2008). This induced dipole has been argued and shown not to damage cells due to the low level voltage passed across the cells as a AC current (Hunt *et al.*, 2008).

Optical tweezers use a laser to trap cells in the centre of the beam due to the conservation of momentum between the light beam and the cell (Laurell *et al.*, 2009). When light hits a cell the momentum of the light beam is transferred to a particle or cell. The Gaussian profile of the laser directs the cell into the centre of the beam allowing the position of the cell to be manipulated.

### 1.3.1 Microwell Arrays

Microwell efficiency in obtaining single cell occupancy is a factor of the well dimensions, flow rate and the number of cells present in the sample. Rettig and Folch looked at these properties to determine well size and shape to increase maximum single cell occupancy using fibroblasts in a large array (Rettig and Folch, 2005). They found that a dimension ratio of  $\sim 1$ , where depth equals width, produced the most efficient single cell loading. As wells get deeper and/or wider, there is a progression towards multicellular occupancy. Whereas, shallow and narrow wells can prevent wells from being occupied by a cell.

Another important factor related to well dimensions is the flow rate of media across the microwell array. Ouyang's group looked at flow rates and patterns affecting yeast cells within a microwell array (Luo *et al.*, 2007). As would be expected, cells were more likely to be retained within the wells at low flow rates, whereas, at higher flow rates the dimensions of the well started play an important factor. Microwells that are as deep, or deeper, than they are wide produced vortices within the well from the cross flowing medium across the well and this helps to retain cells. When the wells become shallower, these vortices do not occur and cells can become dislodged from the wells and be swept out by the flow of the media. Using a flow dampener has also been demonstrated to retain cells within microwells for microscopic analysis by restricting the flow of media during pipetting (Deutsch *et al.*, 2006).

An important factor when looking at adherent cells in microwells is the effect of microwell shape on cell growth. Ochsner *et al.* investigated 3D shape control on adherent cells, whilst cells remained viable, there was actin enrichment around the edge of the microwells (Ochsner *et al.*, 2007).

## **1.4 Surface Modification**

### **1.4.1 Cell Patterning**

Surfaces can have a variety of effects upon cells with some signalling pathways originating from transmembrane proteins. Surfaces can affect how cells migrate or proliferate or even trigger differentiation or cell death (Falconnet *et al.*, 2006). Chemically modified surfaces are not alone in changing cell behaviour, with differing surface topologies also researched for their potential effects (Curtis and Wilkinson, 1997).

Surfaces are needed to encourage and dissuade cell binding (Khan and Newaz, 2010). A good example of this is the research into cell neurons where differing surface patterns, both chemical and topological, have been used to guide neuron growth across a surface. To reduce cell attachment, and often protein binding, hydrophobic surfaces have been developed as well as other modified surfaces such as carbohydrate (Lopina *et al.*, 1996), albumin (Roser *et al.*, 1998), lipid bilayers (Larsson *et al.*, 2003) as well as synthetic materials such as polyethylene glycol (Park *et al.*, 1998). Smart polymers have also been developed that can switch between hydrophilic and hydrophobic with the application of energy. A typical example of this is PNIPAAm poly(N-isopropylacrylamide) which has been modified to change from

superhydrophilic to superhydrophobic with a small increase in heat (Sun and Qing, 2011).

Different techniques have also been employed to increase surface attachment. Surfaces that mimic the extracellular matrix have also been employed and can range from proteins such as fibronectin (Nuttelman *et al.*, 2001) to short peptides such as the RGD (arginine-glycine-aspartic acid) used to help immobilise cells onto a surface (Ratner and Bryant, 2004). Different surface modifications can aid in surface adsorption of extracellular matrix material, with hydroxyl surface groups on gold comparing favourably over carboxyl, amine or methyl (Keselowsky *et al.*, 2003).

#### 1.4.2 Modification of PDMS

The hydrophobic and inert nature of the PDMS surface makes modifying the surface both important and difficult (Lindstrom and Andersson-Svahn, 2011). PDMS has been used for a variety of different functions and, as such, different methods of surface modification have been born out of this (Sugiura *et al.*, 2008). Surface modification of PDMS generally falls into three categories, covalent surface modification such as chemical grafting (Hu *et al.*, 2002), non-covalent surface modification (including surface adsorption) (Zhou *et al.*, 2010) and the generation of interpenetrating networks (Jalili *et al.*, 2009).

#### 1.4.2.1 Covalent Modification of PDMS

Covalent modification of PDMS requires the surface to first be activated (Zhou *et al.*, 2010). This can occur in a variety of different methods providing unique attachment points on which to attach different chemical structures and polymers. Plasma radiation is extensively used to modify surfaces and works by the discharge of oxygen plasma onto the surface for short periods of time, breaking the silicone chains and creating surface hydroxyls (Tan *et al.*, 2010). UV-radiation is another frequently used method that uses atmospheric oxygen and UV radiation to create hydroxyl groups on the surface (Berdichevsky *et al.*, 2004). Coronal discharges are also used to create free radicals and ions on the surface, electromagnetic discharges create ozone using atmospheric oxygen and this degrades to form oxygen free radicals that can react with the surface of PDMS (Hahn *et al.*, 2003).

One key problem after surface modification is the loss of the hydrophilic surface within hours of creation if left exposed to the air (Olah *et al.*, 2005). This is thought to occur through the migration of hydrophobic chains through cracks in the surface (Fritz and Owen, 1995), but the need for further modification is important if a hydrophilic surface is required for a prolonged period of time. This need has brought rise to a variety of solutions to covalently bond polymers to the hydroxyls or free radicals generated or through direct covalent attachment using the hydrosilyl (Si-H) bond which can be made available within the PDMS elastomer (Hu *et al.*, 2002, Guo, 2007, Bhattacharya *et al.*, 2005).

Free radicals can be produced on the surface the UV treatment and coronal discharge. These free radicals can then be used to induce graft polymerisation to the surface using, for example, functionalised acrylate monomers (Schneider *et al.*, 2010).

Hydroxyl groups generated by energy or chemical oxidation of the surface can be used to attach silanes. Sui *et al.* have shown the use of an amine silane and a PEG silane as part of the functionalisation of PDMS surfaces in microchannels(Sui *et al.*, 2006). Using chemical oxidation to produce hydroxyls on the surface and aminopropyltrimethoxysilane or PEG trimethoxysilane was used in the silanisation reaction. The amine surface was then further modified to attach the short RGD peptide to aid in cell attachment.

#### 1.4.2.2 Non-Covalent Modification of PDMS

Non-covalent surface modification can be achieved in a variety of ways, using energy requiring modifications, such as chemical vapour deposition (Im *et al.*, 2009), or more passive methods, such as the use of surfactants (Garcia *et al.*, 2005). Surfactants contain both hydrophobic and hydrophilic regions, the hydrophobic regions interact through Van der Waals forces whilst hydrophilic polymers stretch into the solution.

### 1.4.2.3 Interpenetrating Networks in PDMS

Interpenetrating networks (IPNs) can be used to modify bulk PDMS and exist when two polymers are mixed together, at least one of which is cross-linked (Abbasi *et al.*, 2001). The use of two polymers has been shown to increase the strength of materials but can also increase the wettability of PDMS by incorporating polymers more hydrophilic polymers in to the bulk of the PDMS.

## 1.5 Endocytosis

Many different pathways are employed by the cell to internalise different substrates such as proteins and carbohydrates into endosomes and further along the endocytic pathway. Endocytosis can be split into three broad categories, clathrin-dependant, clathrin independent and phagocytosis. Clathrin independent pathways can be further subdivided into many pathways and include macropinocytosis and calveolin dependent endocytosis.

### 1.5.1 Macropinocytosis

Macropinocytosis is a pathway different from the other endocytic pathways. Although growth factor receptors such as epidermal growth factor receptor (EGFR) and platelet derived growth factor receptor (PDGFR) are associated with macropinocytosis (Jones, 2007), macropinocytosis does not see an increase in regulatory molecules to any specific sites of the plasma membrane. Instead global actin activity can increase at the cell membrane causing ruffles to form at the surface (Lee and Knecht, 2002). It is these ruffles that fold over and fuse enveloping extracellular fluid for uptake into the cell.

For the formation of ruffles to occur new branches of the actin filament are formed. This is initiated by GTPases Rho (Ras homolog), Cdc42 (cell division control protein 42) and Rac (Ras-related C3 botulinum toxin substrate 1) which interact with PI(4,5)P<sub>2</sub> (phosphoinositol 4,5 bisphosphate) and activate WASp (Wiskott-Aldrich syndrome protein) and Scar (suppressor of cAMP receptor) forming the new branching point (West *et al.*, 2000, Seastone *et al.*, 2001).

Although a regulatory mechanism for ruffle binding after folding onto itself is unknown, Pak-1 (p21-activated kinase 1) is known to have a role. Pak-1 is involved in a variety of mechanisms within the cell but has been shown to be essential for the formation of macropinosomes after ruffling (Liberali *et al.*, 2008). The phosphorylation by Pak-1 of CtBP1/BARS (C-terminal binding protein 1/Brefeldin A-ADP-ribosylated substrate) allows the ruffles to fuse (Liberali *et al.*, 2008), whilst depletion of Pak-1 has been shown to reduce macropinosome formation (Karjalainen *et al.*, 2008).

Whilst the localisation for macropinosomes can vary according to the cell type, macropinocytosis remains an important role in uptake of various molecules. For cell penetrating peptides it has shown to have a role in the polycationic peptides polyarginine and Tat (Khalil *et al.*, 2006).

## 1.5.2 Other Key Endocytic Pathways

### *1.5.2.1 Clathrin dependent endocytosis*

In clathrin dependent endocytosis (or clathrin mediated endocytosis, CME), soluble triskelion clathrin is recruited to the vesicle and forms a polygonal

lattice around the budding membrane (Le Roy and Wrana, 2005). This surrounds the vesicle during formation on the plasma membrane as well as some internal compartments. Adapter proteins help recruit clathrin to the site of endocytosis, where the clathrin coated pit can begin to form around a receptor. As clathrin begins to polymerise around the pit the vesicle begins to form. To fully remove the vesicle from the plasma membrane dynamin, a helical GTPase, surrounds the neck and pinches off the vesicle. It is important to note that dynamin is not unique to CME and has been shown to be involved in other endocytic pathways (Doherty and McMahon, 2009).

CME is involved extensively in receptor regulation by trafficking receptors to and from the membrane to up or down regulate signalling pathways (Tsao *et al.*, 2001). A frequently used marker for CME is transferrin, a ~80kDa protein used to traffic iron into the cell (Qian *et al.*, 2002). The transferrin receptor internalises through CME, to the early endosome where it is trafficked back to the plasma membrane through the recycling pathway. Colocalisation studies in live cells often use fluorescently labelled transferrin to mark CME, whilst antibodies to the transferrin receptor can be used during immunolabeling.

#### *1.5.2.2 Caveolin dependent endocytosis*

Caveolin dependent endocytosis, like clathrin dependent endocytosis, involves a protein coat consisting of a caveolin protein, but also utilises four regulatory proteins known as cavins1-4 (Le Lay *et al.*, 2011). The cavin family of proteins were not always known to be associated with calveolae and have a variety of alternate names. Although the full role of these proteins are not fully

understood, it is known that they can precipitate with each other and the caveolin proteins whilst reducing expression of caveolins 1 and 2 has been shown to reduce levels of caveolins and other caveolins (Nichols and Hansen, 2010).

The main markers for caveolae are the toxins, Cholera Toxin B Chain and Shiga Toxin B Chain. Cholera Toxin B Chain has been demonstrated to enter through caveolae-like endosomes (Orlandi and Fishman, 1998) although they can enter through other pathways when this endocytosis pathway has been artificially depleted (Torgersen *et al.*, 2001).

### *1.5.2.3 Phagocytosis*

Phagocytosis is the pathway used for uptake of large structures such as apoptotic bodies and bacteria. As such, like macropinocytosis, involves large restructuring of the plasma membrane, unlike macropinocytosis, phagocytosis is a receptor mediated event (Hillaireau and Couvreur, 2009). Particles, coated with ligands such as IgG and complement proteins which are in turn detected by the cell. This leads to a signalling pathway and the formation of large actin mediated protrusions which engulf the particle into the phagosome. Phagosomes range in size depending upon the particle but are taken directly to lysosomes so the internalised particle can be degraded (Sahay *et al.*, 2010). This means that phagocytosis is abundant in just a few cells, specialising in uptake of extracellular bodies and bacteria, such as macrophages.

## **1.6 Cell Penetrating Peptides**

Cell penetrating peptides (CPPs, or protein transduction domains, as they are also known) can be used to deliver different cargo into a cell. Different peptides have been identified as CPPs and can be described under two different classes, arginine rich peptides, such as oligoarginine (Abes *et al.*, 2008) or Tat (Vives *et al.*, 1997), and amphiphilic peptides, such as penetratin (Derossi *et al.*, 1994), which forms an  $\alpha$ -helical structure with cationic and hydrophobic residues lining up on different sides of the peptide. There are many types of CPP with Tat, oligoarginine (typically R<sub>8</sub> or R<sub>9</sub>) and penetratin among the best defined.

Tat is derived from HIV-1 gp41 protein which was discovered to translocate the membrane on its own (Vives *et al.*, 1997). A short sequence from this protein (amino acids 48-60) that consisted mainly of the cationic amino acids lysine and arginine was shown to be more efficient in entering cells and gave rise to the Tat peptide.

Oligoarginines are synthetically designed peptides that can vary in length and structure. Whilst different length variations of this peptide have been researched, lengths of between seven and ten residues are most common (Rothbard *et al.*, 2000). Structural variations of arginine rich peptides have also been researched in an attempt to optimise peptide uptake (Futaki, 2005).

The full uptake mechanism or mechanisms of octaarginines (R<sub>8</sub>) has not been fully understood. It has been demonstrated that proteoglycans allow the positively charged peptide to bind to the cell surface (Nakase *et al.*, 2007).

Proteoglycans are negatively charged and have been shown to be involved in macropinocytosis by signalling the redistribution of filamentous actin. To further investigate the role of macropinocytosis in oligoarginine uptake, macropinocytosis inhibitors have been used such as the amiloride derived EIPA (5-[*N*-ethyl-*N*-isopropyl] amiloride). Inhibition using EIPA showed a reduction in uptake of the peptide, indicating a role of macropinocytosis in this area (Futaki *et al.*, 2007). However, when low temperature experiments are performed, oligoarginine is still internalised into the cell with a very different fluorescence profile (Fretz *et al.*, 2007). Oligoarginine forms punctate structures typical of endocytic pathway at 37°C, at 4°C, the peptide is diffused throughout the cytoplasm and displaying nuclear labelling. Cholesterol depletion using methyl- $\beta$ -cyclodextran, another method to reduce macropinocytosis, showed similar diffuse labelling indicating a role for another uptake mechanism.

Addition of hydrophobic moieties, such as myristoyl (Lee and Tung, 2010) or cholesterol (Futaki *et al.*, 2001), has been shown to increase uptake of CPPs. Changes to the hydrophobic domain of pVEC, resulting in a reduction in hydrophobicity, have been shown to significantly reduce uptake of this peptide (Elmqvist *et al.*, 2006). As seen in Chapter 5, a single change in a peptide sequence can have a great effect on peptide uptake and activity (Watkins *et al.*, 2011).

Whilst much research has focussed on understanding CPP uptake mechanisms and evaluating novel CPPs, some CPPs have moved further towards

therapeutic use (Grdisa, 2011). A major hurdle in any drug design is getting drugs across the membrane and CPPs can be used to achieve this (Mason, 2010). Already some CPP chimeras have been used in early clinical trials to target proteins, such as PKC $\delta$  (Protein Kinase C delta), to reduce pain lighting the way for potential CPP therapeutics (Inagaki *et al.*, 2003).

### **1.7 Aims of this Thesis**

The overall aim of this thesis was to investigate the use of microwells as a method for multi-image analysis for non-adherent cells.

Chapter 2 outlines the materials and methods used in the experiments analysed in the following chapters.

Chapter 3 studied the manufacture of microwells and aimed to increase the quality of production as well as find a suitable polymer for sectioning. Laser ablation was used to manufacture the microwells and debris produced during ablation reduced overall well quality. Autofluorescence of the surface was a major problem interrupting imaging of the surface and PDMS as an alternative material for imaging was introduced. Microwell design was further investigated, the need to track a single well through different image processes was discussed and different microwell designs were devised.

Chapter 4 looked at surface chemistry with the aim of determining suitable surface modification techniques to aid cytocompatibility of PDMS. Techniques such as silanisation and hydrosilylation were investigated as methods to covalently modify the surface, whilst alternative methods such as the production of an interpenetrating network within PDMS was devised as a method to modify the bulk polymer.

Chapter 5 investigated cell imaging of cell penetrating peptides and aimed to better understand the role of macropinocytosis in uptake of r8 and r8 linked cargoes and the role of membrane blebbing in pro-apoptotic peptides r8-PAD

and fsr-r8. Macropinocytosis of octaarginine was investigated, along with two octaarginine linked pro-apoptotic cargoes, PAD and the Bcl-2 converter peptide. The differences in apoptotic and necrotic blebbing were discussed and the similarities and differences of apoptotic and necrotic blebbing in r8-PAD and Bcl-2 converter peptide treated cells.

## **1.8 References**

- ABBASI, F., MIRZADEH, H. & KATBAB, A. A. (2001) Modification of polysiloxane polymers for biomedical applications: a review. *Polymer International*, 50, 1279-1287.
- ABES, R., ARZUMANOV, A., MOULTON, H., ABES, S., IVANOVA, G., GAIT, M. J., IVERSEN, P. & LEBLEU, B. (2008) Arginine-rich cell penetrating peptides: design, structure-activity, and applications to alter pre-mRNA splicing by steric-block oligonucleotides. *J Pept Sci*, 14, 455-60.
- BERDICHEVSKY, Y., KHANDURINA, J., GUTTMAN, A. & LO, Y. H. (2004) UV/ozone modification of poly(dimethylsiloxane) microfluidic channels. *Sensors and Actuators B-Chemical*, 97, 402-408.
- BETZIG, E., PATTERSON, G. H., SOUGRAT, R., LINDWASSER, O. W., OLENYCH, S., BONIFACINO, J. S., DAVIDSON, M. W., LIPPINCOTT-SCHWARTZ, J. & HESS, H. F. (2006) Imaging intracellular fluorescent proteins at nanometer resolution. *Science*, 313, 1642-5.
- BHATTACHARYA, S., DATTA, A., BERG, J. M. & GANGOPADHYAY, S. (2005) Studies on surface wettability of poly(dimethyl) siloxane (PDMS) and glass under oxygen-plasma treatment and correlation with bond strength. *Microelectromechanical Systems, Journal of*, 14, 590-597.
- BOZZOLA, J. J. (2001) - Electron Microscopy.
- BROWN, E., MANTELL, J., CARTER, D., TILLY, G. & VERKADE, P. (2009) Studying intracellular transport using high-pressure freezing and Correlative Light Electron Microscopy. *Seminars in Cell & Developmental Biology*, 20, 910-919.

- BURKHOLDER, P. M. & BERGERON, J. A. (1970) Spontaneous glomerulonephritis in the prosimian primate Galago. A correlative light, immunofluorescence and electron microscopic analysis. *Am J Pathol*, 61, 437-56.
- CORTESE, K., DIASPRO, A. & TACCHETTI, C. (2009) Advanced correlative light/electron microscopy: current methods and new developments using Tokuyasu cryosections. *J Histochem Cytochem*, 57, 1103-12.
- CROFT, W. J. (2006) *Under the microscope: a brief history of microscopy*, Singapore, World Scientific Publishing Co. Pte. Ltd.
- CURTIS, A. & WILKINSON, C. (1997) Topographical control of cells. *Biomaterials*, 18, 1573-83.
- DEROSI, D., JOLIOT, A. H., CHASSAING, G. & PROCHIANTZ, A. (1994) THE 3RD HELIX OF THE ANTENNAPEDIA HOMEODOMAIN TRANSLOCATES THROUGH BIOLOGICAL-MEMBRANES. *Journal of Biological Chemistry*, 269, 10444-10450.
- DEUTSCH, A., ZURGIL, N., HUREVICH, I., SHAFRAN, Y., AFRIMZON, E., LEBOVICH, P. & DEUTSCH, M. (2006) Microplate cell-retaining methodology for high-content analysis of individual non-adherent unanchored cells in a population. *Biomedical Microdevices*, 8, 361-374.
- DOHERTY, G. J. & MCMAHON, H. T. (2009) Mechanisms of endocytosis. *Annu Rev Biochem*, 78, 857-902.
- ELLISMAN, M. H., GAIETTA, G., DEERINCK, T. J., ADAMS, S. R., BOUWER, J., TOUR, O., LAIRD, D. W., SOSINSKY, G. E. & TSIEN, R. Y. (2002) Multicolor and electron microscopic imaging of connexin trafficking. *Science*, 296, 503-507.
- ELMQUIST, A., HANSEN, M. & LANGEL, U. (2006) Structure-activity relationship study of the cell-penetrating peptide pVEC. *Biochim Biophys Acta*, 1758, 721-9.

- FALCONNET, D., CSUCS, G., GRANDIN, H. M. & TEXTOR, M. (2006) Surface engineering approaches to micropattern surfaces for cell-based assays. *Biomaterials*, 27, 3044-3063.
- FATOYINBO, H. O., HOEFTGES, K. F. & HUGHES, M. P. (2008) Rapid-on-chip determination of dielectric properties of biological cells using imaging techniques in a dielectrophoresis dot microsystem. *Electrophoresis*, 29, 3-10.
- FERNANDEZ-SUAREZ, M. & TING, A. Y. (2008) Fluorescent probes for super-resolution imaging in living cells. *Nat Rev Mol Cell Biol*, 9, 929-43.
- FRETZ, M. M., PENNING, N. A., AL-TAEI, S., FUTAKI, S., TAKEUCHI, T., NAKASE, I., STORM, G. & JONES, A. T. (2007) Temperature-, concentration- and cholesterol-dependent translocation of L- and D-oct-arginine across the plasma and nuclear membrane of CD34(+) leukaemia cells. *Biochemical Journal*, 403, 335-342.
- FRITZ, J. L. & OWEN, M. J. (1995) Hydrophobic recovery of plasma-treated polydimethylsiloxane. *Journal of Adhesion*, 54, 33-45.
- FUTAKI, S. (2005) Membrane-permeable arginine-rich peptides and the translocation mechanisms. *Advanced Drug Delivery Reviews*, 57, 547-558.
- FUTAKI, S., NAKASE, I., TACLOKORO, A., TAKEUCHI, T. & JONES, A. T. (2007) Arginine-rich peptides and their internalization mechanisms. *Biochemical Society Transactions*, 35, 784-787.
- FUTAKI, S., OHASHI, W., SUZUKI, T., NIWA, M., TANAKA, S., UEDA, K., HARASHIMA, H. & SUGIURA, Y. (2001) Stearylated arginine-rich peptides: a new class of transfection systems. *Bioconjug Chem*, 12, 1005-11.
- GALBRAITH, J. A. & GALBRAITH, C. G. (2011) Super-resolution microscopy for nanosensing. *Wiley Interdisciplinary Reviews-Nanomedicine and Nanobiotechnology*, 3, 247-255.

- GARCIA, C. D., DRESSEN, B. M., HENDERSON, A. & HENRY, C. S. (2005) Comparison of surfactants for dynamic surface modification of poly(dimethylsiloxane) microchips. *Electrophoresis*, 26, 703-9.
- GIEPMANS, B. N. G. (2008) Bridging fluorescence microscopy and electron microscopy. *Histochemistry and Cell Biology*, 130, 211-217.
- GRDISA, M. (2011) The delivery of biologically active (therapeutic) peptides and proteins into cells. *Curr Med Chem*, 18, 1373-9.
- GUO, D. H., HM; JING-WANG; XIAO, SJ; DAI, ZD (2007) Surface-hydrophilic and protein-resistant silicone elastomers prepared by hydrosilylation of vinyl poly(ethylene glycol) on hydrosilanes-poly(dimethylsiloxane) surfaces. *Colloids And Surfaces A-Physicochemical And Engineering Aspects*, 308, 129-135.
- HAHN, J. H., MAKAMBA, H., KIM, J. H., LIM, K. & PARK, N. (2003) Surface modification of poly(dimethylsiloxane) microchannels. *Electrophoresis*, 24, 3607-3619.
- HELL, S. W. & WICHMANN, J. (1994) Breaking the diffraction resolution limit by stimulated emission: stimulated-emission-depletion fluorescence microscopy. *Opt Lett*, 19, 780-2.
- HESS, S. T., GIRIRAJAN, T. P. & MASON, M. D. (2006) Ultra-high resolution imaging by fluorescence photoactivation localization microscopy. *Biophys J*, 91, 4258-72.
- HILLAIREAU, H. & COUVREUR, P. (2009) Nanocarriers' entry into the cell: relevance to drug delivery. *Cellular and Molecular Life Sciences*, 66, 2873-2896.
- HU, S., REN, X., BACHMAN, M., SIMS, C. E., LI, G. P. & ALLBRITTON, N. (2002) Surface modification of poly(dimethylsiloxane) microfluidic devices by ultraviolet polymer grafting. *Anal Chem*, 74, 4117-23.

- HUANG, B., WANG, W., BATES, M. & ZHUANG, X. (2008) Three-dimensional super-resolution imaging by stochastic optical reconstruction microscopy. *Science*, 319, 810-3.
- HUNT, T. P., ISSADORE, D. & WESTERVELT, R. M. (2008) Integrated circuit/microfluidic chip to programmably trap and move cells and droplets with dielectrophoresis. *Lab on a Chip*, 8, 81-87.
- IM, S. G., BONG, K. W., LEE, C. H., DOYLE, P. S. & GLEASON, K. K. (2009) A conformal nano-adhesive via initiated chemical vapor deposition for microfluidic devices. *Lab Chip*, 9, 411-6.
- INAGAKI, K., CHEN, L., IKENO, F., LEE, F. H., IMAHASHI, K., BOULEY, D. M., REZAEI, M., YOCK, P. G., MURPHY, E. & MOCHLY-ROSEN, D. (2003) Inhibition of delta-protein kinase C protects against reperfusion injury of the ischemic heart *in vivo*. *Circulation*, 108, 2304-7.
- JALILI, K., ABBASI, F., OSKOEI, S. S. & ALINEJAD, Z. (2009) Relationships between the morphology, swelling and mechanical properties of poly(dimethyl siloxane)/poly(acrylic acid) interpenetrating networks. *J Mech Behav Biomed Mater*, 2, 534-41.
- JONES, A. T. (2007) Macropinocytosis: searching for an endocytic identity and role in the uptake of cell penetrating peptides. *J Cell Mol Med*, 11, 670-84.
- KARJALAINEN, M., KAKKONEN, E., UPLA, P., PALORANTA, H., KANKAANPAA, P., LIBERALI, P., RENKEMA, G. H., HYYPIA, T., HEINO, J. & MARJOMAKI, V. (2008) A Raft-derived, Pak1-regulated entry participates in alpha2beta1 integrin-dependent sorting to caveosomes. *Mol Biol Cell*, 19, 2857-69.
- KESELOWSKY, B. G., COLLARD, D. M. & GARCIA, A. J. (2003) Surface chemistry modulates fibronectin conformation and directs integrin binding

- and specificity to control cell adhesion. *Journal of Biomedical Materials Research Part A*, 66A, 247-259.
- KHALIL, I. A., KOGURE, K., FUTAKI, S. & HARASHIMA, H. (2006) High density of octaarginine stimulates macropinocytosis leading to efficient intracellular trafficking for gene expression. *J Biol Chem*, 281, 3544-51.
- KHAN, S. & NEWAZ, G. (2010) A comprehensive review of surface modification for neural cell adhesion and patterning. *J Biomed Mater Res A*, 93, 1209-24.
- KOSTER, A. J., GRIMM, R., TYPKE, D., HEGERL, R., STOSCHEK, A., WALZ, J. & BAUMEISTER, W. (1997) Perspectives of molecular and cellular electron tomography. *J Struct Biol*, 120, 276-308.
- KOSTER, A. J. & KLUMPERMAN, J. (2003) Electron microscopy in cell biology: integrating structure and function. *Nat Rev Mol Cell Biol*, Suppl, SS6-10.
- LARSSON, C., RODAHL, M. & HOOK, F. (2003) Characterization of DNA immobilization and subsequent hybridization on a 2D arrangement of streptavidin on a biotin-modified lipid bilayer supported on SiO<sub>2</sub>. *Anal Chem*, 75, 5080-7.
- LAURELL, T., NILSSON, J., EVANDER, M. & HAMMARSTROM, B. (2009) Review of cell and particle trapping in microfluidic systems. *Analytica Chimica Acta*, 649, 141-157.
- LE LAY, S., BRIAND, N. & DUGAIL, I. (2011) Cavin proteins: New players in the caveolae field. *Biochimie*, 93, 71-77.
- LE ROY, C. & WRANA, J. L. (2005) Clathrin- and non-clathrin-mediated endocytic regulation of cell signalling. *Nat Rev Mol Cell Biol*, 6, 112-26.
- LEE, E. & KNECHT, D. A. (2002) Visualization of actin dynamics during macropinocytosis and exocytosis. *Traffic*, 3, 186-92.
- LEE, J. S. & TUNG, C. H. (2010) Lipo-oligoarginines as effective delivery vectors to promote cellular uptake. *Mol Biosyst*, 6, 2049-55.

- LIBERALI, P., KAKKONEN, E., TURACCHIO, G., VALENTE, C., SPAAR, A., PERINETTI, G., BOCKMANN, R. A., CORDA, D., COLANZI, A., MARJOMAKI, V. & LUINI, A. (2008) The closure of Pak1-dependent macropinosomes requires the phosphorylation of CtBP1/BARS. *EMBO J*, 27, 970-81.
- LINDSTROM, S. & ANDERSSON-SVAHN, H. (2011) Miniaturization of biological assays -- overview on microwell devices for single-cell analyses. *Biochim Biophys Acta*, 1810, 308-16.
- LOPINA, S. T., WU, G., MERRILL, E. W. & GRIFFITH-CIMA, L. (1996) Hepatocyte culture on carbohydrate-modified star polyethylene oxide hydrogels. *Biomaterials*, 17, 559-69.
- LUO, C. X., LI, H., XIONG, C. Y., PENG, X. L., KOU, Q. L., CHEN, Y., JI, H. & OUYANG, Q. (2007) The combination of optical tweezers and microwell array for cells physical manipulation and localization in microfluidic device. *Biomedical Microdevices*, 9, 573-578.
- MASON, J. M. (2010) Design and development of peptides and peptide mimetics as antagonists for therapeutic intervention. *Future Med Chem*, 2, 1813-22.
- MCINTOSH, R., NICASTRO, D. & MASTRONARDE, D. (2005) New views of cells in 3D: an introduction to electron tomography. *Trends Cell Biol*, 15, 43-51.
- MIRONOV, A. A. & BEZNOUSSENKO, G. V. (2009) Correlative microscopy: a potent tool for the study of rare or unique cellular and tissue events. *Journal of Microscopy-Oxford*, 235, 308-321.
- MIRONOV, A. A., POLISHCHUK, R. S. & LUINI, A. (2000) Visualizing membrane traffic *in vivo* by combined video fluorescence and 3D electron microscopy. *Trends in Cell Biology*, 10, 349-353.
- NAKASE, I., TADOKORO, A., KAWABATA, N., TAKEUCHI, T., KATOH, H., HIRAMOTO, K., NEGISHI, M., NOMIZU, M., SUGIURA, Y. & FUTAKI,

- S. (2007) Interaction of arginine-rich peptides with membrane-associated proteoglycans is crucial for induction of actin organization and macropinocytosis. *Biochemistry*, 46, 492-501.
- NICHOLS, B. J. & HANSEN, C. G. (2010) Exploring the caves: cavins, caveolins and caveolae. *Trends in Cell Biology*, 20, 177-186.
- NISMAN, R., DELLAIRE, G., REN, Y., LI, R. & BAZETT-JONES, D. P. (2004) Application of quantum dots as probes for correlative fluorescence, conventional, and energy-filtered transmission electron microscopy. *J Histochem Cytochem*, 52, 13-8.
- NUTTELMAN, C. R., MORTISEN, D. J., HENRY, S. M. & ANSETH, K. S. (2001) Attachment of fibronectin to poly(vinyl alcohol) hydrogels promotes NIH3T3 cell adhesion, proliferation, and migration. *J Biomed Mater Res*, 57, 217-23.
- OCHSNER, M., DUSSEILLER, M. R., GRANDIN, H. M., LUNA-MORRIS, S., TEXTOR, M., VOGEL, V. & SMITH, M. L. (2007) Micro-well arrays for 3D shape control and high resolution analysis of single cells. *Lab on a Chip*, 7, 1074-1077.
- OLAH, A., HILLBORG, H. & VANCOSO, G. J. (2005) Hydrophobic recovery of UV/ozone treated poly(dimethylsiloxane): adhesion studies by contact mechanics and mechanism of surface modification. *Applied Surface Science*, 239, 410-423.
- ORLANDI, P. A. & FISHMAN, P. H. (1998) Filipin-dependent inhibition of cholera toxin: evidence for toxin internalization and activation through caveolae-like domains. *J Cell Biol*, 141, 905-15.
- PARK, K. D., KIM, Y. S., HAN, D. K., KIM, Y. H., LEE, E. H., SUH, H. & CHOI, K. S. (1998) Bacterial adhesion on PEG modified polyurethane surfaces. *Biomaterials*, 19, 851-9.

- PENCZEK, P., MARKO, M., BUTTLE, K. & FRANK, J. (1995) Double-tilt electron tomography. *Ultramicroscopy*, 60, 393-410.
- PEZACKI, J. P., BLAKE, J. A., DANIELSON, D. C., KENNEDY, D. C., LYN, R. K. & SINGARAVELU, R. (2011) Chemical contrast for imaging living systems: molecular vibrations drive CARS microscopy. *Nat Chem Biol*, 7, 137-45.
- POWELL, R. D., HALSEY, C. M. & HAINFELD, J. F. (1998) Combined fluorescent and gold immunoprobes: reagents and methods for correlative light and electron microscopy. *Microsc Res Tech*, 42, 2-12.
- POWELL, R. D., HALSEY, C. M., SPECTOR, D. L., KAURIN, S. L., MCCANN, J. & HAINFELD, J. F. (1997) A covalent fluorescent-gold immunoprobe: simultaneous detection of a pre-mRNA splicing factor by light and electron microscopy. *J Histochem Cytochem*, 45, 947-56.
- QIAN, Z. M., LI, H. Y., SUN, H. Z. & HO, K. (2002) Targeted drug delivery via the transferrin receptor-mediated endocytosis pathway. *Pharmacological Reviews*, 54, 561-587.
- RATNER, B. D. & BRYANT, S. J. (2004) Biomaterials: Where we have been and where we are going. *Annual Review of Biomedical Engineering*, 6, 41-75.
- REBLED, J. M., YEDRA, L., ESTRADE, S., PORTILLO, J. & PEIRO, F. (2011) A new approach for 3D reconstruction from bright field TEM imaging: Beam precession assisted electron tomography. *Ultramicroscopy*, 111, 1504-11.
- REN, Y., KRUHLAK, M. J. & BAZETT-JONES, D. P. (2003) Same serial section correlative light and energy-filtered transmission electron microscopy. *J Histochem Cytochem*, 51, 605-12.
- RETTIG, J. R. & FOLCH, A. (2005) Large-scale single-cell trapping and imaging using microwell arrays. *Analytical Chemistry*, 77, 5628-5634.
- RICHTER, K., REICHENZELLER, M., GORISCH, S. M., SCHMIDT, U., SCHEUERMANN, M. O., HERRMANN, H. & LICHTER, P. (2005)

Characterization of a nuclear compartment shared by nuclear bodies applying ectopic protein expression and correlative light and electron microscopy. *Exp Cell Res*, 303, 128-37.

ROSER, M., FISCHER, D. & KISSEL, T. (1998) Surface-modified biodegradable albumin nano- and microspheres. II: effect of surface charges on *in vitro* phagocytosis and biodistribution in rats. *Eur J Pharm Biopharm*, 46, 255-63.

ROTHBARD, J. B., GARLINGTON, S., LIN, Q., KIRSCHBERG, T., KREIDER, E., MCGRANE, P. L., WENDER, P. A. & KHAVARI, P. A. (2000) Conjugation of arginine oligomers to cyclosporin A facilitates topical delivery and inhibition of inflammation. *Nat Med*, 6, 1253-7.

RUST, M. J., BATES, M. & ZHUANG, X. (2006) Sub-diffraction-limit imaging by stochastic optical reconstruction microscopy (STORM). *Nat Methods*, 3, 793-5.

SAHAY, G., ALAKHOVA, D. Y. & KABANOV, A. V. (2010) Endocytosis of nanomedicines. *Journal of Controlled Release*, 145, 182-195.

SCHNEIDER, M. H., WILLAIME, H., TRAN, Y., REZGUI, F. & TABELING, P. (2010) Wettability Patterning by UV-Initiated Graft Polymerization of Poly(acrylic acid) in Closed Microfluidic Systems of Complex Geometry. *Anal Chem*.

SEASTONE, D. J., HARRIS, E., TEMESVARI, L. A., BEAR, J. E., SAXE, C. L. & CARDELLI, J. (2001) The WASp-like protein scar regulates macropinocytosis, phagocytosis and endosomal membrane flow in *Dictyostelium*. *J Cell Sci*, 114, 2673-83.

SUGIURA, S., EDAHIRO, J., SUMARU, K. & KANAMORI, T. (2008) Surface modification of polydimethylsiloxane with photo-grafted poly(ethylene glycol) for micropatterned protein adsorption and cell adhesion. *Colloids Surf B Biointerfaces*, 63, 301-5.

- SUI, G., WANG, J., LEE, C. C., LU, W., LEE, S. P., LEYTON, J. V., WU, A. M. & TSENG, H. R. (2006) Solution-phase surface modification in intact poly(dimethylsiloxane) microfluidic channels. *Anal Chem*, 78, 5543-51.
- SUN, T. & QING, G. (2011) Biomimetic smart interface materials for biological applications. *Adv Mater*, 23, H57-77.
- TAN, S. H., NGUYEN, N. T., CHUA, Y. C. & KANG, T. G. (2010) Oxygen plasma treatment for reducing hydrophobicity of a sealed polydimethylsiloxane microchannel. *Biomicrofluidics*, 4, 32204.
- TAYLOR, L. C. & WALT, D. R. (2000) Application of high-density optical microwell arrays in a live-cell biosensing system. *Analytical Biochemistry*, 278, 132-142.
- TORGERSEN, M. L., SKRETTING, G., VAN DEURS, B. & SANDVIG, K. (2001) Internalization of cholera toxin by different endocytic mechanisms. *J Cell Sci*, 114, 3737-47.
- TSAO, P., CAO, T. & VON ZASTROW, M. (2001) Role of endocytosis in mediating downregulation of G-protein-coupled receptors. *Trends Pharmacol Sci*, 22, 91-6.
- VERKADE, P. (2008) Moving EM: the Rapid Transfer System as a new tool for correlative light and electron microscopy and high throughput for high-pressure freezing. *J Microsc*, 230, 317-28.
- VIVES, E., BRODIN, P. & LEBLEU, B. (1997) A truncated HIV-1 Tat protein basic domain rapidly translocates through the plasma membrane and accumulates in the cell nucleus. *J Biol Chem*, 272, 16010-7.
- WATKINS, C. L., SAYERS, E. J., ALLENDER, C., BARROW, D., FEGAN, C., BRENNAN, P. & JONES, A. T. (2011) Co-operative membrane disruption between cell-penetrating peptide and cargo: implications for the therapeutic use of the Bcl-2 converter peptide D-NuBCP-9-r8. *Mol Ther*, 19, 2124-32.

- WEST, M. A., PRESCOTT, A. R., ESKELINEN, E. L., RIDLEY, A. J. & WATTS, C. (2000) Rac is required for constitutive macropinocytosis by dendritic cells but does not control its downregulation. *Curr Biol*, 10, 839-48.
- YEW, T. R., LIU, K. L., WU, C. C., HUANG, Y. J., PENG, H. L., CHANG, H. Y., CHANG, P. & HSU, L. (2008) Novel microchip for in situ TEM imaging of living organisms and bio-reactions in aqueous conditions. *Lab on a Chip*, 8, 1915-1921.
- ZHOU, J., ELLIS, A. V. & VOELCKER, N. H. (2010) Recent developments in PDMS surface modification for microfluidic devices. *Electrophoresis*, 31, 2-16.

## **2 Materials and Methods**

### **2.1 Cell Culture**

KG1a, K562, Jurkat and Mcf-7 cells (ATCC, Teddington, UK) were all subcultured twice weekly in RPMI containing 10% (v/v) FBS, 100 IU/ml penicillin, and 100 µg/ml streptomycin (RPMI complete medium, all Invitrogen, Paisley, UK). HeLa cells were subcultured three times weekly in DMEM (Invitrogen, UK) containing 10% (v/v) FBS, 100 IU/ml penicillin, and 100 µg/ml streptomycin (DMEM complete medium). Non-adherent cell types (KG1a, K562 and Jurkat) were removed from the culture flask and centrifuged (Varifuge 3.0RS, Heraeus Instruments, Germany) at 1000 x g for 3 minutes before being resuspended in RPMI complete medium. Cells were seeded into a 125 cm<sup>2</sup> culture flasks (Dow Corning, Fisher, Loughborough, UK) after diluting 1:4 or 1:5 in RPMI complete media to a volume of 20 ml and placed in a 37°C 5% CO<sub>2</sub> incubator (Procell, Jencons-PLS, UK).

Adherent cells (Mcf-7 and HeLa cells) cultured in 125cm<sup>2</sup> culture flasks were washed twice in sterile PBS before being trypsonised (Invitrogen, UK) for 5 minutes in the 37°C incubator. Trypsinised cells were subsequently centrifuged for 3 minutes at 1000 x g and resuspended in 10 ml of their respective complete media. Cells were seeded into a 125 cm<sup>2</sup> culture flask after diluting 1:4 in their respective media to a volume of 20 ml and placed in the 37°C incubator.

When seeding multiwall plates (Corning, Fisher, UK), 50 µl of cell suspension was mixed with 50 µl 0.4% trypan blue (Sigma-Aldrich, Gillingham, UK) and cells were counted in a haemocytometer (Neubauer, Marienfeld, Germany). Cells were diluted to the necessary concentration and seeded into the multiwall plate.

To keep passage numbers low fresh cell lines were defrosted before cell cultures reached 40 passages. Frozen cell stocks were stored in liquid nitrogen in 1ml cryovials (Dow Corning, Fisher, UK) at a density of  $1 \times 10^6$  cells in serum free media containing 36% (v/v) FBS, 4% (v/v) DMSO (Sigma-Aldrich, UK). Cells were thawed at 37°C and immediately resuspended in 10 ml of their respective complete media. Cells were centrifuged at 1000 x g for 3 minutes and resuspended in 5ml of their respective complete media twice before all 5 ml cell suspension was seeded into a 25cm<sup>2</sup> culture flask (Dow Corning, Fisher, UK) and placed into the 37°C incubator. Cells were transferred into a 175cm<sup>2</sup> culture flask using the cell culture method above once they reached 70-80 % confluency by surface area covered with no dilution in cell numbers.

## **2.2 PBS Formulation**

A stock of ten times PBS was made and diluted to the correct concentration using distilled water (produced in house, Option, Elga) and pH balanced at 7.4 when needed or before autoclaving. Ten times PBS consisted of 2 g potassium chloride, 80 g sodium chloride, 17.8 g sodium phosphate dibasic dihydrate and 2.4 g potassium phosphate monobasic (all Sigma-Aldrich, UK).

### **2.3 Laser ablation and Surface Treatment**

Laser machining was used to prepare microwells in glass cover slips (Fisher Scientific, Loughborough, UK) and in polydimethylsiloxane (PDMS, Dow Corning, UK) coated cover slips. To coat glass cover slips in PDMS, PDMS was mixed at a weight ratio of 10 : 1 pre-polymer to curing agent and 35  $\mu\text{l}$  was cast on a 16 mm  $\varnothing$  circular coverslip producing a thickness of 150 – 170  $\mu\text{m}$ . The polymer was degassed in a vacuum oven for 30 minutes before the vacuum was removed and the sample baked at 110 °C for 1 hr and allowed to cool.

Laser machining of microwells was performed in two separate ways. To provide a sacrificial layer, glass cover slips or PDMS coated cover slips were covered in whiteboard ink (Pentel Easyflo, WHSmiths, Cardiff, UK) to provide an easily removable, sacrificial and protective layer upon which laser micro-machining debris would land (known ingredients 42% ethanol and 42% propan-2-ol). For a circular format, microwells of 15  $\mu\text{m}$  or 20  $\mu\text{m}$  diameter were ablated individually in the material using a 157 nm  $\text{F}_2$  excimer laser (metaFAB, Cardiff, UK). Radiation at a wavelength of 157 nm was delivered from a Coherent LPF220i laser source and coupled through an enclosed,  $\text{N}_2$ -perfused, 3 metre long beam line, to a 25x Schwarzschild projection lens. Beam shaping was previously achieved through a pair of 25 element spherical arrays manufactured from  $\text{CaF}_2$ , this was to provide a uniform beam to enable even machining of the substrates during irradiation. Microwells were ablated with exposures of 200 shots per microwell and pulse energy of 24 mJ.

Substrates were held on a precision vacuum chuck supported by X-Y-Z- $\emptyset$ , stage set with a resolution of 50 nm (XY), 500 nm (Z) and 1 arcsecond ( $\emptyset$ ).

For encoded microwells, a mask was made for the microwell design in a 100 $\mu$ m thickness stainless steel sheet using a 795nm Ti : Sapphire femtosecond laser (metaFAB, Cardiff, UK). The microwells were then manufactured in coated glass or PDMS by projection ablation through the mask using a 193nm excimer laser (Micronanics, Didcot, UK).

Substrates were exposed to 200 shots per well at a repetition rate of 17Hz from a Lambda Physik LPX220i source laser, with a fluence of 1J/cm<sup>2</sup>, through a x10 demagnification lens. Sonication of cover slips was achieved by sequential sonication for 20 minutes in each of neat methanol (Fisher Scientific, UK), neat ethanol (Fisher Scientific, UK), 50% (v/v) ethanol/distilled water and distilled water. Wet etching of the glass cover slips was achieved using 7M KOH (Sigma-Aldrich, UK) at 60°C for 1 hour followed by three 30 second washes in distilled water.

#### **2.4 Autofluorescence of laser ablated wells**

Ablated wells were imaged using a Leica SP5 confocal microscope or a Leica wide field epifluorescent microscope. Using confocal microscope, laser excitation was used at 405 nm, 488 nm, 543 nm or 633 nm with fluorescence emission collected between 420 nm – 800 nm, 503 nm – 800 nm, 558 nm – 800 nm and 648 nm – 800 nm respectively. Gain levels were kept at the same level throughout with images obtained every 300 nm in the z-axis. Maximum

projections and fluorescent intensity readings were analysed using the Leica TCS software.

### **2.5 Fluorescence imaging of cells in glass and PDMS microwells**

KG1a were washed three times in PBS and incubated for 1 hour at 37°C with 15 ng/ml Transferrin-Alexa488 (Invitrogen, Paisley, UK) in serum free RPMI medium (Invitrogen, UK). Cells at a density of 150,000 cells/ml were washed and plated onto either glass or PDMS 15µm microwell array in imaging medium (phenol red-free RPMI, 10mM Na-HEPES pH7.4 from Sigma, UK) and imaged at 37°C on the confocal microscope.

### **2.6 SEM Imaging of cells**

KG1a cells were plated onto a 15µm microwell glass cover slip array at a density of 200,000 cells/ml and allowed to settle for 10 minutes. Cells were fixed by incubating with 2% (v/v) glutaraldehyde (Sigma, UK) in PBS for 30 minutes at room temperature. Samples were washed three times in PBS before being post fixed in 1% osmium tetroxide (Sigma, UK) for a further 30 minutes at room temperature. Dehydration of the sample was achieved by 10 minute incubations in 50%, 70%, 80%, 90% (all v/v), and three neat ethanol washes. Cells were dried using a critical point drier (Samdri 780, Tousimis, Rockville, US) and sputter coated (SC7620, Quorum Technologies Ltd, East Grinstead, UK) before being imaged.

### **2.7 Correlative light-SEM**

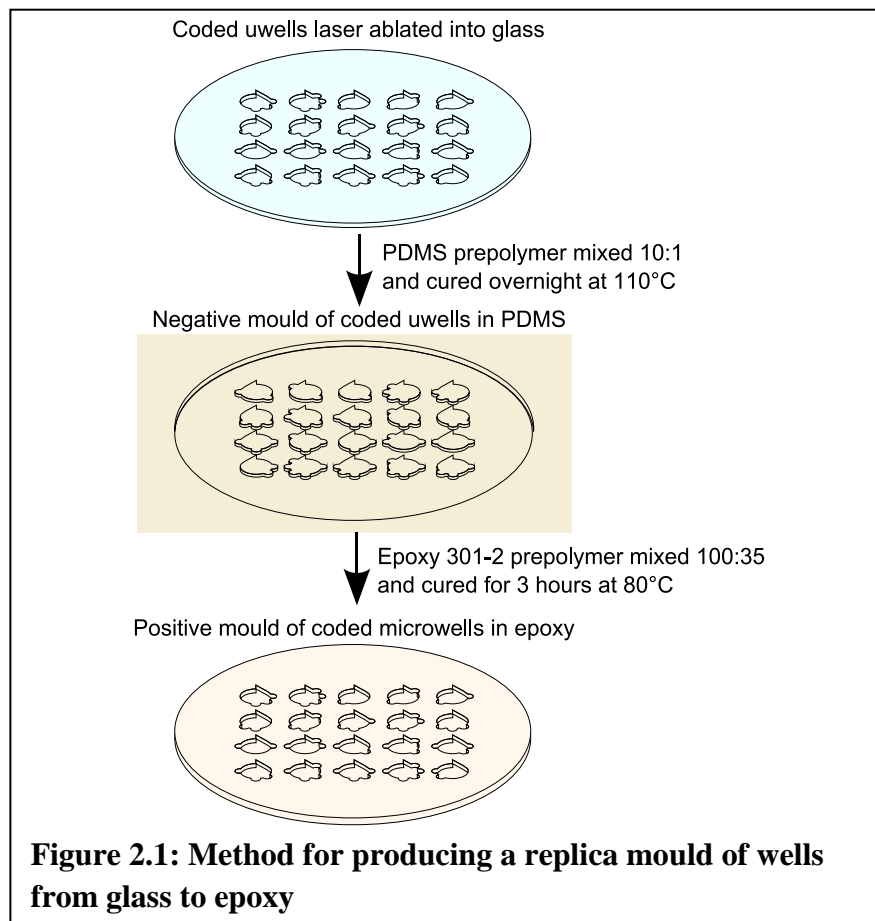
KG1a cells were washed three times in complete media before being plated at 150,000 cells/ml onto glass cover slips containing a 15µm diameter microwell array. Cells were imaged on the confocal microscope at 37°C in 400µl imaging medium before being fixed by adding 400µl of 4% (v/v) glutaraldehyde. Cells were prepared for SEM as above ('SEM Imaging of Cells').

### **2.8 Sectioning of PDMS**

PDMS was made using different ratios of short-chained divinyl-PDMS (Sigma, UK) with long-chained PDMS pre-polymer. These mixes were added with a curing agent at a ratio of 1:1 with the divinyl-PDMS and 1 : 10 with the PDMS pre-polymer. Platinic acid (Sigma, UK) was added to the mix at 1 ul of 20 mg/ml (in tetrahydrofuran, Fisher, UK) for every 100 mg short chained divinyl-PDMS. The different mixes were degassed in a vacuum oven for 30 minutes, then baked at 110 °C for 1 hour and allowed to cool. Pieces of PDMS were attached onto a mounting block, using cyanoacrylate glue (Maplins, Cardiff, UK), for use with a steel knife microtome (5030 Microtome, Bright Instruments Compang Ltd, Huntingdon, England) and attempts were made to section the material at different thicknesses.

## 2.9 Moulding of arrays

To form encoded microwells in epoxy resin cover slips, a positive mould of the encoded microwell array in glass (see ‘Laser Ablation’), was made from PDMS using the following procedure. Cover slips were placed under vacuum in a glass flask and the PDMS polymer mix (10 : 1 pre-polymer to curing agent) was added using a syringe. The vacuum was removed to allow the PDMS to fully penetrate the microwells before being degassed and baked (as previously described). Subsequently the cover slips were removed from the PDMS leaving a positive mould of the microwells. Epoxy resin cover slips were made by first mixing the pre-polymers of epoxy 301-2 (John P Kummer



Ltd, Marlborough, UK) at a ratio of 100 : 35 (part A to part B, part A being diglycidyl ether of Bisphenol A and part B being polyoxypropylenediamine). The polymer was degassed and poured onto the PDMS mould allowing 35  $\mu$ l of resin for each cover slip (this allows for a thickness approximately 160  $\mu$ m, similar to a No.1 glass cover slip). The resin was degassed in a vacuum for 30 minutes before being baked at 60 °C and allowed to cool (Fig. 2.1). Surfaces were sterilised by immersing the cover slips in ethanol for ten minutes followed by three five minute washes in sterile PBS.

### **2.10 Sectioning epoxy**

A range of different hardness epoxies were derived from different Part A : Part B ratios (from 100 : 10 to 100 : 70 part A : part B) degassed in a vacuum oven and hardened as above. Samples were sectioned on an ultramicrotome (Reichert Ultracut 'E') using a glass knife at two thicknesses of 1 $\mu$ m and 100nm. Araldite 506 (Sigma, UK) at component ratios of 5.5 parts resin to 4.35 parts hardener to 0.15 parts accelerator were mixed thoroughly before being degassed and used to backfill microwells made from Epoxy 301-2. Backfilled epoxy microwells were hardened overnight at 60°C before being sectioned using a glass knife at 100 nm and 1  $\mu$ m thicknesses on an ultramicrotome.

### **2.11 Live cell imaging in encoded microwell arrays**

Mcf-7 (breast cancer) cells were seeded onto glass cover slip containing as encoded microwell array at a density of 200,000 cells/ml in twelve well plates

(Fisher, UK) and allowed to adhere overnight. Samples were washed three times in RPMI before being incubated with 15 ng/ml transferrin-Alexa488 for one hour at 37°C 5% CO<sub>2</sub>. Samples were further washed three times in imaging media before being imaged at 37°C on the confocal microscope. Samples were subsequently fixed using 400µl of 4% (v/v) glutaraldehyde added to the 400 µl imaging medium for 30 minutes. Cells were washed three times in PBS, permeabilised in 0.1% (w/v) Triton X-100 (Sigma, UK) for 5 minutes and washed just one further time in PBS. Cells were subsequently labelled using 0.5 µg/ml Hoescht33342 (Invitrogen, UK) for 10 minutes before being washed and imaged on the confocal microscope. Z-stacks and subsequent image alignment were processed using ImageJ.

### **2.12 Silanisation of glass surfaces**

Glass surfaces were sonicated for ten minutes in 10 ml neat ethanol and 10 ml *N,N*-dimethylformamide (Sigma, UK), both for ten minutes, to remove any residue before being activated. Glass surfaces were activated by oxidation using Piranha solution at a volume ratio of 7 : 3 neat hydrosulphuric acid : 30% hydrogen peroxide solution (both from Fisher, UK) at 70°C for 20 minutes. Surfaces were washed in distilled water and dried under nitrogen immediately before silane evaporation. A 1 : 1 w/w ratio of silane (APTES from Sigma, UK or DMDES from Fluorochem, Hadfield, UK) to paraffin oil (Sigma, UK) were mixed thoroughly. Activated glass cover slips were placed surrounding an eppendorf cap in a glass petri dish. The silane-paraffin mix was used to fill the cap and the reaction was covered for ten minutes. After the reaction the

samples were washed three times in distilled water and placed in a 60°C incubator overnight. Following this the samples were sonicated three times in distilled water, dried under nitrogen and stored in neat methanol.

### **2.13 Contact angle measurements**

Samples were placed onto a flat horizontal surface and 2 µl of distilled water was gently lowered vertically onto the surface from a clamped pipette. Digital photographic images were obtained of the side profile of the drop and the centre of the image was aligned parallel to the sample surface. Images were subsequently analysed using Drop\_Analysis plugin for ImageJ.

### **2.14 Cell Surface Imaging**

HeLa cells were seeded onto surfaces at a density of 200,000 cells/ml and allowed to adhere overnight. Cells were fixed in 3% (w/v) paraformaldehyde (Sigma, UK) in PBS for 10 minutes before washing three times in PBS, permeabilised using 0.1% (w/v) triton X-100 (Sigma, UK) for ten minutes and washed once in PBS. Cells were labelled using 1 µg/ml rhodamine-phalloidin (Sigma, UK) and 0.5 µg/ml Hoescht33342 in PBS for ten minutes before being washed three times in PBS and mounted onto a microscope slide (Fisher, UK). Imaging of the cells was performed using either the confocal microscope or the wide field microscope.

### **2.15 Succinic anhydride and succinimidyl ester modification of surfaces**

After silanisation, surfaces were incubated with either 5 mg/ml succinic anhydride (Sigma, UK) or 0.5mg/ml Oregon Green succinimidyl ester (Invitrogen, UK) in tetrahydrofuran (THF) and 5% (v/v) triethylamine (Sigma, UK) for 4 hours. Surfaces were washed twice in distilled water and dried under nitrogen. Oregon Green fluorescence images were taken on a widefield inverted microscope using four second exposure times with gain kept at 0, no binning was used.

### **2.16 Hydrosilylation Reaction on PDMS**

PDMS was cured (as above) using four different ratios of pre-polymer to curing agent, 2 : 1, 4 : 1, 10 : 1 and 20 : 1. Two millilitres of neat THF and 200µl neat PEG (meth)acrylate (PEGMA from Sigma, UK) or 200µl divinyl-PEG (dV-PEG from Sigma, UK) and a final concentration of 50 µg/ml Speier's catalyst (Fluorochem, UK) in THF were mixed and added to the different PDMS samples in glass vials. The samples were allowed to react for thirty minutes at 80°C.

PDMS (at a ratio of 10 : 1, pre-polymer to curing agent) was part cured for thirty minutes before being allowed to swell in 20% (v/v) polymethylhydrosilane (PMHS from Sigma, UK), 50 µg/ml Speier's catalyst in THF for one hour. The part-cured PDMS was then removed from the solution and allowed to dry for two hours before being cured overnight at 80°C. Reactions with dV-PEG and PEGMA proceeded as above.

### **2.17 Activation of PDMS by UV/Ozone treatment**

PDMS was cured at the recommended 10 : 1 ratio of pre-polymer to curing agent. UV/Ozone treatment was performed for 10, 20, 30, 60 or 90 minutes after which the samples were placed immediately in distilled water. Samples were dried under nitrogen and contact angles measured (as above).

### **2.18 Silanisation of PDMS**

Activated PDMS samples were incubated for two hours in 1 or 5 mM APTES or 5 mM TEOS (Sigma, UK) or DMDES at 60°C. After the reaction the samples were washed three times in distilled water and placed in a 60°C incubator overnight. Following this, the samples were sonicated three times in distilled water, dried under nitrogen and stored in neat methanol.

During albumin modification, samples were incubated with 4% (v/v) glutaraldehyde and 0.5 mg/ml albumin (Invitrogen, UK) or 0.5 mg/ml albumin-Alexa 488 (Invitrogen, UK). Samples were washed three times in water before imaging or sterilized by washing in 70% (v/v) ethanol for ten minutes followed by washing three times in sterile PBS before cells were plated.

### **2.19 Thin layer coating**

Glass or PDMS coated cover slips were coated in gold by sputter deposition before being sterilized by washing in 70% (v/v) ethanol for ten minutes and washing three times in sterile PBS. Cells were plated, labelled and imaged as above (Cell Surface Imaging).

### **2.20 Sol-Gel**

Sol-gels were formed by mixing TEOS, ethanol, hydrochloric acid (Sigma, UK), ammonium hydroxide (Sigma, UK) and distilled water at different ratios (see table in figure 4.17 in chapter 4) or with the addition of DMDES (see table in figure 4.18 in chapter 4) and allowed to gel overnight, for 24 hours or for 48 hours at 60°C. Gels were allowed to dry at room temperature under a fume hood for 24 hours.

### **2.21 Swelling of PDMS**

PDMS was cured to a thickness of 3mm at the recommended ratio under previously described conditions, and cut into 20 x 20 mm squares. Each PDMS squares were weighed and subsequently immersed in TEOS, hexane (Fisher, UK), cyclohexane (Fisher, UK), isopropyl alcohol (Fisher, UK), ethanol or distilled water with the squares being removed, the surface liquid removed by blotting and weighed at time intervals of 10, 20, 30, 45 and 60 minutes. The percentage increase of each square was calculated and plotted using excel.

### **2.22 Sol-gel interpenetrating network in PDMS**

PDMS squares were soaked in excess TEOS overnight before being removed, the surface dried by blotting and reacted in 2.5mM ammonium hydroxide, 2.5mM hydrochloric acid and 25 % (v/v) ethanol at 60°C for 0, 2, 4, or 6 hours.

Unreacted TEOS was removed by soaking in ethanol overnight before the gel was left to dry for 24 hours and the contact angle measured.

### **2.23 Sol-Gel Particles in PDMS**

Sol-gel particles were made by mixing 2.5mM ammonium hydroxide, 2.5mM hydrochloric acid and 25% (v/v) ethanol, with the addition of 10mg fluorescein sodium salt (Sigma, UK) for fluorescent particles, to a volume of 10 ml and heated to 60°C in a water bath. A further 5 ml of TEOS was dripped slowly into the mixture from a burette over the course of two hours. The reaction was allowed to continue for a further 1 hour before the solution was removed. The beads were isolated by centrifugation at 1500 x g for 5 minutes and three subsequent washes in neat ethanol were performed by re-suspending the beads in neat ethanol and further centrifugation.

The beads were encased in PDMS by mixing 0.1 % (w/w) beads in pre-mixed PDMS and cured as previously described. For cell imaging, surfaces were sterilised by washing for 10 minutes in 70 % (v/v) ethanol and washing three times using sterile PBS, before cells are seeded, fixed and imaged as previously described.

### **2.24 r8 – Alexa488 and r8-PAD – Alexa488 Uptake in HeLa**

HeLa cells were plated onto 35 mm glass bottomed dishes at a density of 250,000 cells/ml and allowed to adhere overnight on glass bottomed dishes. Cells were washed three times in SFM with imaging medium containing 10% (v/v) FBS replacing the final medium. Immediately before imaging r8-

Alexa488 or r8-PAD-Alexa488 was added at a concentration of 10 $\mu$ M. Samples were imaged on the confocal microscope at 37°C with images taken every 30 seconds.

### **2.25 EGF and Peptide treatment on HeLa cells fixed cell imaging**

HeLa cells were seeded onto cover slips in six well plates at a density of 250,000 cells and allowed to adhere overnight in a 37°C 5% CO<sub>2</sub> incubator. Cells were incubated with 20  $\mu$ M r8, (GS)<sub>4</sub> or 1 $\mu$ M EGF for 2, 5 or 10 minutes in complete medium at 37°C. Cells were fixed and labelled with rhodamine-phalloidin and Hoechst 33342 as previously described.

### **2.26 Live cell imaging of transfected cells**

HeLa cells were seeded at a density of 150,000 cells/ml onto 35mm glass bottom dishes and left to adhere overnight in the 37°C incubator. OptiMEM (105 $\mu$ l; Invitrogen, UK) was mixed gently with 3.3  $\mu$ l of Fugene 6 (Roche, Burgess Hill, UK), to this was added 2.2  $\mu$ g of plasmid DNA and mixed gently by pipetting. Cells were washed and the media replaced with complete medium. Fugene/DNA solution (100 $\mu$ l) was added drop wise onto the cells and returned to the 37°C incubator overnight. Cells were washed once with imaging medium containing serum and imaged at 37°C on the confocal microscope using the resonant scanner.

### **2.27 SEM of peptide treated cells**

HeLa cells were seeded onto cover slips in six well plates at a density of 250,000 cells/ml and allowed to adhere overnight. Cells were incubated with 20  $\mu$ M r8, GS<sub>4</sub> or 1 $\mu$ M EGF for 10 minutes in complete medium at 37°C. Cells were fixed and prepared for SEM as previously described.

### **2.28 Nucleus volume measurements**

HeLa cells were seeded onto glass cover slips in six well dishes at a density of 250,000 cells/ml in complete medium and allowed to adhere overnight at 37°C. Samples were incubated with 20 $\mu$ M r8 or 1, 2, 5, 10 or 20 $\mu$ M r8-PAD for 10 minutes before being fixed and labelled as previously described. Confocal z-stack images were obtained of the nuclei with 1 $\mu$ m between each z-layer. Nucleus volume was calculated by using the ‘Analyze Particles’ method in ImageJ. This was achieved by opening up the image stacks and converting them to greyscale by splitting the colour channels (Image>Color>Split Channels). Threshold intensity for the nucleus was selected using the Huang method in ImageJ (Abramoff *et al.*, 2004) and applied to the stack (Image>Adjust>Threshold). Nucleus area for each slice was automatically calculated using the ‘Analyze Particles’ method with size and circularity set as default and ‘include holes’ (includes any non-fluorescent regions if it is surrounded by fluorescence) and ‘exclude on edges’ (doesn’t count if the fluorescent region touches the edge of the screen) selected. An algorithm was produced in excel to determine the total nucleus volume for each cell and the

mean volume was determined using individual nucleus volumes from three individual cover slips.

### **2.29 Live cell imaging of peptide treated cells**

Mcf-7 cells were plated onto 35 mm glass bottomed dishes at a density of 250,000 cells and allowed to adhere overnight on glass bottomed dishes. Cells were washed three times in imaging medium containing 10% (v/v) FBS replacing the final medium. Immediately before imaging on confocal peptides 20  $\mu$ M fsr- r8 or asr-r8 were added. Samples were imaged on the confocal microscope at 37°C with images taken every 30 seconds.

KG1a were washed three times in imaging medium containing 10% (v/v) FBS and allowed to settle in 15  $\mu$ m microwells before imaging. Immediately before imaging on confocal peptides 10  $\mu$ M fsr- r8 or asr-r8 were added. Samples were imaged on the confocal microscope at 37°C with images taken every 30 seconds.

### **2.30 Pak-1 siRNA treated cells**

100,000 cells HeLa cells were seeded onto 35 mm glass bottom dishes and left to adhere overnight in the 37°C incubator. One hundred and five microlitres of OptiMEM (Invitrogen, UK) was mixed gently with 3.3  $\mu$ l of Fugene 6 (Roche, Burgess Hill, UK), to this was added 2.2  $\mu$ g of Pak-1 siRNA and mixed gently by pipetting. Cells were washed and the media replaced with complete medium. One hundred microlitres of Fugene/DNA solution was added drop wise onto the cells and returned to the 37°C incubator for 48 hours. Cells were

washed once with imaging medium containing serum and imaged at 37°C on the confocal microscope.

### **2.31 Cytochalasin D and Blebbistatin inhibition in HeLa cells**

HeLa cells were seeded onto cover slips and allowed to adhere overnight as previously described. Cells were washed three times in serum free medium before being incubated with either 10 µM Cytochalasin D or 100 µM blebbistatin (both Sigma-Aldrich, UK) for 30 minutes. Cells were subsequently washed three times in imaging medium plus 10 % (v/v) FBS, 20µM r8-PAD was added to the cells and the cells imaged immediately at 37°C on the confocal microscope.

### **2.32 References**

ABRAMOFF, M. D., MAGELHAES, P. J. & RAM, S. J. (2004) Image processing with ImageJ. *Biophotonics Int*, 11, 36-42.

### **3. Design and Manufacture of Encoded Microwell Arrays**

Microwells have been extensively used to retain cells, thus enabling individual cell analysis, whether that is for imaging or to test the effects of probes on cells. This retention of cells allows individual cells to be analysed in greater detail, obtaining more information from typically heterogeneous populations. This analysis at a single cell level can give a researcher more information about how individual cells may react within a population.

Microscopes are extensively used throughout cell biology (Galbraith and Galbraith, 2011) and different microscopes allow for the analysis of different aspects, from studying uptake of probes in fluorescence microscopy to the detailed cell structure in electron microscopy. The use of different microscopes to analyse the same single cell or same population of cells is one of the key aims in correlative microscopy.

This chapter will look at the use of microwells for correlative microscopy of both adherent and non-adherent cells.

#### **3.1 Introduction**

An implicit pre-requisite for correlative microscopy is the retention and identification of a cell's position during imaging. Optical tweezers (Luo *et al.*, 2007), both positive and negative dielectrophoresis (Mittal *et al.*, 2007) and

microfluidic traps (Nalayanda *et al.*, 2007) have all been used to retain cells, but using microwells is, by far, the most common technique, probably due to the ease with which microwells can be manufactured and used (El-Ali *et al.*, 2006). Microwells have been developed in various shapes and sizes but the most common shapes are either round or square-sectioned wells, typically provided in an array. These microwells have been used for a wide variety of purposes, for example, testing a B-cell array against an antigen (Tokimitsu *et al.*, 2007), or looking at how the shape of microwells can be used to control stem cell growth (Ochsner *et al.*, 2007).

Commercially available microwells are commonly made from a few materials, such as glass or polystyrene (Haigh *et al.*, 2006). Whilst these materials are suitable for machining, moulding or casting, they cannot be sectioned into thin slices (typically 1 $\mu$ m-100 $\mu$ m for TEM). Therefore, an alternative material is needed that would not only satisfy the essential requirements of biocompatibility and light transmission, but also can be serially sectioned using conventional microtome equipment.

At the moment there are few methods which enable correlative microscopy and none that provide access to its routine application. One approach is to grow adherent cells on a surface marked with a grid, perform live cell imaging and then use high-pressure freezing before preparing them for electron microscopy (Verkade, 2008). Using this technique, researchers have been able to obtain good correlative images of the dynamics of endocytic pathway including fusion (Brown *et al.*, 2009), albeit with specialist equipment.

### 3.1.2 Aim

The work in this chapter will describe the development of a microwell array for cellular imaging. Different materials will be looked at for their suitability towards cell imaging and sectioning. Whilst different encoded microwell array designs will be investigated that allow for the tracking of a single microwell through the different processes required for correlative microscopy.

## 3.2 Results

### 3.2.1 Laser Ablation and Optimisation of Microwell Quality in Glass Surfaces

Laser ablation is a simple method of creating repeated structures, such as microwells, in a suitable surface (Selimovic *et al.*, 2011). By using different wavelengths of light, different materials can be ablated depending on their transmissibility/absorption at this wavelength. Using a deep UV laser, such as 157nm laser, allows almost all materials to be ablated (Greuters and Rizvi, 2003).

Using a femtosecond laser allows for fast ablation with little thermal damage to the resultant fabricated structure in glass (Eaton *et al.*, 2008). Exposure of a material to the laser shot is short, in comparison to the time between shots, thus allowing the material to cool down and minimise thermal damage. However, when ablation was performed on borosilicate glass cover slips debris from the laser was ejected during each shot onto the surrounding surface (see figure 3.1). Attempts were made to remove this debris from the surface using three

different methods. Simple sonication in neat ethanol followed by distilled water managed to remove the majority of the debris. Whilst the second method used a sacrificial layer placed on the surface before ablation. The third method involved wet etching whereby glass microwell arrays were submerged in 7 M potassium hydroxide at 60°C for 1 hour before being washed was also used to remove some of this debris.

It has been shown previously that using a layer of whiteboard ink on the surface before ablation allowed the debris to be caught and subsequently removed (Shin *et al.*, 2006). Originally this was done using the simple method

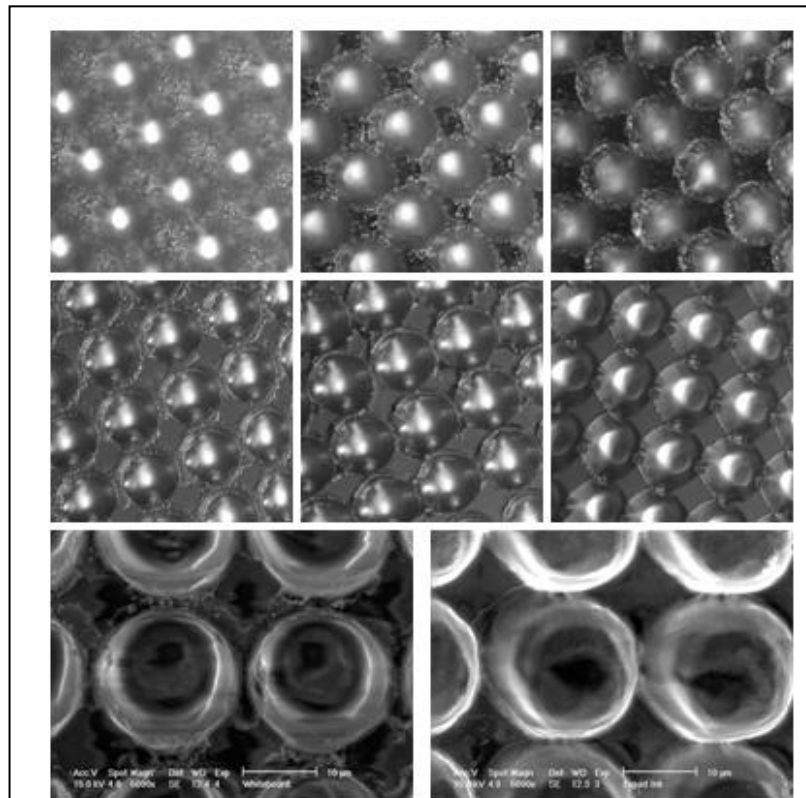


**Figure 3.1: Microwell debris removal after different treatments.**

Microwells were ablated into glass cover slips after no treatment (a & d), dry marker (b & e) or liquid ink marker (c and f). Surfaces were then cleaned either using tape (a-c) or by sonication in ethanol (d-f). SEM images of dry marker (g) and liquid ink marker (h) after sonication. Microwells 20µm in diameter.

of placing tape over the ablated area and removing the sacrificial layer and the debris. Whiteboard ink consists of the dye (carbon black) along with a release agent, allowing the ink to be removed after it has been applied (Shin *et al.*, 2006). When debris from ablation falls onto the surface, it falls onto the carbon black instead of the exposed surface (in this case glass) where it could easily bond. Of the two different types of white board ink used, one was more successful than the other. Using ‘liquid ink’ whiteboard marker as the sacrificial layer showed an improved surface quality over using dry marker (figure 3.1g and 3.1h), with the liquid ink marker sacrificial layer having visibly less debris than the dry marker sacrificial layer. This could be due to the amount of ink laid down as liquid ink markers leave a visibly darker layer when drawn onto the surface of the glass cover slip. It was also found that sonicating the surfaces in ethanol after ablation allowed for a better removal of the ink than using tape as was originally described. This is most likely due to the amount of debris/ink that can be removed as all of the ink was removed during sonication. However, when using tape, some of this ink remained, leaving the need for the surface to be cleaned further. Additionally, using tape would leave residue on the surface which could affect later experiments and would have to be removed before an experiment was performed.

### 3.2.2 Autofluorescence in Glass Microwells

The debris from laser ablation has shown to be strongly fluorescent after

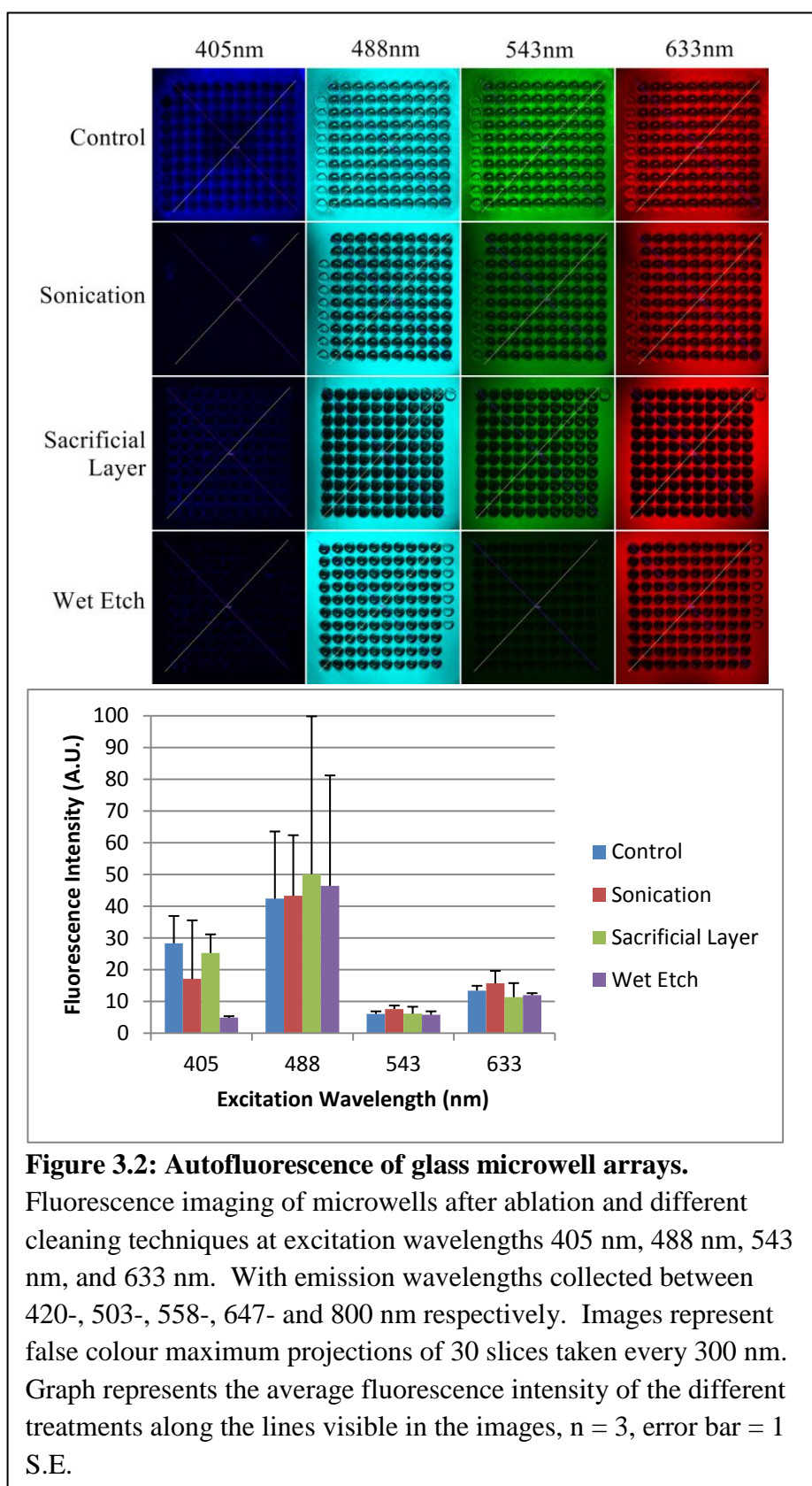


**Figure 3.2: Autofluorescence of glass microwell arrays.**

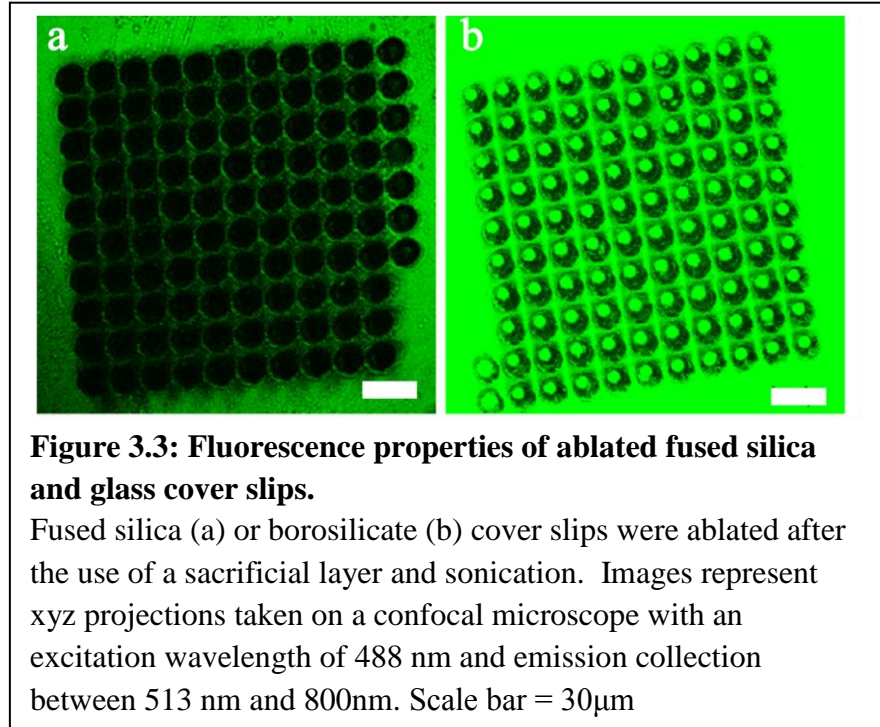
Fluorescence imaging of microwells after ablation and different cleaning techniques at excitation wavelengths 405 nm, 488 nm, 543 nm, and 633 nm. With emission wavelengths collected between 420-, 503-, 558-, 647- and 800 nm respectively. Images represent false colour maximum projections of 30 slices taken every 300 nm. Graph represents the average fluorescence intensity of the different treatments along the lines visible in the images,  $n = 3$ , error bar = 1 S.E.

excitation at 488nm, a wavelength frequently used in fluorescence microscopy corresponding with the commonly used fluorescent probe GFP (green fluorescent protein (Tsien, 1998)), whilst there was also fluorescence at other wavelengths (figure 3.2). The different methods used to remove the debris were imaged on a laser scanning confocal microscope (LSCM) and the autofluorescence of the surface was analysed using Leicas LAS AF software. None of the methods produced a statistically significant difference to the surface autofluorescence.

The reasons behind the differences of autofluorescence are difficult to determine. This effect is mainly seen on the LSCM, whilst there is less autofluorescence seen on epifluorescent systems suggesting that it has something to do with the system. Alternative materials, such as fused silica and quartz, would need to be investigated to try and determine the cause of this effect.

### 3.2.3 Autofluorescence in polydimethylsiloxane (PDMS) and Fused Silica

Borosilicate glass is used for cover slips and contains up to 13% borate (QVF, 2000) as well as other impurities, whilst fused silica is made up almost exclusively of silicate and having almost no impurities (UQGOptics, 1999). Laser ablation of fused silica proved successful, whilst auto-fluorescence of the material was visibly reduced (figure 3.3) but not completely irradiated at the worst affected excitation wavelength 488 nm. It is likely that the autofluorescence effect is an effect between the microscope and the glass.



PDMS was investigated as an alternate material for imaging with reduced autofluorescence. When compared with glass, PDMS showed a much lower level of surface autofluorescence (figure 3.4) when used for imaging KG1a cells after uptake of the fluorescent probe transferrin-Alexa488. The autofluorescence visible in PDMS was most likely due to impurities introduced during the curing process and can be reduced after curing in a more sterile environment. Using PDMS over glass allowed clearer imaging of non-adherent cells, this is important because endosomal labelling has become confused with background fluorescence when using the glass wells.

The difference between glass and PDMS indicates a likely surface effect of the glass when interacting with the laser rather than laser light directly being reflected back from the surface.

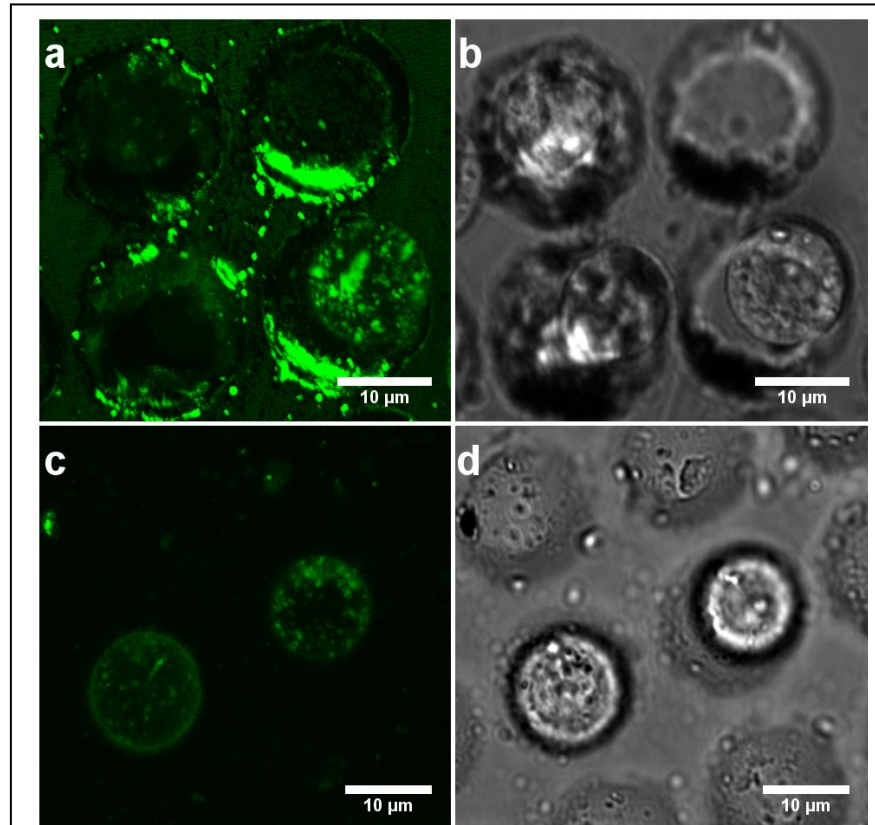


**Figure 3.4: Live KG1a cells imaged in glass and PDMS microwells.**

KG1a cells were incubated for 15 minutes with transferrin-Alexa488 before being imaged in either glass (a and b) or PDMS (c and d) microwell arrays. Fluorescence images (a and c) represent xyz projections taken on a confocal microscope.

#### 3.2.4 Development of a Cover Slip Manifold for Live Cell Imaging

Microwells were ablated directly onto glass cover slips and a manifold was required to hold a cover slip in place during live cell imaging. This manifold had to be non-toxic, suitable for sterilisation in an autoclave or in 70% ethanol, hold imaging media for live cell imaging and be compatible with an inverted microscope. The design developed involved two metal plates which clamp

together using six screws (figures 3.5, 3.6 and 3.7). The base plate had two features, the first was a sloping base underneath which tapers to meet flush with the cover slip. This is designed to not damage the microscope lens by not exposing the glass lens to any sharp edges. The second feature was a recessed lip in which the coverslip and o-ring was placed. This formed a seal between the top plate and the bottom plate sandwiching the cover slip and the o-ring in between.

The exposed surface for imaging was an 8 mm diameter circle, which was a small surface but allows enough space to image a microwell array which was typically 2-3mm across. The material chosen was stainless steel, as this was a robust material suitable for autoclaving and resistant to many chemicals used during live cell microscopy.

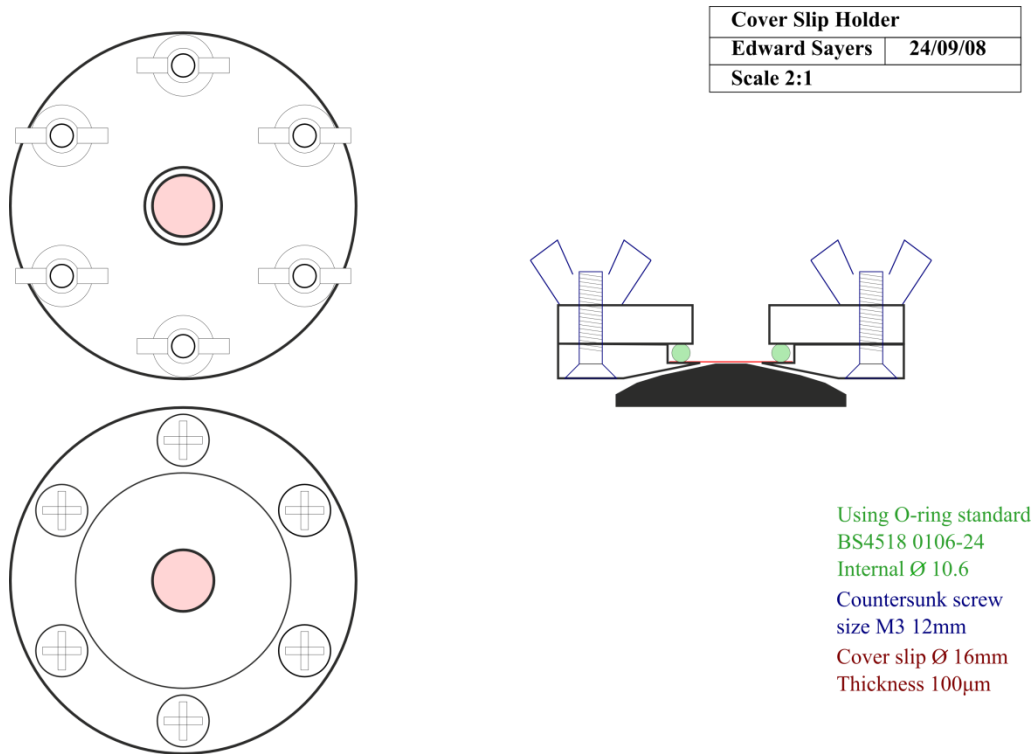


Figure 3.5: Manifold design.

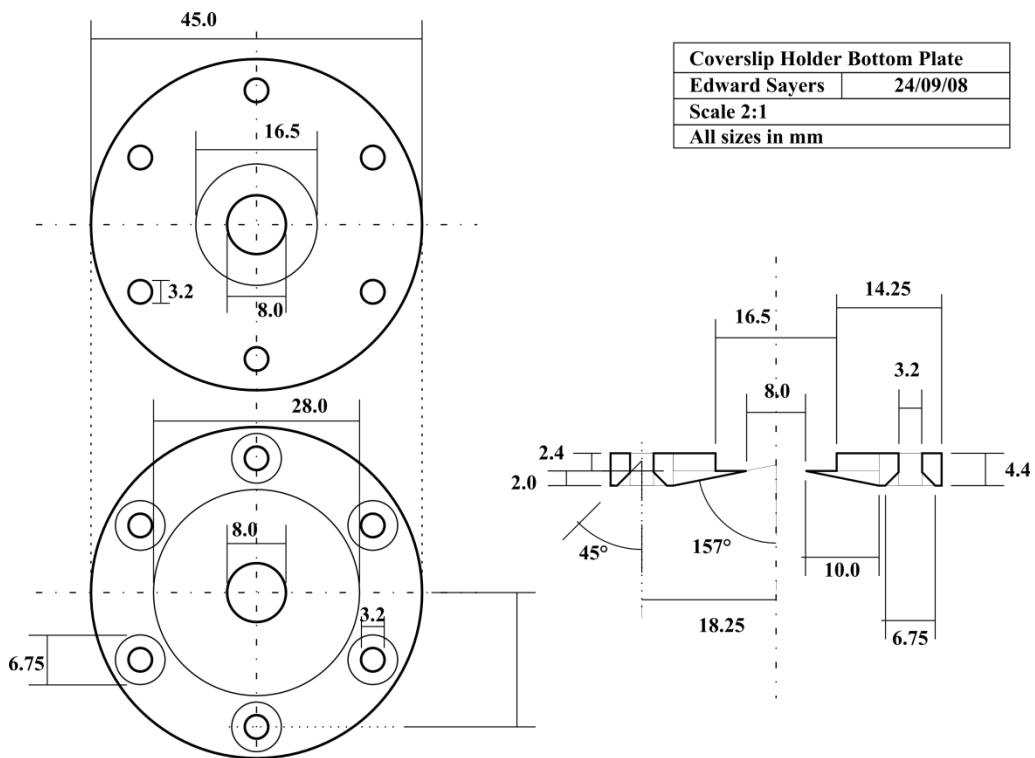
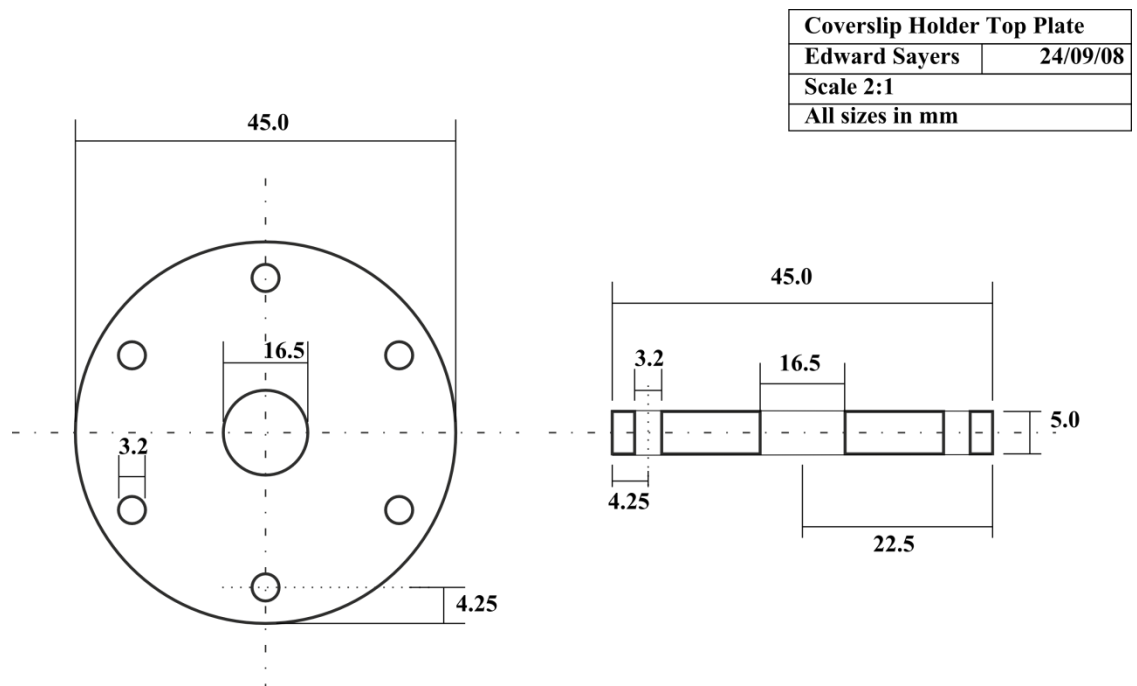


Figure 3.6: Bottom plate of manifold.



**Figure 3.7: Top plate of manifold.**

### 3.2.5 SEM Imaging of Non-Adherent Cells in Microwells

The microwell arrays have been successfully used for live cell imaging (see Chapter 5 – Cell penetrating peptides and ‘Co-operative membrane disruption between cell penetrating peptide and cargo – implications for the therapeutic use of the Bcl-2 converter peptide D-NuBCP-9-r8’ in Appendix) but they can also be used for back-scattered SEM imaging. KG1a (acute myelogenous leukaemia) cells were fixed and imaged resting within microwells (figure 3.8). Cells imaged in the microwells showed similar morphology to KG1a imaged on normal glass indicating that the wells had little morphological effect on cells

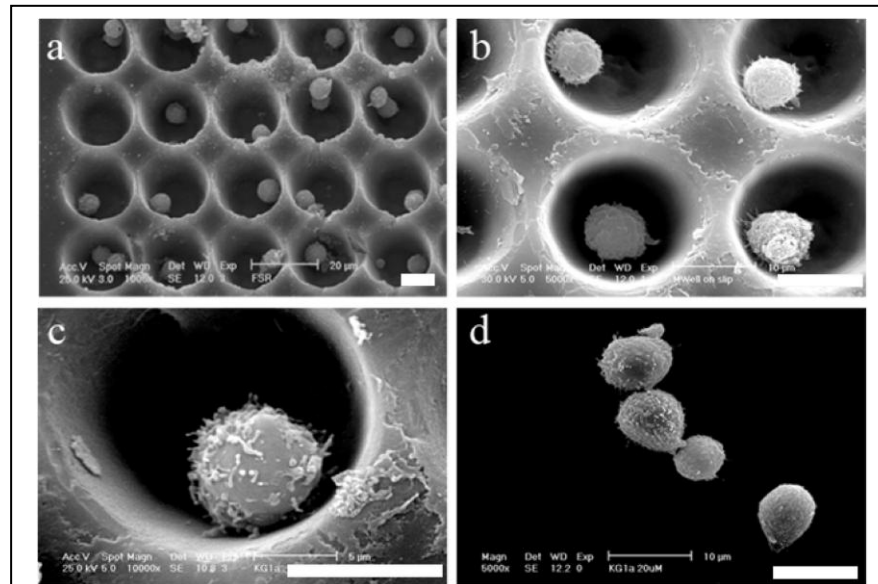


**Figure 3.8: SEM of KG1a cells in microwells.**  
 KG1a cells were fixed either in microwells (a-c) or on glass (d) and prepared for SEM. Scale bars = 10μm

at these microwell sizes. The use of chemical fixatives had caused the cells to shrink during fixation.

### 3.2.6 Correlative Live-SEM Imaging of Non-Adherent Cells in Microwells

Cell imaging using live and scanning electron microscopy were both possible using the microwells to retain non-adherent cells. It was also possible to obtain

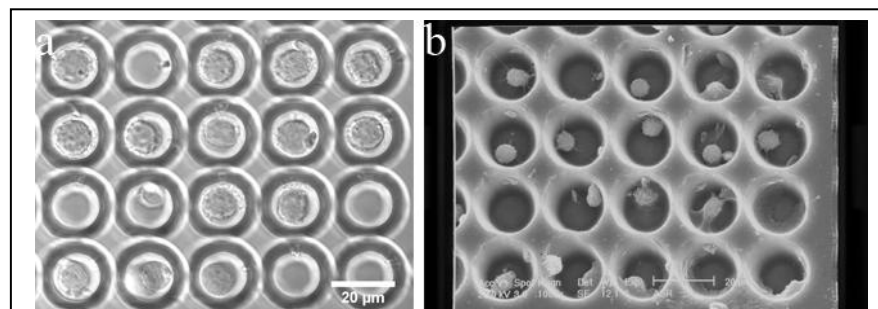


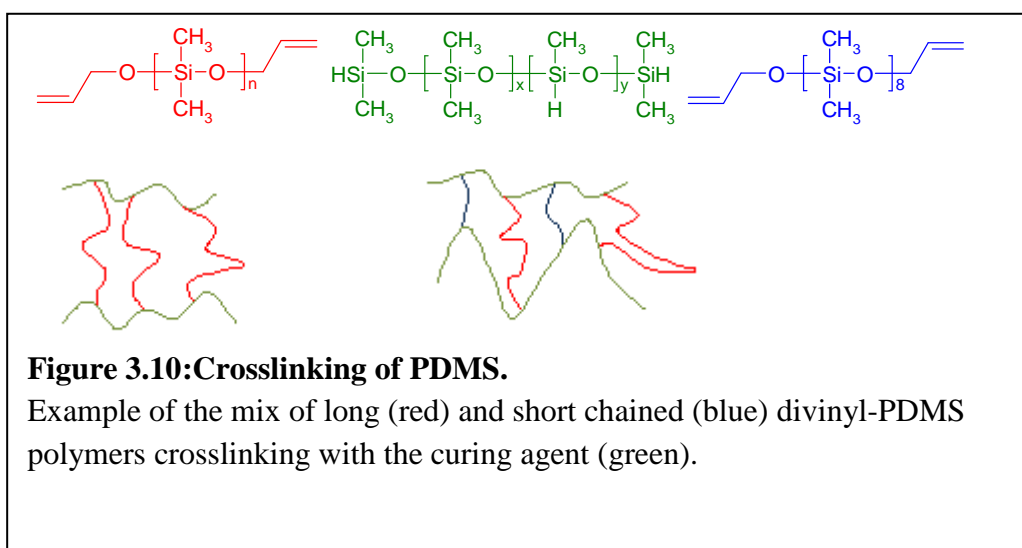
**Figure 3.9: Correlative microscopy of KG1a cells in microwells.**  
 Live KG1a cells were imaged (a) before being fixed and prepared for SEM (b). Scale bar = 20μm

correlative images of live and scanning electron micrographs of KG1a cells resting in the microwells (figure 3.9). Cell positioning between live cell

imaging and SEM imaging were identical indicating a high chance that there was correlative microscopy between both these images. The chemical fixation method employed caused the cells to shrink within the microwell array and with cryofixation not available, a better fixation method would need to be employed. The matching of both light and SEM images provided proof-of-concept demonstration that correlative light-electron microscopy of non-adherent cells was possible.

### 3.2.7 Sectioning PDMS

To obtain correlative light-TEM images, cells needed to be imbedded and sectioned. Sectioning through the well immediately negated the use of hard materials such as glass since this cannot be sectioned using any commonly available laboratory equipment. A different material was therefore required, and needed to be optically clear from 405 nm – 800 nm, non-toxic towards cells and sectionable using common equipment.



PDMS Sylgard 182 (Dow Corning), consists of a pre-polymer with a viscosity of 5000 cSt (precise molecular weight unknown, but PDMS with a similar viscosity provided by a different supplier is known to be 50 kDa) and a curing agent (510 cSt, molecular weight unknown due to unknown ratio of methylhydrosilyl groups to dimethylsilyl groups) which, when cured, formed long chain length crosslinks between the vinyl moiety of the pre-polymer and the hydrosilyl moiety of the curing agent (figure 3.10).

To increase crosslinking within PDMS, short-chained divinyl-PDMS polymers (4-7 cSt, molecular weight 700-850 Da) were mixed in with the pre-polymer and curing agent. By altering the ratios between the divinyl-PDMS, the pre-polymer and the curing agent the properties of the PDMS were altered to produce a harder polymer (table 3.11) more suitable to sectioning. These polymers were produced and tested on a steel knifed microtome to test their ability to be sectioned. Whilst the PDMS polymers differed in rigidity with increased crosslinking, brittleness also increased. Sectioning the different PDMS polymers proved too difficult due to either the polymer being too soft and deforming around the blade, or, being too brittle and breaking too easily when exposed to the blade.

dvPDMS	PDMS	Curing Agent	Description
1	1	1.1	Very brittle, quick to break forms, long fractures
1	2	1.2	Brittle, breaks easily, moderate fractures
1	3	1.3	Flexible, still brittle, moderate fractures
1	4	1.4	Flexible, still brittle, very short fractures
1	5	1.5	Strong, no breaks, very short fractures

**Table 3.11: Properties of different mixing ratio of dvPDMS, PDMS pre-polymer and curing agent.**

### 3.2.8 Sectioning Epoxy

Obtaining the required characteristics by chemically modifying PDMS was problematic and attention was turned to epoxy resin. Epoxies, such as Araldite, are commonly used in sample preparation for TEM in order to embed cells and tissue samples for sectioning. Araldite could not be used as it fluoresces at multiple wavelengths, making live cell fluorescence imaging too difficult. A commercially available epoxy, EPO-TEK 301-2, suitable for liquid crystal display (LCD), optical lamination and light emitting diode (LED) encapsulation, and, as such, is transmissive between 400 nm and 800 nm as required for light microscopy (Epoxy-Technology, 2010). This epoxy is biologically inert providing a suitable substrate for fluorescence imaging. Sectioning a block of epoxy resin at the recommended ratio of 100 : 35 part A (diglycidyl ether of bisphenol A) : part B (polyoxypropylenediamine) was not possible due to the hardness of the material. Different ratios of the two parts of the epoxy were subsequently mixed to determine the most suitable material for sectioning, aiming for the material to have similar properties to Araldite 506 (table 3.12). Most ratios proved too hard for sectioning, but ratios of either 100 : 20 and 100 : 60 were most effective with a ratio of 100 : 60 chosen as the

most suitable epoxy mix to continue to work with, ratios outside of this range proved too soft (Table 3.12). The final material was still rigid but soft enough to allow sections to be cut at thickness of both 1  $\mu\text{m}$  and 100 nm.

Epoxy Part A	Epoxy Part B	Sectioning Notes
10	100	Can be sectioned but too soft
20	100	Forms good sections at 1 $\mu\text{m}$ and 100nm
40	100	Too hard
50	100	Too hard
60	100	Forms good sections at 1 $\mu\text{m}$ and 100nm
70	100	Can be sectioned but material is soft
80	100	Material is too soft

**Table 3.12: Mixing ratios of epoxy 301-2 and the ability of the resultant polymer to be sectioned.**

Light imaging of sectioned encoded microwells were obtained but the microwells were not parallel to the glass knife causing the resulting image to show elongated microwells (figure 3.13). The sectioning showed the two polymers Araldite 506 and EPO-TEK's 301-2 can be used in conjunction with

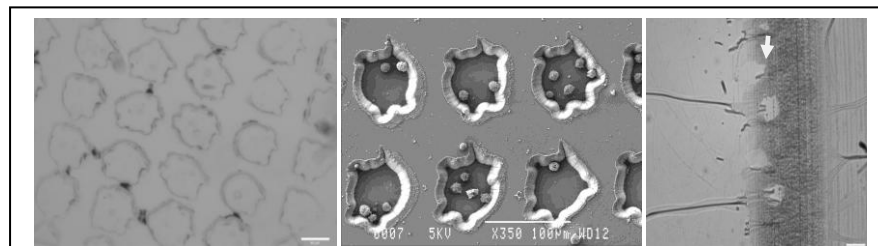


**Figure 3.13: Microscopy and sectioning of encoded microwells.**

Bright field image of encoded microwells (a), SEM image of K562 cells in encoded microwells (b); 1 $\mu\text{m}$  ultramicrotome section of encoded microwell array in 301-2 and araldite (c). Arrow points to the direction triangle on microwell. Scale bars = 50 $\mu\text{m}$

each other, using Araldite 506 as a back fill to 301-2 made microwells.

### 3.2.9 Designing an Encoded Array

It is important to be able to track the positions of cells or samples through two or more imaging processes such as light microscopy and electron microscopy. During sectioning a microwell position can be easily lost if circular wells in a repetitive pattern were to be used. This would be due to rotation, inversion and possible fragmentation of an array. This means that unless a full asymmetric array is recovered, the sample would be useless. Therefore, to enable a user to quickly find a location of a microwell, an identification system is required. An added complication is that any array code must be readable in every section thus negating the use of simply writing an ID number next to each microwell.

A number of different designs were considered but these fell into two categories: (i) spatially encoded arrays, and (ii) protrusion encoded arrays (figure 3.14). The first feature required of the well was the need to make the well asymmetric. This was achieved by placing a small triangle at the

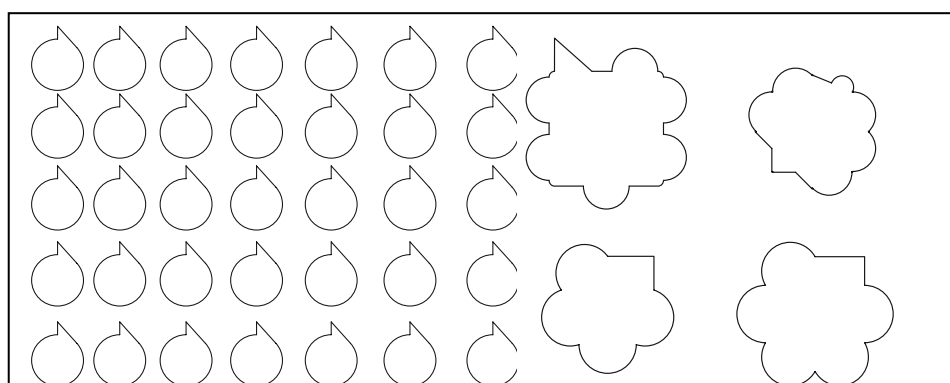


**Figure 3.14: Possible microwell designs.**

Spatially encoded design (left) where each well is a known distance from the others. Protrusion encoded well (right) where different protrusion positions encode for different wells and each well has its own unique shape and thus code.

periphery and off-centre from the well. This would make sure that if a section from the well became inverted; it would be quick and easy to determine which way up the sample needs to be.

Spatially encoded wells used the space between the wells to calculate which well the user was imaging. This had the advantage of the wells being repetitively uniform in shape but had a number of disadvantages. To be able to determine a well's position a user would have to be able to image at least two other wells which are at right angles to the well. To calculate the position accurately the user would then have to compare the width of the well with the distance from the edge of the examined well to the edge of the adjacent wells. This known ratio would then be compared to a known map and the well position could be determined. The main disadvantage in this method is the complication involved in calculating the position. The second disadvantage was if the section was not parallel to the base of the well, it would be difficult to determine the distance between the well and thus, the well position. Thirdly, any manufacturing would require all the wells to be precisely uniform in their 3D shape with vertical walls so as not to complicate any calculation when a section has been cut. Finally, the number of wells able to be encoded in this fashion is limited by the maximum space needed between them. There is a confliction in needs to the layout, such as to reduce error the spaces between the wells need to increase by a large amount, whilst to increase the number of wells available to a user the space between the wells needs to increase by a small amount.

The second form of encoding devised were protrusion encoded designs (figure 3.14). In this case the well number was encoded by a series of protrusions (or recesses) around the periphery of the well where the presence or absence of each protrusion corresponded to a bit in a binary code. By having, for example, five protrusion positions going around the well, we have 32 wells each with a unique shape ( $2^5$ ). By placing the protrusions around the periphery of the well in a logical fashion, such as using a binary layout, it is easy to develop a code for each well.

A number of designs were considered for producing a protrusion encoded array, using increasing numbers and multiple shapes of protrusions around the edge of the microwell, the maximum number of microwells can be increased. The maximum number of wells possible can be defined by the simple equation:

$$W_{max} = (1 + P_s)^{P_n}$$

Where:  $W_{max}$  represents the maximum number of wells

$P_s$  represents the number of differently shaped protrusions

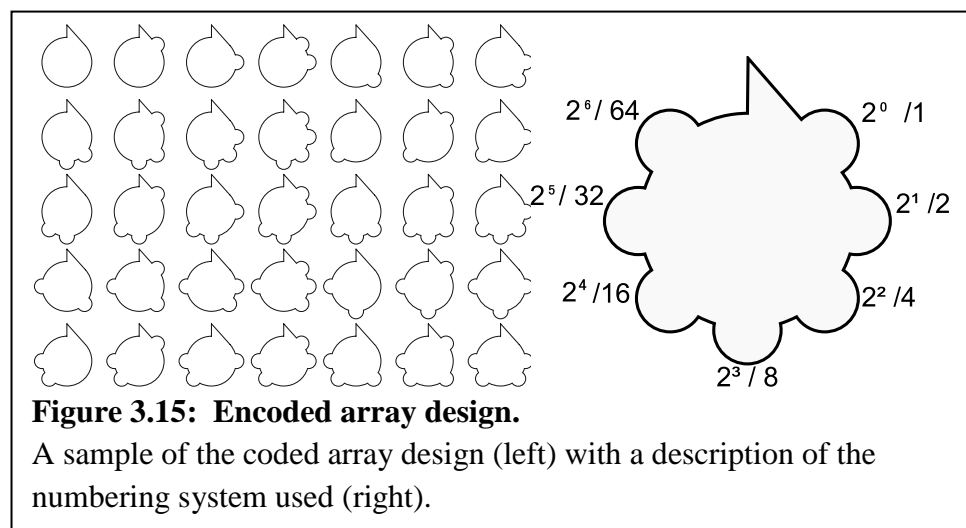
$P_n$  represents the number of protrusions

This means that having an increase in the number of possible protrusions around the well increased the number of possible wells geometrically ( $W_{max} = a^{P_n}$ ). For example, if there were 3 positions for protrusions to be placed there would be  $2^3$  or 8 combinations of different wells, whereas, if there were 7, there would be  $2^7$  or 128 combinations. This was assuming that each protrusion position counts as being present, or not, or one bit of a binary code. The other section to the equation defines the number of different forms in

which a protrusion could occur ( $W_{max} = [Ps]^a$ ), which increased exponentially. For example, if the protrusion takes the form of two different shapes, plus its presence or absence, each position can have three options. So if there were three possible positions defined, there would be  $3^3$  or 27 combinations.

Using this system, we developed a new protrusion encoded microwell array (figure 3.15) where each microwell had an individual identity so that its original position within the array could be easily determined (Sayers *et al.*, 2011). The final coded array comprised three key design features:

- i. The microwell itself, within which a cell could rest during imaging and preparation;
- ii. The encoding protrusions around the circumference of the microwell with their presence/absence forming a binary code;
- iii. A singular triangular protrusion to make the microwell non-superimposable on its mirror image, *i.e.* the microwell is chiral and can be read no matter which way the section is orientated.



This design with seven protrusions was chosen due to the need to have 100 different well designs, whilst the design was kept simple to enable it to be easily interpreted. Seven protrusions allows for 128 wells whilst only having protrusions present, or not, keeps the design simple and less likely to cause errors during reading of the design.

### 3.2.10 Live and Fixed Cell Imaging in the Encoded Array

Mcf-7 (breast cancer) cells were imaged in the encoded microwell array both

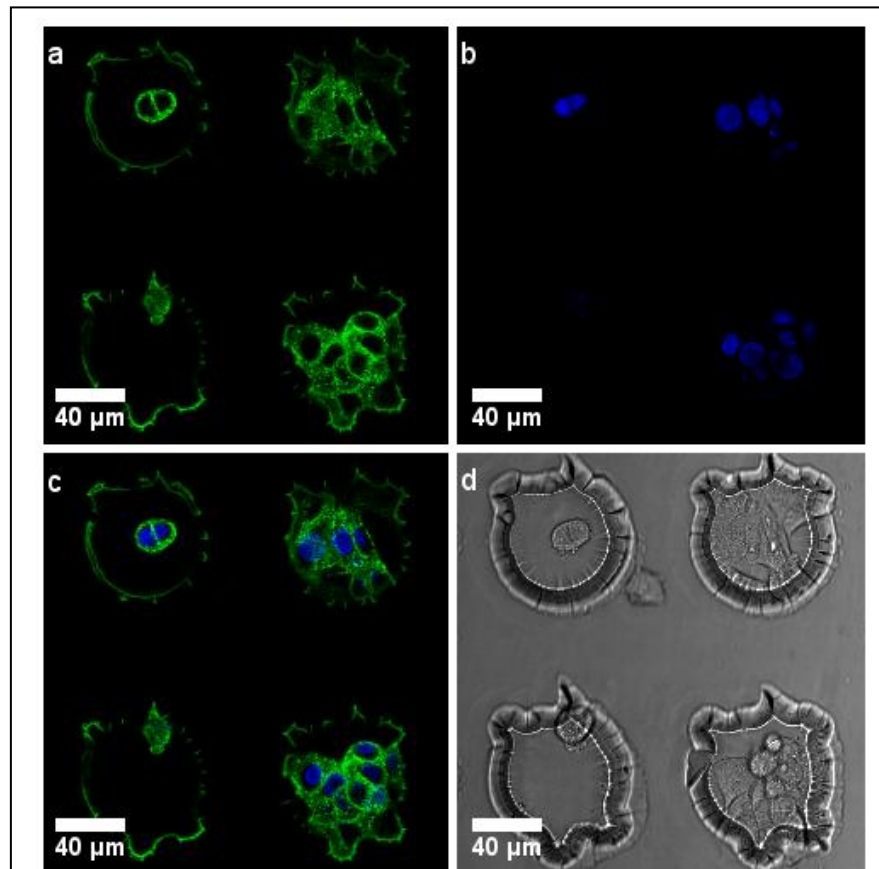


**Figure 3.17: Correlative live-fixed imaging of Mcf-7 cells in encoded microwells.**

Mcf-7 cells were labelled using transferrin-Alexa 488 for one hour before being imaged live (a and d). Cells were fixed and nucleus stained with Hoescht33342 (b). Images were processed and overlay produced in ImageJ (c). Confocal images (a and b) represent xyz projections.

live and after fixation (figure 3.17). Correlative live-fixed imaging was achieved using this method, whilst the different microwell shapes can be seen using the DIC image. It is possible to read the code, despite the wells not being completely clear after ablation. The directional triangle is at the top of the well with the diagonal sloping to the right, the protrusions mark (going clockwise from the image in the top left) microwells 64, 65, 77 and 76. This means the whole array did not have to be viewed and the location of the well can be determined from the pictures after the images have been taken. Overlaying of the live and fixed cell images have not produced an exact match due to the slight misalignment of the cell's nucleus, which is most likely due to shrinking of the cell during fixation after the live cell imaging. To overcome this better methods of fixation would be needed, ideally, cryofixation.

### **3.3 Discussion**

#### **3.3.1 Improving Quality of Laser Ablated Material**

Laser ablation remains a good method for producing different shaped microwells in glass or PDMS. Other methods typically used involve the production of a master and replica moulding from this. This, for example, could be the use of a photoresist such as SU-8, where a mask is used to selectively polymerise a design in the polymer using UV light (Whitesides *et al.*, 2000). Methods similar to this typically need clean room facilities to prevent dust and other particles damaging the mask.

Lasers can be used to either individually produce a repeating structure on a surface or, through using a mask, produce larger more complicated features (Kim and Na, 2007). One of the downsides to using a laser is the debris thrown off from the material during ablation. This debris can reduce the quality of the final item and can produce undesired affects under microscopy such as auto-fluorescence. Cleaning off the debris was therefore important in producing a suitable microwell array. Different methods were attempted including sonication, use of a sacrificial layer and wet etching of the surface. The best results were obtained by using all three of these methods as each step provided its own advantage. Using a sacrificial layer reduced the amount of debris on the surface of the wells, whilst sonication removed the majority of any debris left. Finally wet-etching allowed for a surface layer to be removed and the overall surface improved.

The use of a sacrificial layer was successful as an inexpensive and replicable way of cleaning the surface. Using a liquid ink marker was the easiest and most inexpensive way to provide this. Other methods would most likely be suitable as well. Spin coating a layer of carbon black dissolved in a suitable solvent, such as ethanol, may also provide a suitable alternative, whilst also allowing for a uniform layer to be coated onto the surface. The low cost of using a liquid ink marker and the ease of removal provides a simple method that is unlikely to damage or mark materials such as glass and PDMS.

Sonication was used to remove large particles. It was found sonication in water and ethanol removed the majority of the particles however some debris

remained on the surface. It may also be possible to use harsher chemicals when attempting to remove these particles from the surface, but the need not to damage the surface is important. It is likely that when glass debris falls onto the glass surface some bonding may occur. UV light in the presence of oxygen can be used to create hydroxyl groups on the surface which can later be modified (see UV/Ozone in chapter 4). On top of this effect, ablation is the process of removing the material by breaking apart bonds within the material (Morales and Lieber, 1998). It is not inconceivable that debris may have bonded to the surface, making extremely difficult to remove by most methods of cleaning. Using a sacrificial layer would have stopped the bonding of the debris to the surface by stopping this interaction all together.

Wet etching proved to be the best final step in improving microwell quality. Using a high molar concentration of potassium hydroxide can be used to etch glass, whilst holding it at higher temperatures can speed up the reaction. Etching of glass can be done using a variety of harsh chemicals. Hydrofluoric acid can be used to etch through glass (Spierings, 1993), but suitable facilities are needed due to the danger created using this method and etching can occur rapidly. Using 7M KOH at 60°C provided a low speed etch for borosilicate glass, which has been shown previously to have a slow etch rate of 1µm per hour (Manea *et al.*, 2003). The relatively slow etch speed is more suited to the needs required as it allows a more controlled etch of the surface. Etching may not be suitable for all purposes though. Whilst suitable for 15µm round wells, any highly detailed sub microscale structures can be quickly lost.

### 3.3.2 PDMS as an Alternative Material

Using these methods on glass to improve surface quality has been shown to be successful but other materials are not as suitable. PDMS is a commonly used material in microfluidics (Whitesides *et al.*, 2000) and we have produced microwells in PDMS using laser ablation. Improving surface quality of ablated PDMS is similar to those used for glass with the exception of wet etching. Wet etching PDMS using the high temperature and concentration of KOH causes a fast etch to occur. This is not unexpected as PDMS has a polymer structure of silicone and is a much more flexible and softer material (Whitesides *et al.*, 2000). Surface improvements were suitable using a sacrificial layer and sonication.

### 3.3.3 Autofluorescence of Glass

Reducing the auto-fluorescence of the glass proved to be difficult. Fluorescent probes are an important part of imaging in cell biology and allow for multiple targets to be imaged at the same time (Demandolx and Davoust, 1997). Any autofluorescence in the visible light region would interfere with the imaging quality of the research. Some of the autofluorescence was due to debris, and the removal of the debris aided in reducing the fluorescence. However, a consistent surface effect remained throughout the imaging making it difficult to image properly when using the confocal laser system. On a standard epifluorescent system these effects were reduced and standard imaging on the confocal system has produced these effects when the focal plane approaches the glass. Microscopes such TIRF (total internal reflection fluorescence) microscope use a surface effect to allow greater quality imaging at the surface

cell interface and standard confocal microscopes are being used less to image at this interface (Axelrod, 2001). Using microwells the surface effects from the glass becomes more dramatic as imaging at the top or centre of a cell resting within the microwell may be on the same plane as the surface of the glass enhancing this effect.

Switching to alternative materials can reduce this effect. PDMS didn't suffer from the surface effect and a higher quality of imaging can be produced. Comparison of live cell imaging between glass and PDMS microwells showed PDMS to produce a much clearer image where endosomes are more visible and clearer.

#### 3.3.4 Imaging in Microwells

Scanning electron microscopy imaging of cells within the microwells proved to be successful with little morphological difference between cells imaged in the wells and those imaged outside. Correlative live cell – scanning electron microscopy was shown to be possible using the microwell system. Non-adherent cells can easily be moved across the surface during washing steps in preparation for SEM. The microwells managed to retain the cells in the position during fixation and subsequent washes allowing for comparison between the live cell and the fixed cell images.

### 3.3.5 Sectioning PDMS and Epoxy

To allow for correlative TEM, cells need to be sectioned. Using PDMS proved to be difficult as the material was too soft whilst introducing short chained crosslinking to the PDMS created a brittle polymer. Whilst this approach was abandoned in favour of using an epoxy, using PDMS as a polymer may still be possible. The difference in estimated molecular weight was quite large and this mix may not have helped produce a stable structure. Using the short chained PDMS alone also produced a very brittle polymer. By using chain lengths that are similar or the same may produce a more suitable polymer. An investigation into the length of chain and the possible use of different chemical side groups in the siloxane rubber may strengthen the polymer without making it too brittle. Using different side groups may, however, reintroduce the autofluorescence problem. The next chapter looks at surface chemistry of PDMS and its cytophobicity. One of the alternate surfaces investigated was a sol-gel made up of silicate, but this too produced a brittle polymer that was unsuitable. The distances between crosslinks were very short indicating that reducing the length of the chain may make PDMS too brittle.

Epoxy proved to be a more suitable material for sectioning. It was possible to image cells in the encoded microwells in the epoxy as it was selected for its non-toxicity as well as its optical properties (>94% transmission at 320nm and >99% transmission between 400-1200nm) and its chemical resistance (Epoxy-Technology, 2010).

### 3.3.6 Encoded Microwells

Different encoded microwell designs were investigated and a simple well was devised using binary coding in the form of protrusions around the circumference of the well. Whilst more complicated designs could provide a greater number of different combinations and therefore, more wells that can be imaged at once, the simpler design was chosen. Different researchers want different properties out of their equipment. If the encoded microwells were to be designed for high throughput then a design would be needed that could code for over 1,000 different wells at one. For correlative microscopy however, a user is unlikely to use great numbers. Current methods can find it difficult to track just a few cells, so typical user may not need to track more than 100 different cells at a time, especially if they are tracking the events in only one cell in detail. One of the major advantages of this method is the ability to use any cell type, whether they are adherent or non-adherent, as the size of the well can be easily modified as well as the chemistry of the surface.

### 3.3.7 Conclusion

Microwells are a good method for correlatively light – SEM imaging non-adherent cells. For imaging under TEM, materials need to be sectioned, glass is clearly unsuitable, whilst PDMS proved difficult to modify and make suitable. Using an epoxy proved suitable for sectioning the microwells. To allow for the tracking of individual microwells, a coding system was developed. The encoded microwells can be imaged under light and scanning electron microscopes allowing for the following of a cell between the two techniques.

### **3.4 References**

- AXELROD, D. (2001) Total internal reflection fluorescence microscopy in cell biology. *Traffic*, 2, 764-74.
- BROWN, E., MANTELL, J., CARTER, D., TILLY, G. & VERKADE, P. (2009) Studying intracellular transport using high-pressure freezing and Correlative Light Electron Microscopy. *Seminars in Cell & Developmental Biology*, 20, 910-919.
- DEMANDOLX, D. & DAVOUST, J. (1997) Multicolour analysis and local image correlation in confocal microscopy. *Journal of Microscopy-Oxford*, 185, 21-36.
- EATON, S. M., ZHANG, H., NG, M. L., LI, J., CHEN, W. J., HO, S. & HERMAN, P. R. (2008) Transition from thermal diffusion to heat accumulation in high repetition rate femtosecond laser writing of buried optical waveguides. *Opt Express*, 16, 9443-58.
- EL-ALI, J., SORGER, P. K. & JENSEN, K. F. (2006) Cells on chips. *Nature*, 442, 403-411.
- EPOXY-TECHNOLOGY (2010) EPO-TEK 301-2 Technical Data Sheet. Billerica.
- GALBRAITH, J. A. & GALBRAITH, C. G. (2011) Super-resolution microscopy for nanosensing. *Wiley Interdisciplinary Reviews-Nanomedicine and Nanobiotechnology*, 3, 247-255.

- GREUTERS, J. & RIZVI, N. H. (2003) Laser micromachining of optical materials with a 157nm fluorine laser. IN OSTENDORF, A. (Ed.) *Laser Micromachining for Optoelectronic Device Fabrication*.
- HAIGH, S., SCHROEN, D., ZURGIL, N. & DEUTSCH, M. (2006) Multiparametric assays on individual cells - Temporal measurement of reactive oxygen species generation. *Genetic Engineering News*, 26, 18-20.
- KIM, J. & NA, S. (2007) Metal thin film ablation with femtosecond pulsed laser. *Optics and Laser Technology*, 39, 1443-1448.
- LUO, C. X., LI, H., XIONG, C. Y., PENG, X. L., KOU, Q. L., CHEN, Y., JI, H. & OUYANG, Q. (2007) The combination of optical tweezers and microwell array for cells physical manipulation and localization in microfluidic device. *Biomedical Microdevices*, 9, 573-578.
- MANEA, E., CERNICA, I., LUPU, M. & PODARU, C. (2003) Optimization of deep wet etching borosilicate glass substrates technological process for biomedical applications. *Semiconductor Conference, CAS 2003*.
- MITTAL, N., ROSENTHAL, A. & VOLDMAN, J. (2007) NDEP microwells for single-cell patterning in physiological media. *Lab on a Chip*, 7, 1146-1153.
- MORALES, A. M. & LIEBER, C. M. (1998) A laser ablation method for the synthesis of crystalline semiconductor nanowires. *Science*, 279, 208-11.
- NALAYANDA, D. D., KALUKANIMUTTAM, M. & SCHMIDTKE, D. W. (2007) Micropatterned surfaces for controlling cell adhesion and rolling under flow. *Biomedical Microdevices*, 9, 207-214.

OCHSNER, M., DUSSEILLER, M. R., GRANDIN, H. M., LUNA-MORRIS,

S., TEXTOR, M., VOGEL, V. & SMITH, M. L. (2007) Micro-well arrays for 3D shape control and high resolution analysis of single cells.

*Lab on a Chip*, 7, 1074-1077.

QVF (2000) Composition and Corrosion Resistance of Borosilicate Glass.

[http://www.qvf.com/en/equipment\\_1/borosilicate%20glass/Composition.shtml](http://www.qvf.com/en/equipment_1/borosilicate%20glass/Composition.shtml), De Dietrich Process Systems GmbH, .

SELIMOVIC, S., PIRAINO, F., BAE, H., RASPONI, M., REDAELLI, A. &

KHADEMHOSEINI, A. (2011) Microfabricated polyester conical microwells for cell culture applications. *Lab Chip*, 11, 2325-32.

SHIN, D. S., LEE, J. H., SUH, J. & KIM, T. H. (2006) Elimination of surface

debris generated by KrF excimer laser ablation of polyimide. *Materials Science and Engineering a-Structural Materials Properties*

*Microstructure and Processing*, 416, 205-210.

SPIERINGS, G. (1993) Wet Chemical Etching Of Silicate-Glasses In

Hydrofluoric-Acid Based Solutions. *Journal of Materials Science*, 28, 6261-6273.

TOKILMITSU, Y., KISHI, H., KONDO, S., HONDA, R., TAJIRI, K.,

MOTOKI, K., OZAWA, T., KADOWAKI, S., OBATA, T., FUJIKI, S.,

TATENO, C., TAKAISHI, H., CHAYAMA, K., YOSHIKATO, K.,

TAMIYA, E., SUGIYAMA, T. & MURAGUCHI, A. (2007) Single

lymphocyte analysis with a microwell array chip. *Cytometry Part A*, 71A, 1003-1010.

TSIEN, R. Y. (1998) The green fluorescent protein. *Annu Rev Biochem*, 67, 509-44.

UQGOPTICS (1999) SCHOTT® BOROFLOAT,  
[http://www.uqgoptics.com/materials\\_optical\\_borosilicateBorofloat.aspx](http://www.uqgoptics.com/materials_optical_borosilicateBorofloat.aspx).

VERKADE, P. (2008) Moving EM: the Rapid Transfer System as a new tool for correlative light and electron microscopy and high throughput for high-pressure freezing. *J Microsc*, 230, 317-28.

WHITESIDES, G. M., MCDONALD, J. C., DUFFY, D. C., ANDERSON, J. R., CHIU, D. T., WU, H. K. & SCHUELLER, O. J. A. (2000) Fabrication of microfluidic systems in poly(dimethylsiloxane). *Electrophoresis*, 21, 27-40.

## **4. Surface Modification and Cell Surface Interaction**

In the previous chapter the design and manufacture of microwells was investigated. These microwells were made into both glass and polydimethylsiloxane (PDMS). Whilst glass surfaces are commonly used for imaging cells, PDMS is less suitable since it is cytophobic. However other properties of PDMS, its optical performance and ease with which it can be moulded and manipulated *e.g.* laser ablation, make it a useful material for use in this study. Therefore in order to use PDMS in this study a number of chemical modification techniques were evaluated with the aim of making the PDMS surface more cell-friendly..

### **4.1 Introduction**

PDMS is a versatile material often used in the fabrication of microscale devices (Whitesides *et al.*, 2000). Its strengths are its simplicity for microfabrication, being a mouldable polymer, and its resistance to a variety of chemicals. However, PDMS is hydrophobic, the stable dimethylsiloxane polymer is relatively inert making it difficult to modify. Hydrophobic solvents readily swell PDMS, whilst hydrophilic solvents do not. The surface of PDMS poorly wetted by hydrophilic solvent such as water (Lee *et al.*, 2003). Because of this there has been extensive research into methods that can be used to modify the surface to make it more polar..

One of the earliest approaches was to oxidise the surface. This can be achieved in a variety of ways either by plasma or corona discharge, using energy such as

UV (Berdichevsky *et al.*, 2004) or chemically using strong oxidizing solutions. Oxidised surfaces have been shown to revert back to their hydrophobic states when not immersed in water-based solvents (Olah *et al.*, 2005). It is suggested that this hydrophobic recovery is due to migration of polymer chains from within the bulk of the material towards the surface. This process is aided by cracks induced during energy mediated surface modifications (Hahn *et al.*, 2003).

It is therefore imperative to further modify the surface immediately after activation, in order to retain a surface change. One of the easiest ways to do this is by silanisation, where silanols covalently cross-link the surface resulting in a permanent modification. Other covalent approaches have also been employed such as the use of free radicals generated under UV to graft different polymers to the surface (Li *et al.*, 2002), or catalytic hydrosilylation where polymers can be grafted to the surface using hydrosilyl bonds incorporated into the PDMS (Zhang *et al.*, 2008) (Guo, 2007).

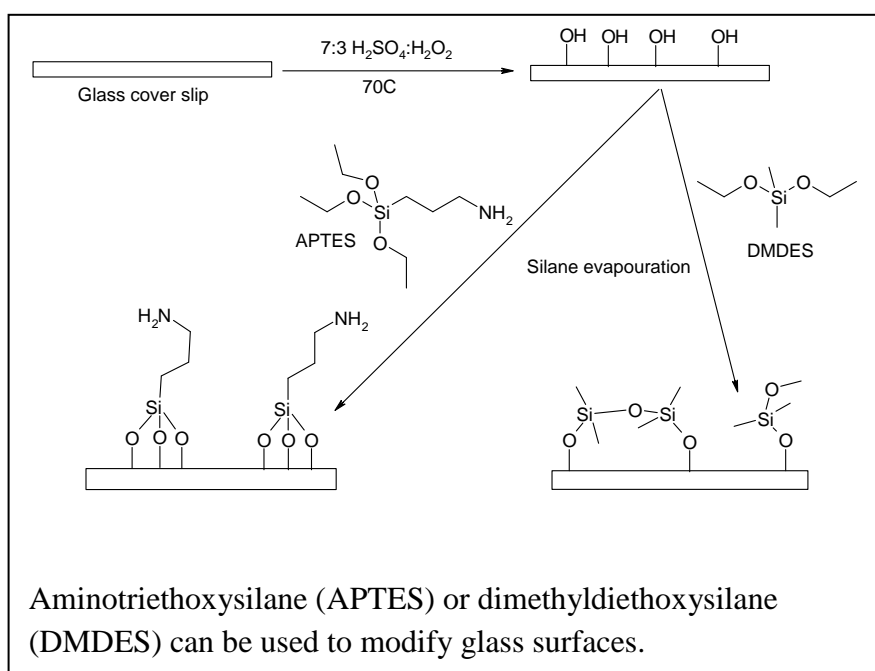
#### 4.1.4 Aim

This chapter will investigate different surface chemical modification techniques for both glass and PDMS to provide a surface suitable for cell imaging studies. The chapter will cover two main techniques, direct surface reactions and interpenetrating networks using sol-gels.

## 4.2 Results

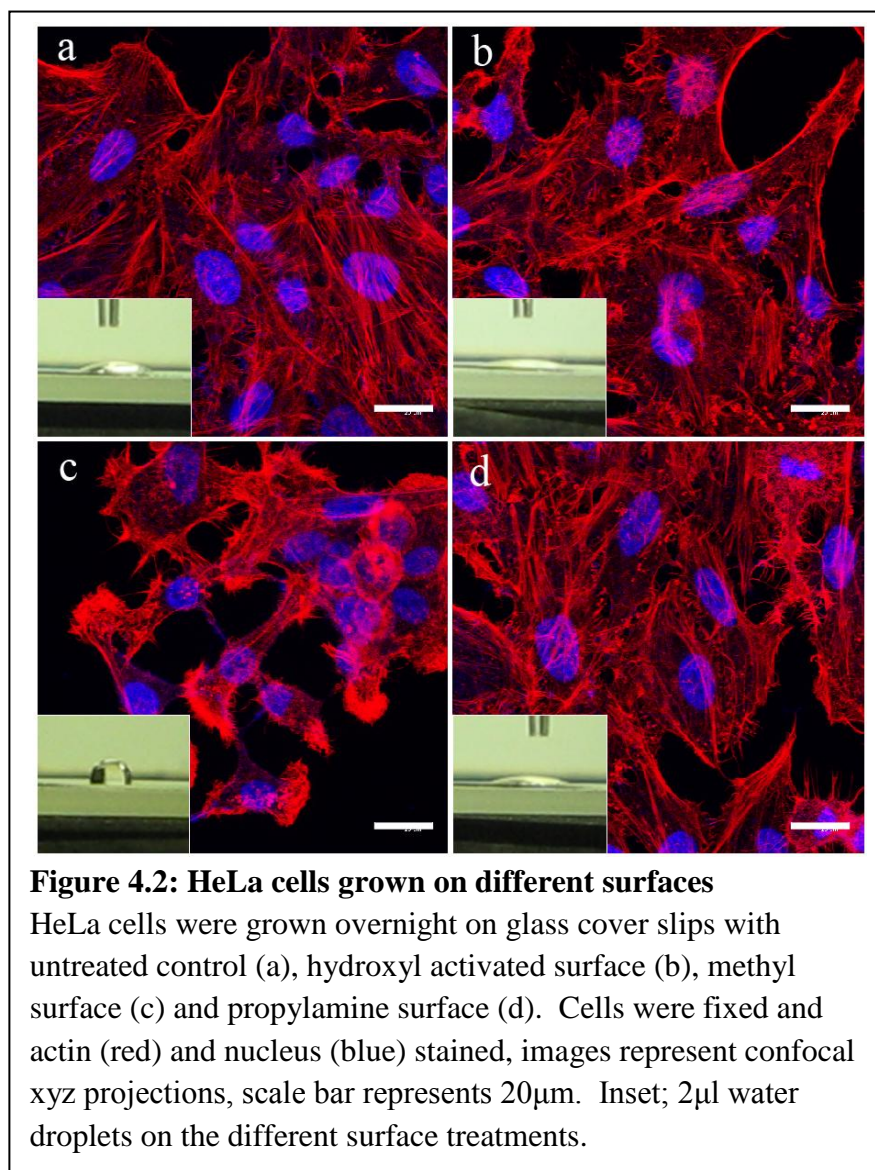
### 4.2.1 Surface Modification of Glass

Glass surfaces can be readily modified, so as to tailor surface properties to suite a particular need. One of these methods uses silanes to functionalise glass surfaces so as to enable further chemical modifications (Munoz *et al.*, 1983). The first step in this process was surface activation. Whilst a number of



different techniques have been described, such as plasma etching, one of the simplest to perform was the Piranha technique. This involved treating the glass surface with a sulphuric acid - hydrogen peroxide solution. This treatment cleaves the siloxane bonds providing hydroxide moieties on the surface on the glass. Silanes were subsequently used to attach chemical functionality on to the hydroxy modified surface (figure 4.1).

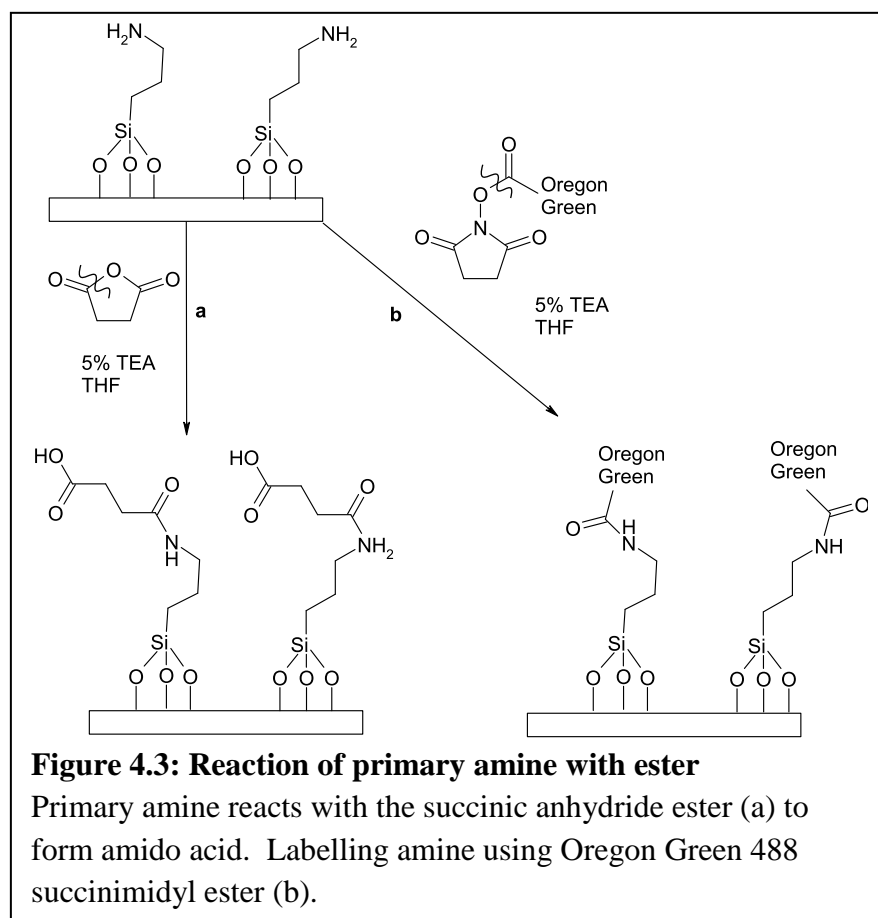
Glass surfaces modified with different silanes were difficult to characterise. Contact angle measurements indicated an expected decrease in contact angle



following Piranha activation (figure 4.2; insets). Methyl modified surfaces showed a large increase in the contact angle indicating a significant increase in the hydrophobicity of the surface. Propylamine modified surfaces showed a similar contact angle to that obtained after just activation of the glass surface.

Cells grown on both the activated (hydroxylated) surface and the amine modified surface showed little difference to the unmodified control (figure 4.2). In contrast, cells grown on a methyl modified surface showed different cell morphology. Cells had a reduced level of surface attachment and demonstrated actin enrichment at the available attachment sites around the cell. The morphology of cells grown on the methyl modified surface was similar to cells grown on PDMS (see 4.2.2 'Modification of PDMS Surfaces'). Calculating the ratio between the area of the picture containing actin (red) and the area of the picture containing the nucleus (blue), it was possible to obtain a numerical measurement for the morphology of the cells found in figure 4.2. On the control surface and the propylamine surface this ratio was 8.7 (there was 8.7 times more of the surface donated to actin than the nucleus,  $n = 2$ ), for the hydroxyl surface this ratio had dropped slightly to 8.1 ( $n = 2$ ). However, for cells grown on the methyl surface this had dropped to 4.0 ( $n = 2$ ). Whilst these results give an indication of morphology difference, a number of factors have to be taken into account. The images contained no more than fourteen cells, do not take into account the cell stacking seen in the methyl surface sample and do not take into account cell cycle. Analysis of a large number of cells could reduce this effect and the calculation of cell surface area to volume from 3D projections could also provide more accurate detail. However, the range obtained for the calculation of just two samples was narrow and indicates this could be a suitable tool for analysing cell morphology.

Amine groups were further functionalised using succinic anhydride or succinimide esters. These reagents reacted with the amine to, in the case of a succinic anhydride, give a carboxyl terminated surface, or, using a succinimide ester, attach larger molecules onto the surface, such as proteins or fluorescent probes (figure 4.3).



Methyl modification yielded a surface with a significantly larger contact angle than either the activated surface or the amine derivatised surface (figure 4.4) indicating a large difference in hydrophobicity of the samples. By adding succinic anhydride (SA) it was hoped the amine modified surface would react with the SA producing a carboxylated surface. Again, contact angle analysis

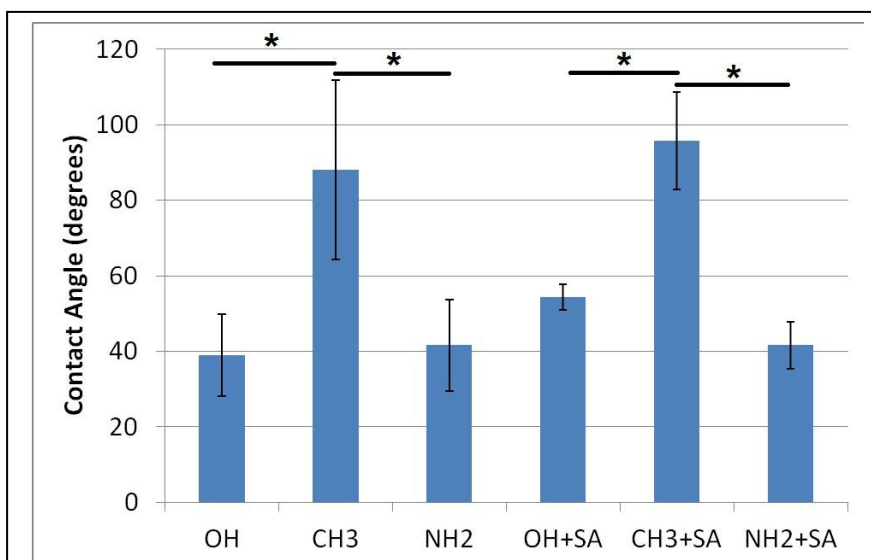


**Figure 4.4: Contact angle of glass surfaces following treatment with different silanising reagents.**

Contact angles of water droplets on activated glass surfaces (OH) before silane evaporation using APTES (NH<sub>2</sub>) or DMDES (CH<sub>3</sub>). Succinic anhydride (SA) was added to the three surfaces to form amido acid (NH<sub>2</sub> +SA) with other two samples providing a control. Error bars represent 1 S.E., n=3, \* P<0.05 using two tailed students t-test.

showed a significant difference between methyl plus SA and either the activated surface plus SA or amine surface plus SA. There was, however, no difference between either the amine modified surface or the amine plus SA surface. This suggests that the reaction had not taken place but it does not rule out the possibility that both amine and the amine plus SA surfaces have similar contact angles or that the efficiency of the original amine modification was low.

To test whether amine was present on the surface, the activated fluorescent probe Oregon Green succinimidyl ester was incubated with the six different surfaces evaluated in figure 4.4. The resulting surface fluorescence was imaged using a fluorescent microscope (figure 4.5). Little difference in fluorescence intensity was observed between any of the surfaces with the exception of the amine surface that had not been incubated with succinic

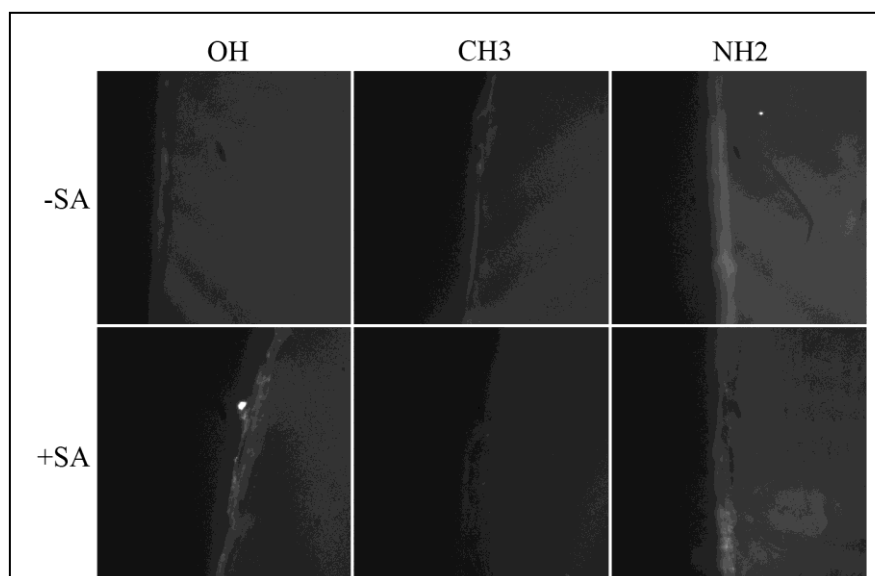


**Figure 4.5: Surfaces incubated with a fluorescent probe to amines.**

Glass surfaces were activated (OH) and reacted with either DMDES (CH<sub>3</sub>) or APTES (NH<sub>2</sub>), surfaces were incubated in the presence or absence of succinic anhydride (SA) and all surfaces incubated with Oregon Green succinimidyl ester. Fluorescent images obtained using a standard fluorescence microscope.

anhydride (5 mg/ml in THF for 4 hrs). It might have been expected that amine modified surfaces would have a higher fluorescence due to the availability of amines for labelling with Oregon Green succinimidyl ester. Reaction of the amine modified surface with SA prior to fluorescent labelling would have prevented the attachment of the fluorescent probe due to the unavailability of

the amine. The effect is small and this again may have been due to the low availability of amines on the surface after silane evaporation.

Cells grown on unmodified, amine modified or amido modified glass showed little difference in morphology, whilst cells grown on methyl modified surfaces again showed abnormal morphology and disrupted actin arrangement (figure 4.6). Typically, the mammalian cell membrane has an outer sugar rich layer that gives the membrane a negative charge and some cells have been shown to modulate external carbohydrates (glycocalyx) to modify their adhesion (Sabri

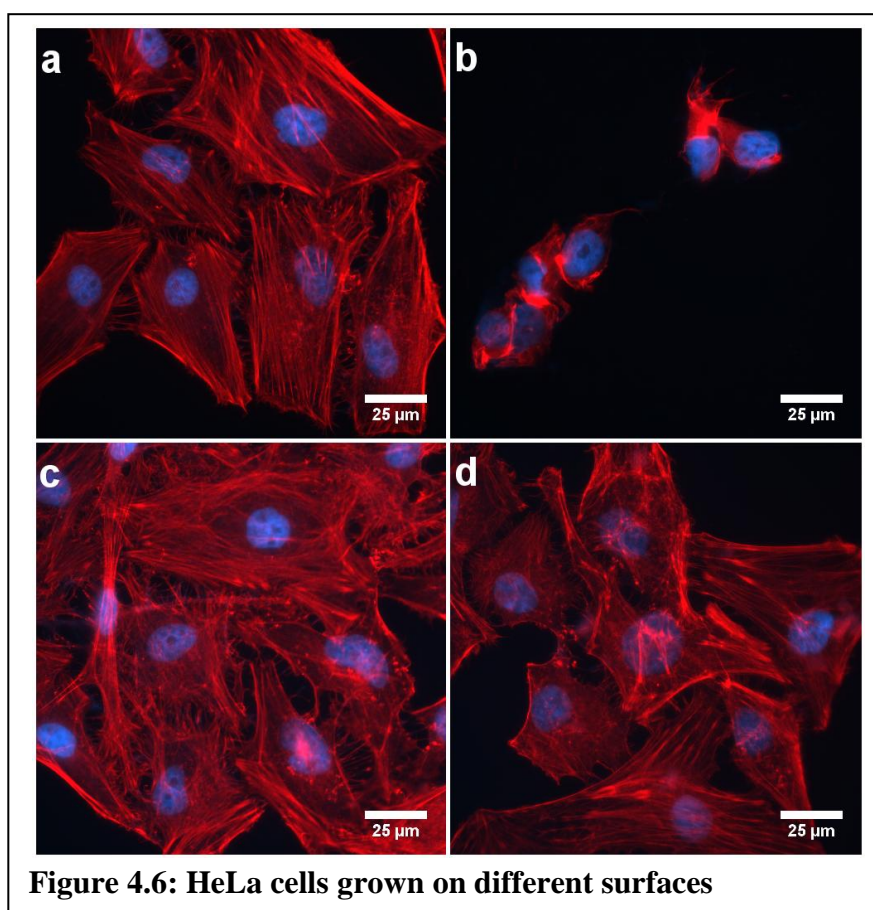


**Figure 4.6: HeLa cells grown on different surfaces**

HeLa cells were grown overnight on glass (a), DMDDES modified glass (b), APTES modified glass (c) or APTES plus SA modified glass (d). Images are taken after fixation and labelling of actin (red) and nucleus (blue) on a fluorescence microscope and processed in ImageJ.

*et al.*, 2000). It might be predicted that cells grown on carboxyl modified surfaces would show different morphology with the negatively charged surface significantly reducing cell-surface interaction. However, little difference in morphology was observed between cells grown on amine and cells grown on carboxyl surfaces. This could be due to either inefficient conversion of amine to amido acid or the different surfaces having little difference in their effects on cells.

#### 4.2.2 Surface modification of PDMS

Microwells can be laser ablated in a wide range of materials and it has been shown previously that a suitable material for microwell arrays is PDMS (see chapter 3). PDMS has many advantages over glass, being flexible and softer, it is, however, very hydrophobic with methyl groups present on the surface. As discussed in section 4.2 (Surface Modification of Glass), methyl modified surfaces are poor substrates for cell attachment. Therefore, if PDMS microwells are to be manufactured it would be necessary to modify its surface properties so as to make it more compatible with adherent cells.

A number of different methods were used to modify PDMS where the surface, or the whole material itself. Surfaces were modified by direct chemical reactions such as the use of silanes, in a similar manner to glass, or by hydrosilanisation where vinyl groups were used to provide direct covalent links between the silane and the surface modifying groups. Alternatively,

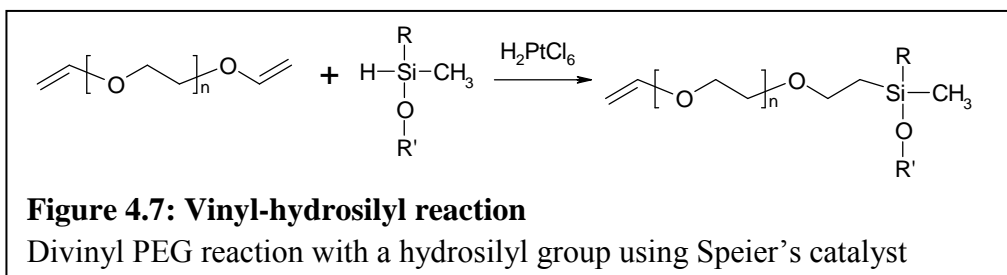
interpenetrating networks of alternative materials were made throughout PDMS, providing a more hydrophilic polymer supported by PDMS.

#### 4.2.2.1 Surface Chemistry

Modifications have commonly been used to modify PDMS to promote cell adhesion and deter protein adsorption (Heyries *et al.*, 2007, Whitesides *et al.*, 2000). Methods attempted in this study involve direct modification of the surface using chemical modification and interpenetrating networks weaved into the PDMS to change the properties of the surface.

##### 4.2.2.1.1 Modification of PDMS by Catalytic Hydrosilylation

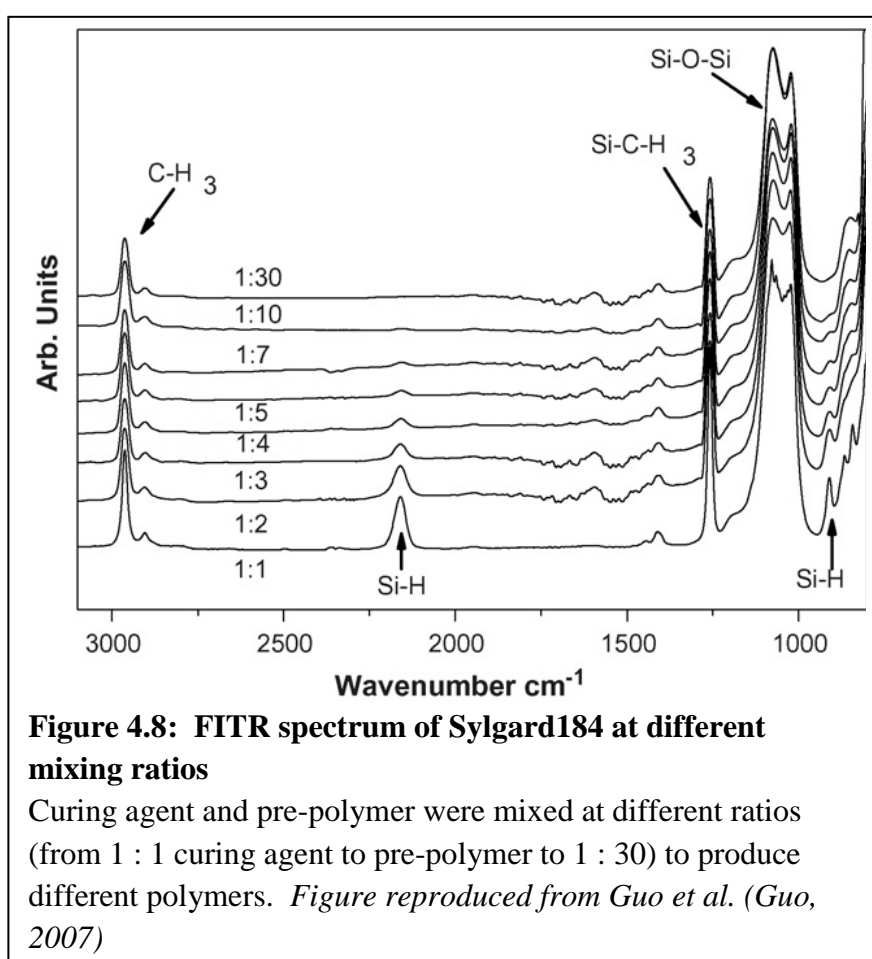
Hydrosilylation is an addition reaction where a hydrosilyl group is added to a vinyl group (figure 4.7).



PDMS sylgard184 is composed of two parts (see chapter 3), the curing agent contains hydrosilyl groups to which the vinyl terminated PDMS can bond and form a crosslink (Heyries *et al.*, 2007). At the recommended ratio of curing agent to PDMS prepolymer of 1 : 10, the hydrosilyl groups in the curing agent are almost saturated by the vinyl terminated pre-polymer. By increasing the

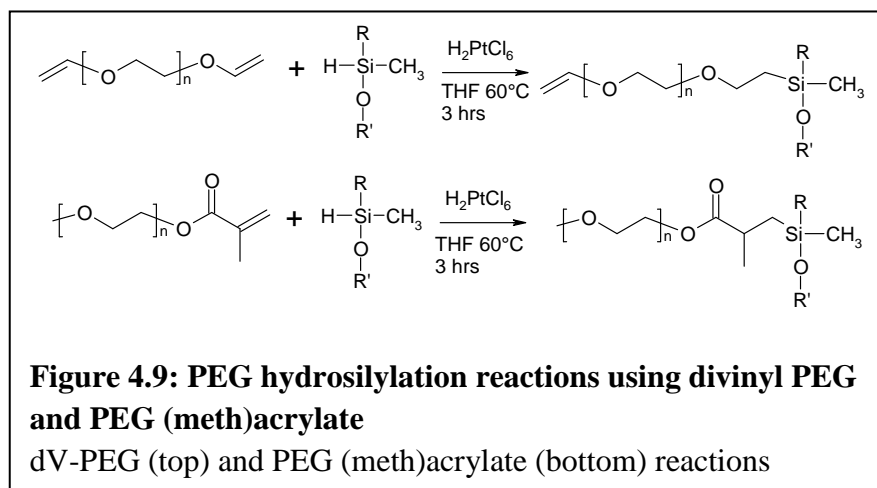
ratio of curing agent to the pre-polymer, hydrosilyl groups become less saturated leaving more available for further reactions (figure 4.8).

Alternatively, polymethylhydrosiloxane (PMHS, a similar polymer with multiple hydrosilyl groups) was used instead of, or alongside, the curing agent to increase the number of available hydrosilyl groups for cross-linking by reacting with the vinyl terminated portion of the PDMS polymer, integrating the polymer into the network. Polymers such as divinyl-polyethyleneglycol

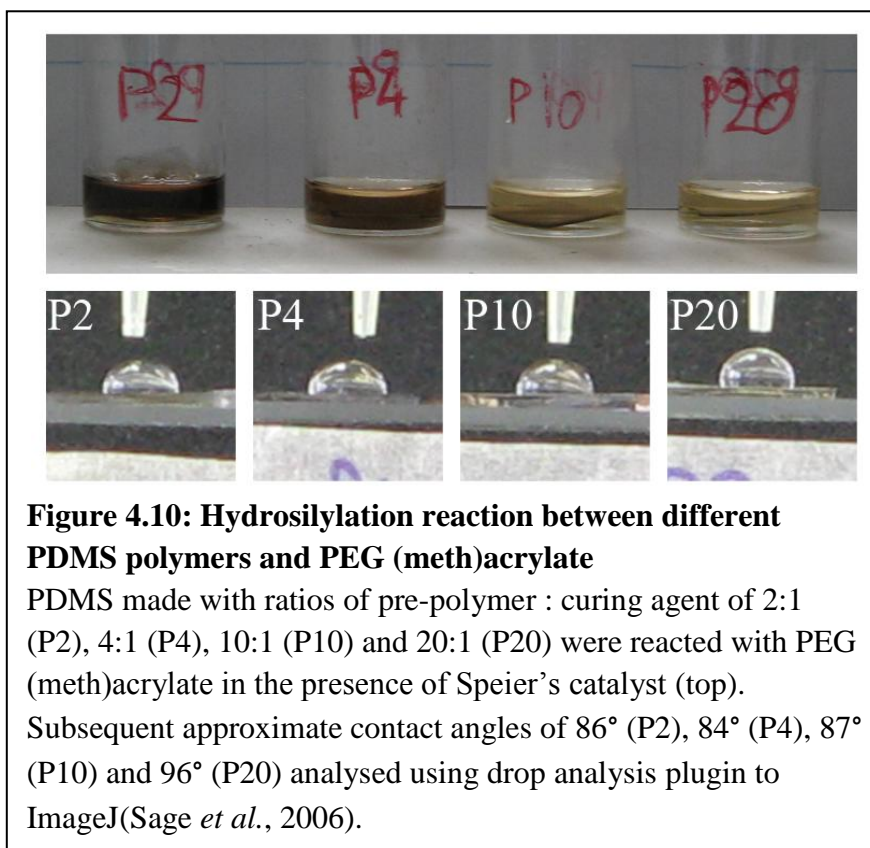


(dV-PEG) and PEGMA (PEG methacrylate) were used to react with any hydrosilyl groups in PDMS, and reduce the overall hydrophobicity (figure 4.9).

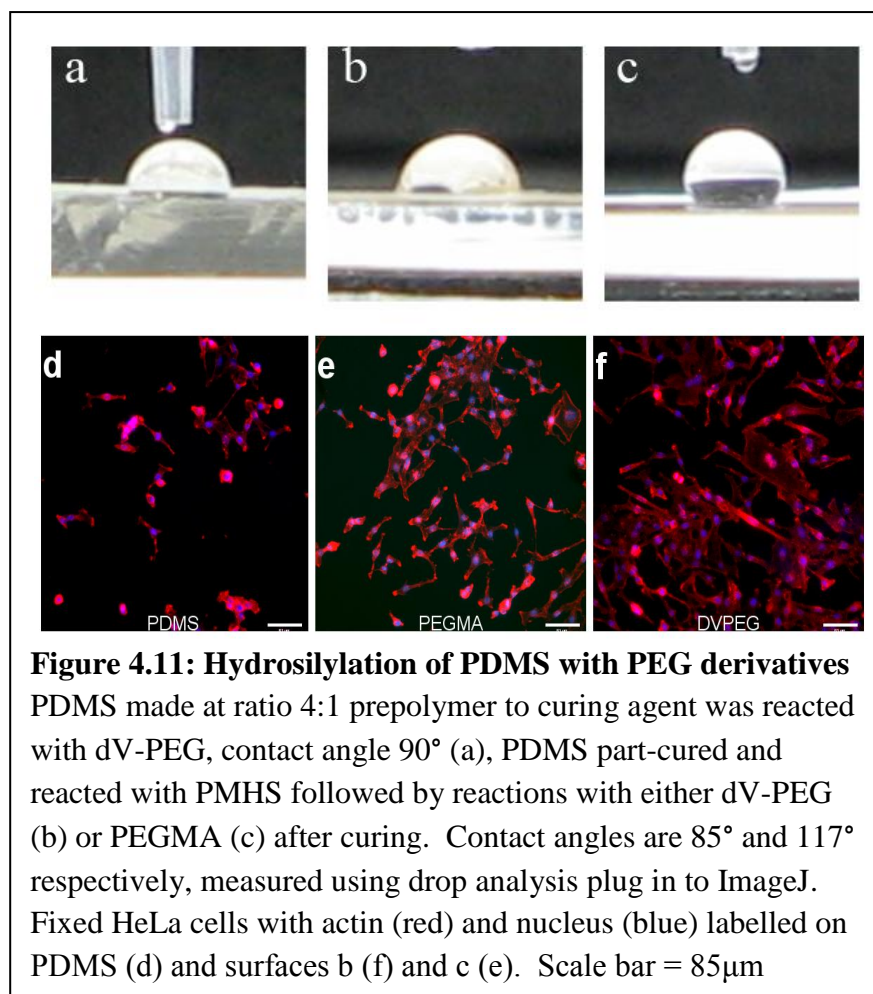
At optimum ratios of 10:1 prepolymer to curing agent there are few hydrosilyl groups available after curing (Guo, 2007). Reducing the proportion of prepolymer, to 4:1 or 2:1, increases the available hydrosilyl groups for reaction with a (meth)acrylate modifier. Speier's catalyst (chloroplatinic acid),



catalyses the reaction between the vinyl group of the reactant and the hydrosilyl group of the polymer (Rao and Zhang, 2012) leaving a dark brown residue (figure 4.10). There was little difference between the contact angles produced by reacting different ratios of PDMS curing agent and pre-polymer with PEG (meth)acrylate (PEGMA). This would indicate that either the reaction has not occurred or PEGMA does not produce a large change in contact angle.



Reactions using divinyl PEG produced similar contact angles to those obtained when using PEGMA under the same conditions (figure 4.11). PMHS was added to part-cured PDMS (10:1) to increase the number of hydrosilyl groups available for hydrosilylation. Reactions of PDMS-PMHS with dV-PEG and PEGMA produced differing results. dV-PEG produced a much lower contact angle than with the same reaction using PEGMA. This indicated a difference in the reactions with dV-PEG much more successful at producing an altered surface than PEGMA in the presence of PMHS. This was substantiated using cell morphology experiments, where surfaces derivatised using dV-PEG showed improved cell morphology compared to PDMS control and surfaces derivatised using PEGMA (figure 4.11d-f). Whilst cell morphology was not



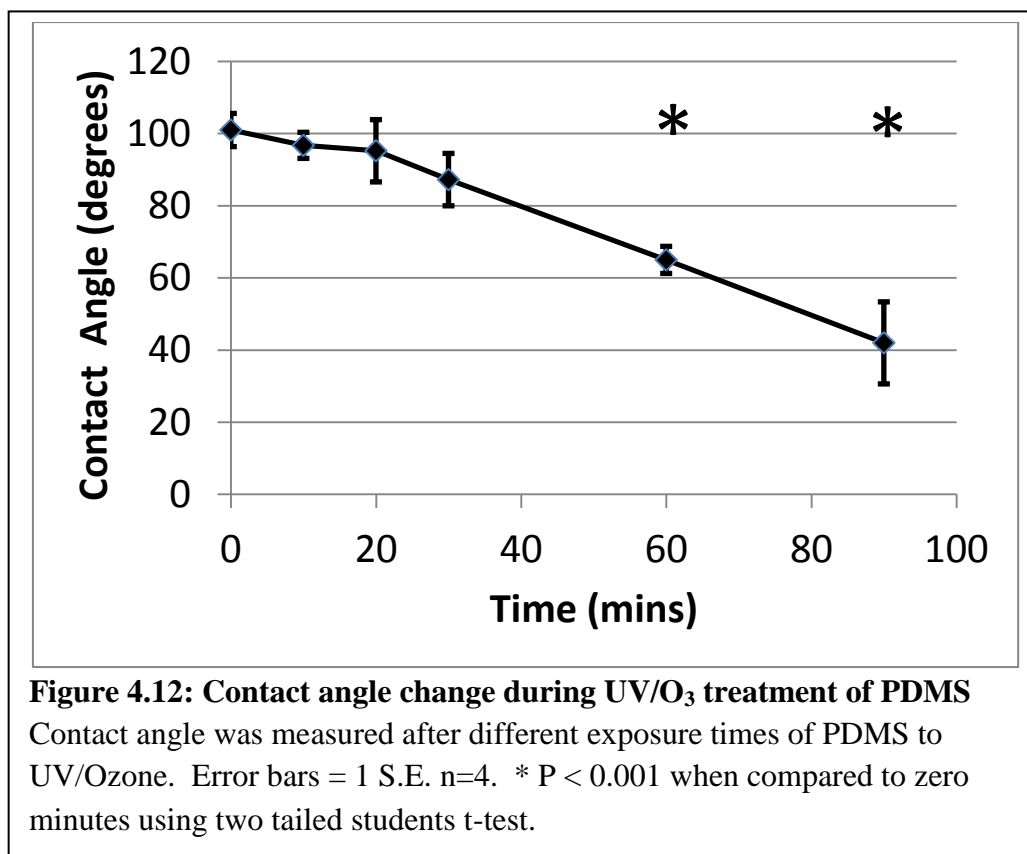
optimal, improvements over controls were observed suggesting there is value in using this derivatisation approach.

Hydrosilylation of PDMS surfaces using vinyl-PEG chemicals can produce an improved surface for cell adhesion. Whilst methacrylate terminated PEGs showed less potential than the vinyl terminated PEG molecules in altering the polymer surface. This is surprising as methacrylate normally produces a more reactive double bond than a terminal vinyl group. However, PDMS was cured using just terminal vinyl groups indicating there could be more happening with this reaction.

#### 4.2.2.1.2 Modification of PDMS Surfaces using *Silanes*

The dimethylsiloxane chains within PDMS make it hydrophobic and relatively inert but also create the challenge of how to modify it by chemical means. When working with Sol-Gels (see Sol-Gel Modification of PDMS below) Si-O-Si bonds can be easily hydrolysed back to Si-OH, just by exposing it to water or a weak alkali. However, in PDMS, these bonds are much stronger. Attempts were made, using Piranha solution to activate the surface in a similar fashion to glass. However, when PDMS was exposed to Piranha solution a white layer built up on the surface of the PDMS and the contact angle remained the same. An alternative method for activating the surface for silane chemistry was therefore needed.

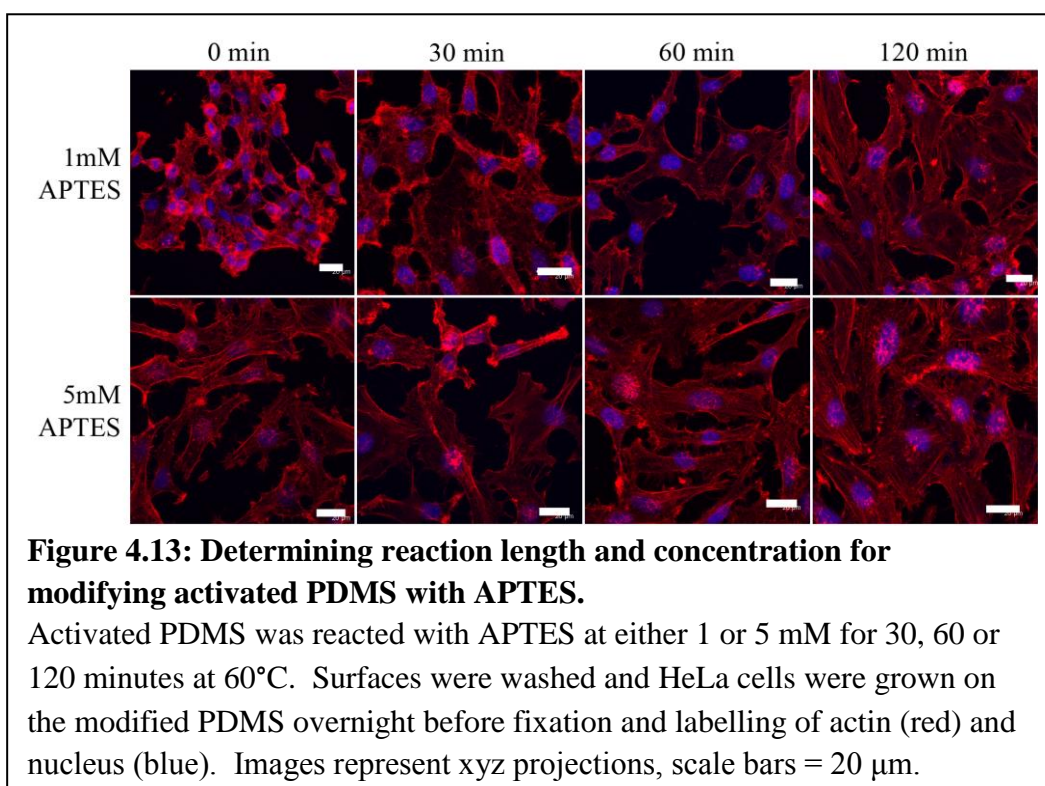
The most commonly used method for activating the surface of PDMS is oxygen plasma etching (McDonald *et al.*, 2000). This involves targeting oxygen ions at the surface of the PDMS to break open the siloxane linkage. Another method, which has much the same effect, is UV/ozone treatment. This approach is commonly used to clean surfaces prior to experiments, but has also been shown to activate the surface of a variety of polymers and plastics. It works by exposing the surface to two wavelengths of UV light. The first, 185nm, breaks the oxygen-oxygen bonds and produces ozone, whilst the second, 254nm, brings about a reaction between ozone and the PDMS to break open siloxane linkages (Olah *et al.*, 2005). Exposure of an hour or more to UV/ozone created a reduction in contact angle of PDMS (figure 4.12).



After activation of the surface using UV/Ozone the surface was modified using silane chemistry techniques similar to that used for glass. PDMS surfaces were modified with APTES and TEOS (tetraethylorthosilicate), and DMDES was used as a positive control. Attempts were also made to further modify the amine derivatised surfaces by adding albumin as an alternative surface with which to attach cells.

To optimise reaction conditions different concentrations of APTES were incubated with activated PDMS over two hours (figure 4.13). Contact angle measurements of APTES modified surfaces showed little difference to unmodified PDMS. To determine the best reaction conditions HeLa cells were grown on APTES modified surfaces and the cell morphology on the different surfaces was imaged. After reaction of 1 mM APTES with the activated

PDMS for two hours, subsequent cell morphology showed improvement over when the reaction was performed for less than two hours.



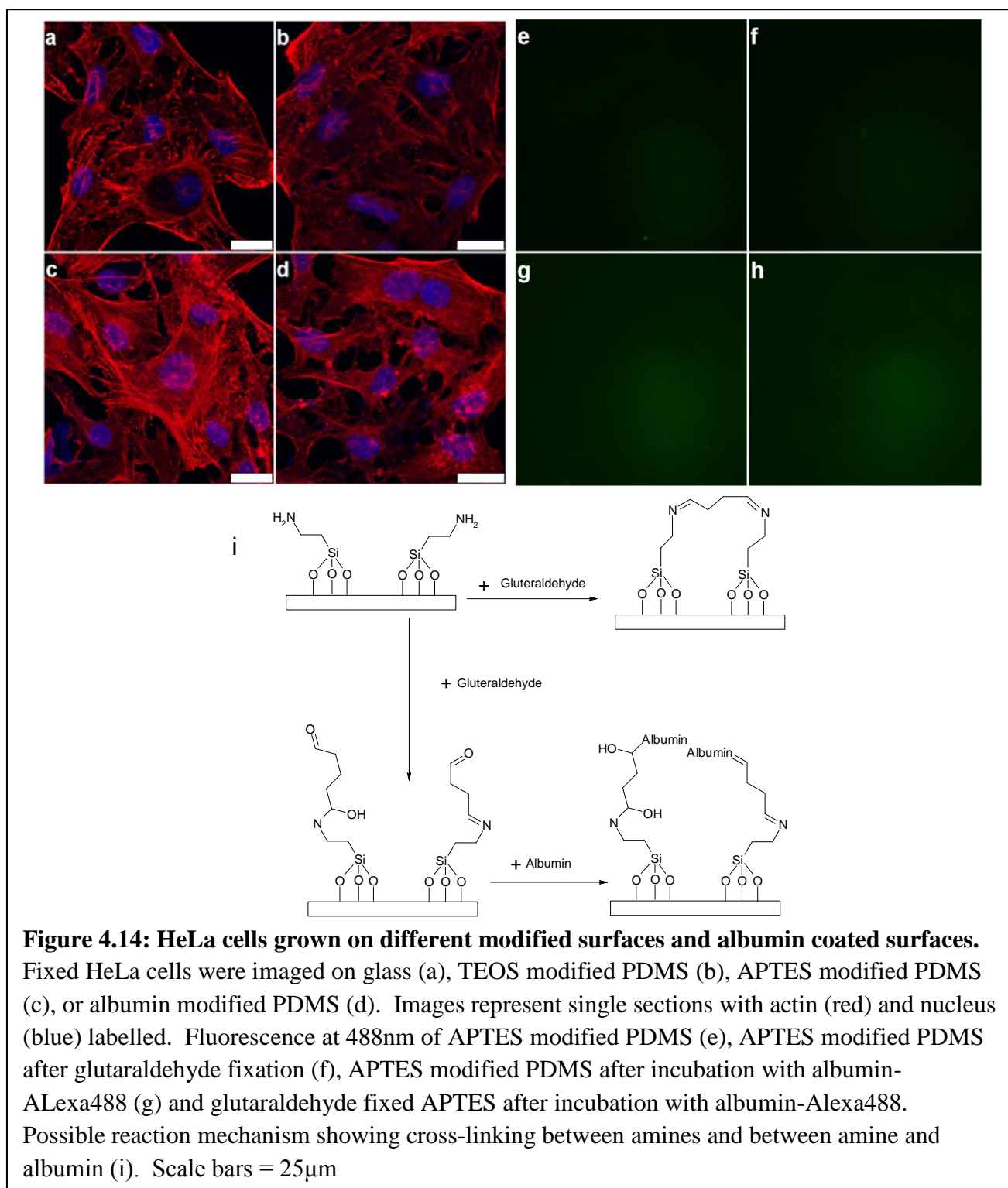
APTES modified PDMS provided a surface that gave similar cell morphology to cells grown on glass. The surface of glass normally has a neutral charge, whereas the amine group of the APTES modified glass is protonated at physiological pH and so carries a positive charge. TEOS is a silane which can be used to form thin layers across an activated surface providing a different surface with which to test. In the presence of water and on a suitably activated surface, siloxane bonds formed between TEOS molecules in this thin layer, can hydrolyse forming hydroxyls (Kim *et al.*, 1999). This could provide a more suitable surface for cell attachment.

An alternate method for helping cells bind to a surface is coating the surface with proteins. Using the amine from APTES, it could be possible to cross-link

between proteins and the surface amine using fixatives such as glutaraldehyde (figure 4.14i).

Cells grown on APTES and TEOS modified PDMS surfaces showed a similar morphology to cells grown on glass (figure 4.14a-d). However, cells grown on the albumin modified surfaces showed a poorer morphology. This could be due either to cells not binding to albumin or glutaraldehyde cross-linking between the amine moieties of the APTES modified PDMS. This cross-linking would provide an additional hydrophobic alkane chain between the amines potentially masking the surface amine (figure 4.14i).

To understand which of these options is responsible for the observed effect fluorescently labelled albumin was cross-linked using glutaraldehyde to an APTES modified surface (figure 4.14e-h). Images showed a slight increase in fluorescence in the samples exposed to albumin-Alexa488 but no difference between the APTES control and the APTES plus glutaraldehyde sample. This indicates that cross-linking between the amine and the albumin was unlikely to have occurred whilst fluorescence on the surface would be produced by albumin that had been adsorbed onto the surface. Cell imaging also shows poor cell morphology suggesting that glutaraldehyde has cross-linked between the amine of the APTES rather than between the APTES and albumin.

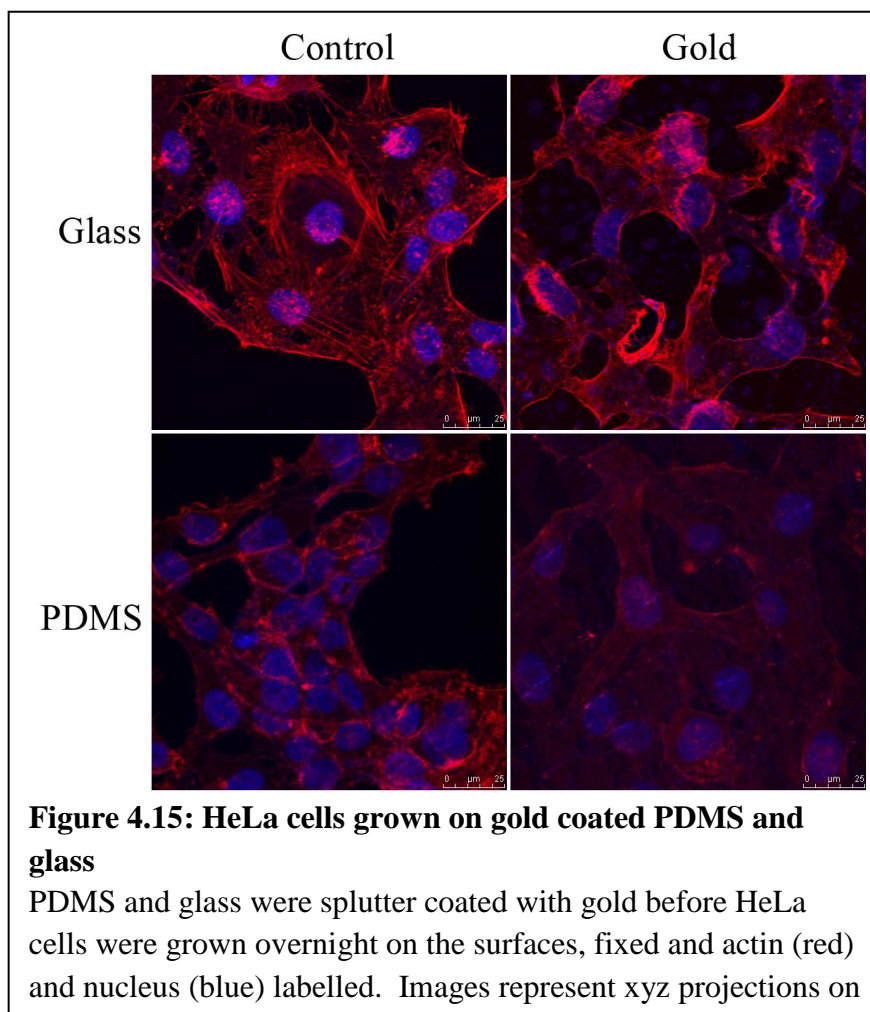


Modification of PDMS surfaces using UV/Ozone treatment produced an activated surface for silane chemistry. Although a variety of surfaces were produced using different silane functionalisations, simple surfaces such as amine from APTES or siloxane/hydroxyl from TEOS were the most successful surfaces for cell attachment. UV/Ozone treatment on its own produces a hydroxyl surface but studies have shown hydroxyl groups produced during hydroxylation of the surface either by plasma etching or to a lesser extent plasma etching react with each other returning the PDMS to its natural state (Berdichevsky *et al.*, 2004). It is therefore imperative that some form of surface chemistry is performed to keep the surfaces suitable for cell growth.

#### ***4.2.2.2 Thin layer coating***

The easiest and simplest form of modifying glass slides was to spin-coat them. This provides a modifiable thin layer on to which cells can grow .

Gold surfaces are naturally hydrophobic. Sputter coating PDMS or glass with gold can produce a thin layer on which cells should not be able to adhere. Cells grown on glass showed normal morphology whilst cells grown on PDMS are in closer proximity to each other and lack proper adhesion and morphology (figure 4.15). Cells grown on both the gold modified PDMS and gold modified glass surfaces showed poor adhesion and morphology. Gold coated glass showed cells of a morphology typical of cells on a more hydrophobic surface, whilst cells grown on gold coated PDMS, showed better morphology than those grown on PDMS alone, but again the morphology is poor. It was hoped



gold would provide a cytophobic surface where cells would find it difficult to attach. Instead there was an improved adhesion over plain PDMS marking no overall improvement in the prevention of cells growing on the surface. There was also an increase in background fluorescence from the gold at UV excitation levels, further discouraging the use of gold to prevent cell adherence.

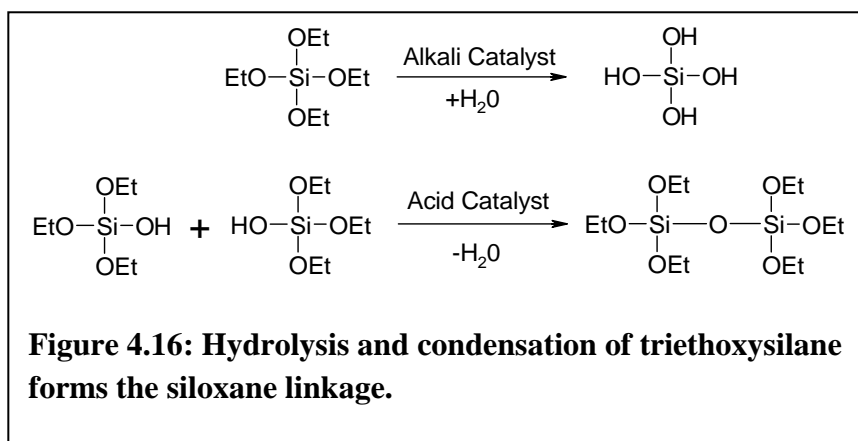
#### 4.2.3 Interpenetrating Network

Interpenetrating networks (IPN) provide a secondary polymer interweaved within a primary polymer as a means to change the properties of the primary polymer. Using an IPN it is possible to create a hydrophilic polymer inside the

hydrophobic PDMS (Abbasi *et al.*, 2006). Two methods researched were to create an interpenetrating polymer within the bulk silicone and the use of silanes to create a sol-gel within PDMS.

#### 4.2.3.1 Sol-Gel

Sol-gels are formed following hydrolysis and condensation of silanes (figure 4.16). By controlling the relative rate of the hydrolysis and condensation reactions it is possible to create different gel properties. By reducing pH, hydrolysis becomes the rate limiting step slowing the conversion of ethoxy side chains to hydroxyl side chains. This lack of hydroxyl groups slows down the condensation step producing a more ordered structure, this, in turn, produces a clearer gel.



A series of reactions were performed in order to optimise the production of a clear gel (figure 4.17). Two of the gels formed produced a clear disc after drying that had a very hydrophilic surface, whilst the other gels produced were less optically clear, readily cracking during drying. The dried discs, however, were very brittle and would therefore not be suitable for cell work. Although the brittleness was not quantified, the gel quickly lost structural integrity when

Sample	TEOS (ml)	EtOH (ml)	HCl (10mM, ml)	NH <sub>4</sub> OH (10mM, ml)	dH <sub>2</sub> O (ml)
A	0.5	0.5	0.25	0.25	0.5
B	0.5	0.25	0.25	0.25	0.25
C	0.5	0.5	0.5	0.5	0
D	0.5	0.25	0.5	0.5	0.25
E	0.5	0.5	0.25	0.5	0.25
F	0.5	0.25	0.25	0.5	0.5

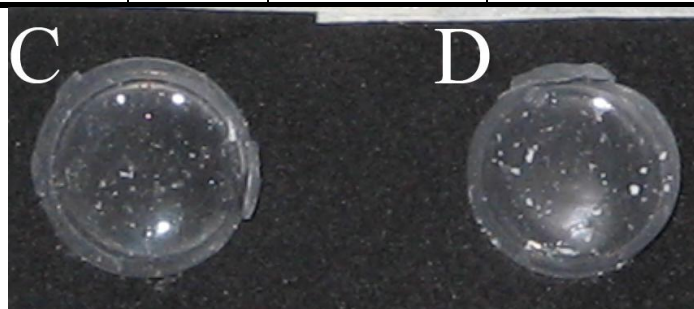


**Figure 4.17: Sol-gel reaction and dried gel**

Different concentrations of reactants were mixed (table) and allowed to gel overnight at 60°C to form sol-gel. Resulting gels were dried at room temperature for 24 hrs to form dried gel (image).

a small force was applied. They were more fragile than glass cover slips or PDMS polymers of a similar size and shape. This brittleness of the gel was a factor of the cross-linking between siloxane molecules and the speed at which the sample is dried. A more ordered structure would produce a stronger gel and this would be achieved by the slow removal of water from the gel.

However, attempts to achieve this strength did not produce a better gel and an alternative method was sought.

In order to improve gel strength, new gels were created incorporating DMDES as an alternative crosslinker. This gives rise to a material similar in structure to PDMS (figure 4.18). After 24 hrs only two samples formed a gel, one with only TEOS, and the other using a 3 : 1 ratio of TEOS : DMDES. Additional ammonium hydroxide was added to the remaining samples to try and increase gelation. Only one additional sample formed a gel, when equal amounts of TEOS and DMDES were used.



TEOS	1	0.75	0.5	0.25	0.2	0.1	0
DMDES	0	0.25	0.5	0.75	0.8	0.9	1
Gel – 24hrs	Y	Y	N	N	N	N	N
Gel – 48hrs	-	-	Y	P	P	N	N

**Table 4.18: Formation of sol-gel using TEOS and DMDES**  
TEOS and DMDES were mixed with 2.5 mM HCl and NH<sub>4</sub>OH in 2ml and allowed to gel at 50°C. After 24hrs an additional 200 µl of 10mM NH<sub>4</sub>OH were added to samples C-G and samples were allowed to gel for a further 24hrs at 50°C. Y indicates formation of gel, N, no formation of gel, and P partial formation of gel.

In all cases of gel formation the subsequent dried gel was brittle, whilst using an increasing proportion of DMDES in the gel produced increasingly more brittle gels. This would indicate that DMDES has a negative effect on gel morphology perhaps resulting from the formation of a less ordered structure. It was hoped that TEOS would form chains of hydroxyl terminated polydimethylsiloxanes whereas the TEOS would provide crosslinking between

these molecules. Alternate reactions were attempted in an attempt to provide a strong gel mix, these included reaction of DMDES on its own before adding TEOS at different rates. Interestingly the most useful reactions occurred with a high proportion of TEOS, indicating a possible lack of involvement of DMDES in the polymerisation.

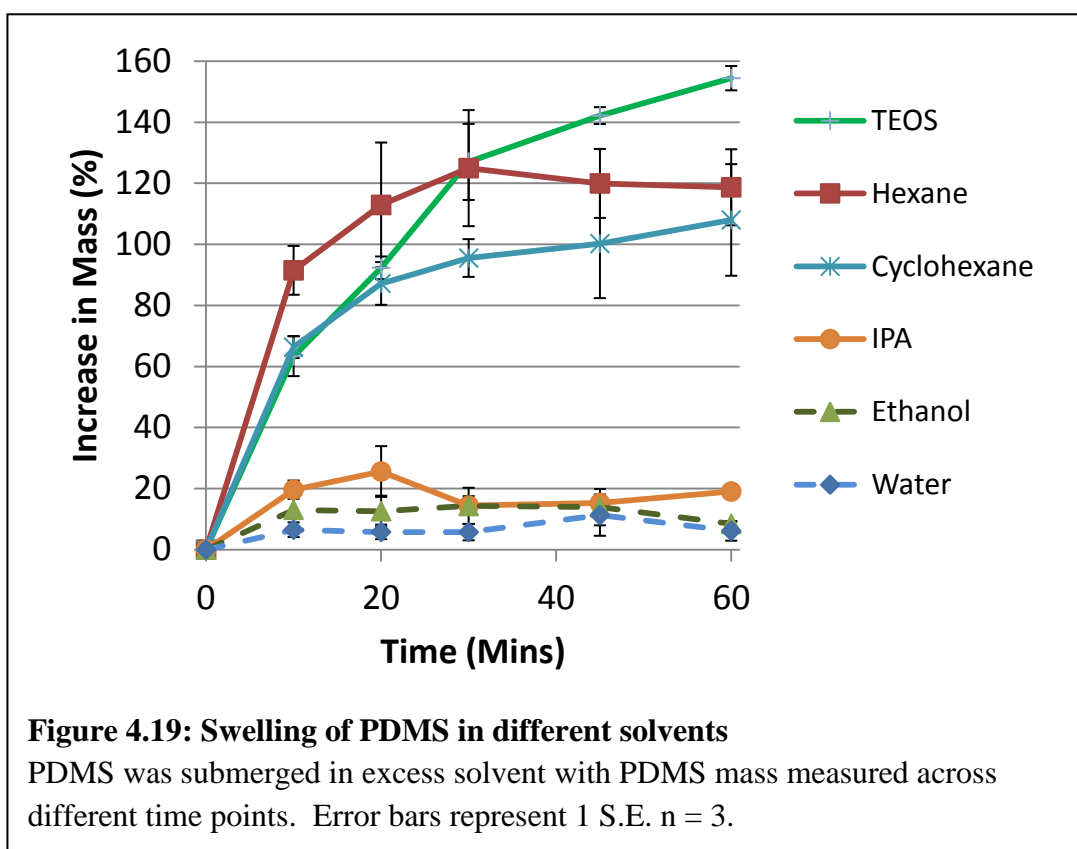
Producing a sol-gel for fluorescence cell imaging proved to be challenging. Most sol-gels, when dried, became too brittle to be suitable, although it was possible to make an optically clear gel that was suitable hydrophilic. Whilst forming a sol-gel material proved too challenging, it may be possible to use the sol-gel as a network within a stronger material.

#### *4.2.3.2 PDMS-Sol-Gel interpenetrating network*

Interpenetrating networks involve growing a polymer that interweaves within PDMS to change its bulk or surface chemical properties. Such networks can be grown either by modifying the pre-polymerisation PDMS solution or by introducing the secondary polymer (monomer) by using a good solvent to swell the PDMS. .

Swelling PDMS requires a solvent able to penetrate PDMS. Trying to introduce polar groups was inherently difficult due to the hydrophobicity of PDMS preventing uptake of charged molecules. Hydrophilic solvents like alcohol and water did not swell PDMS, whereas the hydrophobic compounds hexane and cyclohexane were easily absorbed into the PDMS (figure 4.19). TEOS (tetraethoxyorthosilicate) was also readily absorbed sharing a similar structure to PDMS itself. The ease at which TEOS was taken up by the PDMS suggested it was a suitable reagent for creating a sol-gel IPN within the PDMS.

Creating the sol-gel within the PDMS requires the reaction to occur within the



PDMS. Contact angle images of a TEOS in PDMS reaction showed no improvement in contact angle during different reaction lengths within the PDMS polymer (figure 4.20). The creation of a sol-gel network using this

method was not possible. This could be due to the high hydrophobicity of the internal PDMS structure preventing the polar alkali and acid catalysts from being taken into the PDMS polymer. Reaction of the TEOS requires a

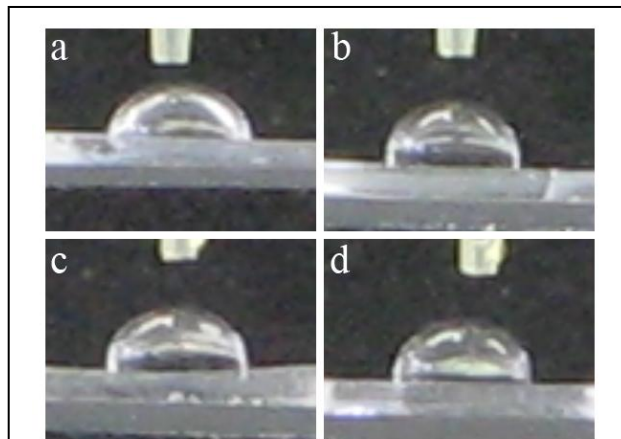


**Figure 4.20: Water droplets on IPN of TEOS sol-gel in PDMS**

PDMS was soaked in TEOS overnight before reacting in 2.5 mM  $\text{NH}_4\text{OH}$ , 2.5 mM HCl and 25% ethanol for 0 (a), 2 (b), 4 (c), or 6 (d) hours at  $60^\circ\text{C}$ . Gels were left overnight in excess neat ethanol before being imaged.

condensation step, producing water, which would also be unfavourable in these conditions. Using a different acid catalyst was also attempted, as well as supplementing TEOS before curing PDMS. In all these cases, a suitable sol-gel IPN was not produced.

An alternative method was devised where silica particles made from TEOS were added to PDMS before curing. This would provide a nucleation site for further reaction of the sol-gel network within the PDMS (figure 4.21). Contact angle images showed a reduction in contact angle after the formation of a sol-gel over untreated PDMS, indicating that a change in surface conditions had occurred. The silica particles produced were tested with cells and it was found

that cells endocytosed the fluorescent particles. Co-incubation of fluorescent particles with the HeLa cells showed perinuclear labelling similar to that found with lysosomal or late endocytic labelling. Cell morphology was altered as well with lamellipodial like structures around the periphery of the cell (see chapter 5) when cells are incubated with 0.5mg / ml and to a lesser extent 1mg / ml of fluorescent protein. At greater concentrations cells start to lose morphology, although this could be due to the large amounts of particles residing on the surface preventing the cells from binding properly.

Simple sol-gel chemistry proved unsuitable for either providing a substrate for

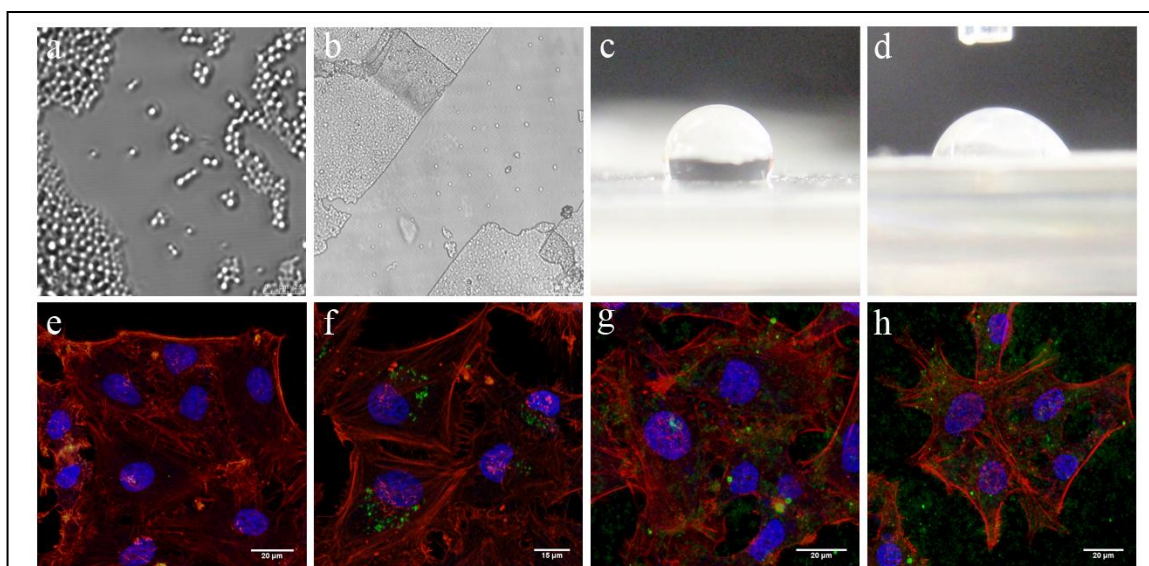


**Figure 4.21: Effect of silica beads on sol-gel IPN in PDMS and HeLa cells**

Silica beads (a) were mixed into PDMS before curing and sol-gel polymerised within PDMS (b). Images of contact angles on PDMS (c) and sol-gel IPN in PDMS (d). HeLa cells were co-incubated with untreated control (e), 0.5mg / ml (f), 1mg / ml (g) and 2mg / ml (h) fluorescein labelled particles (green) overnight before fixation and actin (red) and nucleus (blue) labelled. Images e-h represents xyz projections.

cell imaging or as an IPN within PDMS. Whilst it was possible to create a clear gel, the gels formed were brittle making them unsuitable for the constant handling which can occur during cell imaging. Attempts to improve the

strength relied on creating a crosslinked structure that contained PDMS like chains. This proved difficult to achieve in the time-scale but would have produced an easily modifiable gel and surface with which to work with.

Using the strength of PDMS to counteract the brittleness of the sol-gel proved possible but, again, unsuitable for cell work. Trying to make a sol-gel within the PDMS by allowing the reactants to swell the PDMS proved difficult to achieve, most likely due to the high hydrophobicity of the PDMS rubber.

Using silicone particles to nucleate sol-gel growth was more promising, however the undesired uptake of the particles into cells could lead to problems in subsequent applications although silicone particle uptake might be interesting as a cell delivery mechanism. Observations suggest that actin rearrangement has a role in the uptake indicating the particles that are either macropinocytosed or more likely phagocytosed.

### **4.3 Discussion**

#### **4.3.1 PDMS**

Cell imaging requires a suitable material which is non-fluorescent and optically clear. It must also be non-toxic to cells and provide a cytophilic surface and must not interfere with cell experiments by overstimulating the cell. Glass is often used for cell imaging as it complies with all of these conditions. However, to create a microwell array, we also needed a substrate with reduced autofluorescence (see chapter 3), can be treated with chemicals such as

fixatives and alcohols and be able to be ablated or molded to provide surface structures. One of the key materials we used in this study was PDMS. PDMS is non-fluorescent, optically clear, inert and can be easily molded or ablated but, however, it is a poor surface for cell attachment (Mata *et al.*, 2002). Methods were therefore sought to modify the material so that the surface was more conducive to cell attachment.

There are a number of ways to chemically modify the surface of PDMS. These include direct chemical reactions, such as hydrosilylation or silane chemistry, the introduction of interpenetrating networks within the PDMS or through the modification of the surface by chemical deposition or adsorption.

Two different methods were investigated to chemically modify the surface. Hydrosilylation, where PEG derivatives were covalently attached to the surface, and silane chemistry, where different silanes were used to directly modify an activated surface.

#### 4.3.2 Hydrosilylation

Hydrosilylation proved to be the less successful method of the two. By reacting vinyl groups with the surface it was possible to create a surface that was more cytophilic. A successful modification of the surface was possible but the hydrosilyl groups available in native PDMS proved too few with which to adequately perform the reaction. By increasing the amount of curing agent, it was hoped that more hydrosilyl groups would become available, using, a more hydrosilyl rich reactant proved to be successful. The greater number of

hydrosilyl groups allowed adequate attachment of vinyl terminated PEG to produce a change on the surface.

#### 4.3.3 Silinisation

Using silanes to modify the surface proved much more successful. In any silane chemistry, the first step is to activate the surface. Silicon rich substrates, such as glass and silicon wafers, are commonly activated by the strong hydrolysing solution containing hydrogen peroxide and hydrogen sulphide. Using this solution it is possible to create an active solution on which silane evaporation can be performed. Silane evaporation creates a uniform layer of silanes across the surface of the activated material providing multiple functional groups with which to perform further chemistry. Two different silanes were tested, DMDES, which produced a methyl surface and APTES, which produced an amine surface on glass. It was shown that amine modified surface provided a good surface on which to grow cells. Whereas the methyl modified surface prevented adequate attachment of adherent cells on to glass. It is difficult to verify the surface has changed. The most direct method is to measure the surface contact angle of water or other test solvents. Contact angle measurements can provide an indication of how hydrophobic or hydrophilic a surface is. A large change in contact angle indicates a change has occurred that has resulted in the surface becoming either more polar or more non-polar. Similarly, cell morphology experiments can provide great detail of the suitability of the surface for cell-surface attachment but cannot provide details of the full chemical nature of the surface. Using fluorescent markers can test for specific moieties on the surface but the downside is the relatively low

number of available bonds on the surface can make differences difficult to measure. Alternatives also have advantages and disadvantages. AFM measurements require a clean environment and minor changes of surface chemistry would be difficult to detect. The best way of measuring a chemical reaction would be to use FTIR spectroscopy. However, the reaction is only on the surface providing a thin layer against the large thickness of the glass or polymer being measured with which to test. Specialist set-ups would be required to test the surface, normally involving the reflection of the infra-red from the surface of the material. Although it was not possible to directly measure changes of the surface chemistry in this project, secondary measurements provided strong indications that changes to surface chemistry has occurred. With the main aim of providing surfaces that are both strongly suited and not suited to cell adhesion, cell morphology assays provides the best indication of whether a surface is suitable or not.

#### 4.3.4 Interpenetrating Network

The alternative method for modifying PDMS was using an interpenetrating network. Whilst it was possible to create optically clear sol-gels that had hydrophilic surfaces, dried gels proved to be brittle. Using PDMS to provide strength, it was speculated that it would be possible to create a sol-gel IPN within PDMS. This would provide a hydrophilic surface that can be easily modified further using silane chemistry. Direct reactions within PDMS proved difficult to produce. This was most likely due to the high hydrophobicity of the internal environment within the silicone rubber. This would prevent polar molecules such as the acid and base catalysts from entering the rubber whilst

also making it energetically unfavourable for the condensation reaction to occur. This was overcome by using small silica particles as nucleation points from which to grow the gel within the PDMS polymer. Whilst a sol-gel IPN was produced using this method, any silica beads escaping from the PDMS polymer would have an effect on cell morphology and endocytosis studies. Silica beads have been used to deliver drugs into the cell and this potential was shown using fluorescent silica beads which localised to a region deep within the cell, typically where the lysosome is found. Although beyond the scope of this project it would be interesting to investigate the use of these beads, what the uptake mechanism is and what effect they could have when attached to functional peptides similar to those used in Chapter 4.

#### 4.3.5 Conclusions

Overall, surface modification of PDMS is necessary because of its hydrophobic nature which prevents proper cell adhesion. Directly modifying the surface by activating the surface followed by reaction with silanes such as APTES or TEOS can provide a suitable surface for cell adhesion with few visible effects on cell morphology.

**4.4 References**

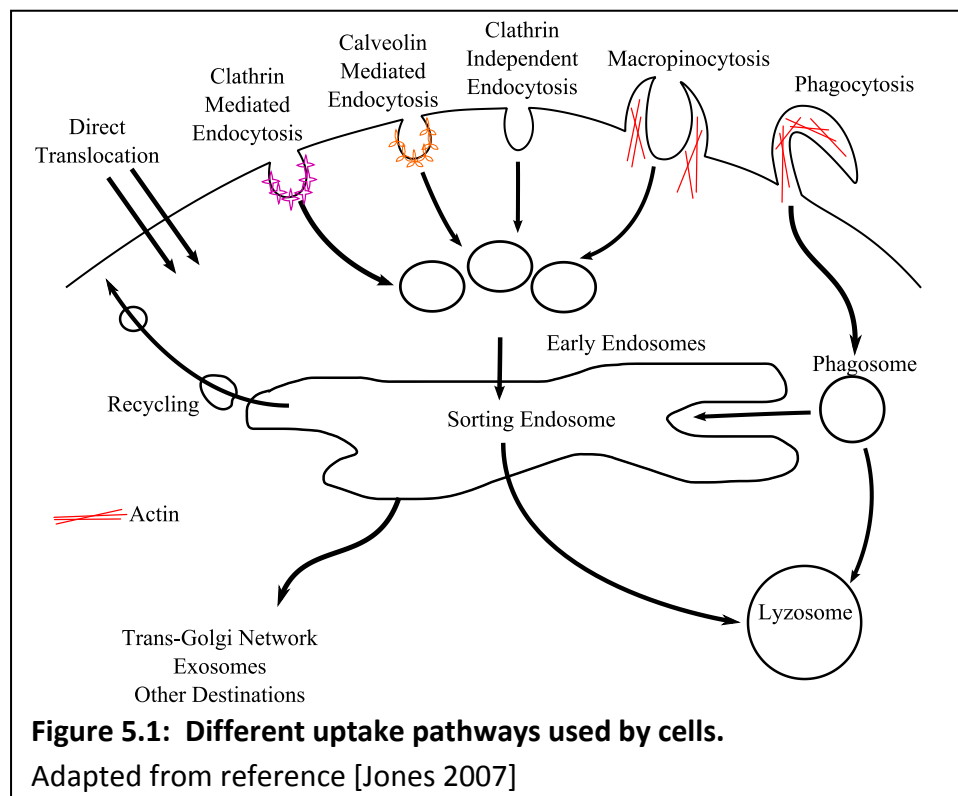
- ABBASI, F., MIRZADEH, H. & SIMJOO, M. (2006) Hydrophilic interpenetrating polymer networks of poly(dimethyl siloxane) (PDMS) as biomaterial for cochlear implants. *J Biomater Sci Polym Ed*, 17, 341-55.
- BERDICHEVSKY, Y., KHANDURINA, J., GUTTMAN, A. & LO, Y. H. (2004) UV/ozone modification of poly(dimethylsiloxane) microfluidic channels. *Sensors and Actuators B-Chemical*, 97, 402-408.
- GUO, D. H., HM; JING-WANG; XIAO, SJ; DAI, ZD (2007) Surface-hydrophilic and protein-resistant silicone elastomers prepared by hydrosilylation of vinyl poly(ethylene glycol) on hydrosilanes-poly(dimethylsiloxane) surfaces. *Colloids And Surfaces A-Physicochemical And Engineering Aspects*, 308, 129-135.
- HAHN, J. H., MAKAMBA, H., KIM, J. H., LIM, K. & PARK, N. (2003) Surface modification of poly(dimethylsiloxane) microchannels. *Electrophoresis*, 24, 3607-3619.
- HEYRIES, K. A., MARQUETTE, C. A. & BLUM, L. J. (2007) Straightforward protein immobilization on Sylgard 184 PDMS microarray surface. *Langmuir*, 23, 4523-7.
- KIM, G.-D., LEE, D.-A., MOON, J.-W., KIM, J.-D. & PARK, J.-A. (1999) - Synthesis and applications of TEOS/PDMS hybrid material by the sol-gel process. - 13, - 372.

- LEE, J. N., PARK, C. & WHITESIDES, G. M. (2003) Solvent compatibility of poly(dimethylsiloxane)-based microfluidic devices. *Anal Chem*, 75, 6544-54.
- LI, G. P., HU, S. W., REN, X. Q., BACHMAN, M., SIMS, C. E. & ALLBRITTON, N. (2002) Surface modification of poly(dimethylsiloxane) microfluidic devices by ultraviolet polymer grafting. *Analytical Chemistry*, 74, 4117-4123.
- MATA, A., BOEHM, C., FLEISCHMAN, A. J., MUSCHLER, G. & ROY, S. (2002) Growth of connective tissue progenitor cells on microtextured polydimethylsiloxane surfaces. *Journal of Biomedical Materials Research*, 62, 499-506.
- MCDONALD, J. C., DUFFY, D. C., ANDERSON, J. R., CHIU, D. T., WU, H. K., SCHUELLER, O. J. A. & WHITESIDES, G. M. (2000) Fabrication of microfluidic systems in poly(dimethylsiloxane). *Electrophoresis*, 21, 27-40.
- MUNOZ, J. L., DEYHIMI, F. & COLES, J. A. (1983) Silanization of glass in the making of ion-sensitive microelectrodes. *J Neurosci Methods*, 8, 231-47.
- OLAH, A., HILLBORG, H. & VANCISO, G. J. (2005) Hydrophobic recovery of UV/ozone treated poly(dimethylsiloxane): adhesion studies by contact mechanics and mechanism of surface modification. *Applied Surface Science*, 239, 410-423.
- RAO, H. & ZHANG, Z. (2012) - Preparation, characterization, and permeation property of a liquid crystal/PDMS membrane material. - 123, - 199.

- SABRI, S., SOLER, M., FOA, C., PIERRES, A., BENOLIEL, A. & BONGRAND, P. (2000) Glycocalyx modulation is a physiological means of regulating cell adhesion. *J Cell Sci*, 113 ( Pt 9), 1589-600.
- SAGE, D., STALDER, A. F., KULIK, G., BARBIERI, L. & HOFFMANN, P. (2006) A snake-based approach to accurate determination of both contact points and contact angles. *Colloids And Surfaces A- Physicochemical And Engineering Aspects*, 286, 92-103.
- WHITESIDES, G. M., MCDONALD, J. C., DUFFY, D. C., ANDERSON, J. R., CHIU, D. T., WU, H. K. & SCHUELLER, O. J. A. (2000) Fabrication of microfluidic systems in poly(dimethylsiloxane). *Electrophoresis*, 21, 27-40.
- ZHANG, T. Y., LIN, F., SONG, M. Z. & HE, Z. Z. (2008) Synthesis and structural characterization of methacrylic acid/octadecyl acrylate-graft-poly(methylhydrosiloxane) by hydrosilylation. *Journal of Applied Polymer Science*, 107, 3773-3780.

## 5. Live Cell Microscopy and Cell Penetrating Peptides

The previous chapter looked at the suitability of a range of materials for sectioning and for cell imaging. This chapter investigates methods for microscopic analysis of the dynamics of cell penetrating peptides (CPPs) in cells and specifically the role of a specific endocytic pathway called macropinocytosis in uptake of CPPs. Finally the techniques developed allowed for investigations into the mechanism of action of CPP-peptide chimeras that have been described to promote apoptosis in cells.



## **5.1 Introduction**

### **5.1.1 Macropinocytosis**

Cell uptake of macromolecules occurs through a variety of pathways (figure 5.1), depending on the demands of the cell. Uptake pathways differ in the protein machinery involved in their regulation, the size of the endosome formed, the molecules that are internalised and their final subcellular fate or in some case their recycling out of the cell. Cell uptake can be generally divided into two classifications, endocytosis and phagocytosis. Endocytic uptake may involve recruitment of coat proteins such as clathrin to the plasma membrane and the clathrin mediated pathway represents the most well studied uptake route (Doherty and McMahon, 2009). However a number of other clathrin independent pathways exist, such as those regulated by other proteins, for example, caveolin and flotillin. Invaginations formed from these uptake routes bud to form endosomal vesicles, typically <120nm in diameter that are then transported to endosomal sorting stations that then mediate traffic to a range of other cellular locations such as lysosomes or the *trans*-Golgi network. Larger molecules need to be internalised using different processes and phagocytosis defines the method by which bacteria, apoptotic cells and other large particles are internalised. With the exception of macropinocytosis (described below), phagocytosis, unlike other endocytosis pathways, uses a mechanism that involves large protrusions of the cell membrane, engulfing and internalising large particles forming the phagosome. Upon internalisation, the phagosome often fuses with the

lysosome forming a phagolysosome, allowing the contents to be degraded (Luzio *et al.*, 2007). Phagocytosis is limited to a few cell types, such as macrophages and dendritic cells, which swallow large particles for degradation as part of the immune system and for degradation of apoptotic and dead cells.

Macropinocytosis has been mostly characterised as a manifestation of the membrane of cells in response to growth factors such as epidermal growth factor (EGF) and platelet-derived growth factor (PDGF) (Jones, 2007). Like phagocytosis, macropinocytosis involves plasma membrane remodelling; this normally occurs in the form of membrane ruffling. Ruffles allow the membrane to engulf extracellular fluids by forming large cups which close around the extracellular matter and allow the cells to take in these fluids. When macropinocytosis is occurring there is therefore an increase in the uptake of fluid phase endocytic probes such as dextran and horseradish peroxidase.

Macropinocytosis is regulated by a range of different proteins. Actin filaments are required to provide a backbone for the ruffles, providing the shape and flexibility, whilst another cytoskeletal component, myosin, interacts with the actin to provide the movement needed to engulf this extracellular material (Lee and Knecht, 2002). Proteins, such as the Rab family proteins, cdc42 (cell division control protein 42) and Rac1 (Ras-related C3 botulinum toxin substrate 1) are involved in this actin remodelling through interaction with Pak-1. Pak-1 (p21-activated kinase 1) has been shown to be

heavily involved in the regulation of macropinocytosis (Liberali *et al.*, 2008). Depletion of Pak-1 reduces membrane ruffling and can prevent the actin polymerised circular dorsal ruffles, whilst having no effect on clathrin-mediated endocytosis (Karjalainen *et al.*, 2008).

### 5.1.2 Cell Penetrating Peptides

Cell penetrating peptides (CPPs), or protein transduction domains as they are also known, have been shown to be able to enter cells but also have the capacity to co-internalise a range of different cargo molecules such as DNA, RNA, peptides and proteins into (Dietz and Bahr, 2004) (Fawell *et al.*, 1994) (Meade and Dowdy, 2007). Several of these have therapeutic potential thus raising the profile of these entities from being of general interest to being candidate drug delivery vectors. Hundreds of CPPs sequences have now been listed and these range from being highly hydrophobic to extremely cationic. As a result they are unlikely to have a common mechanism and detailed uptake analysis has only been performed on a few such as HIV-TAT and octaarginine (R8) (Heitz *et al.*, 2009). R8 has been shown to enter through endocytosis and direct translocation at 37°C but the peptide has also been shown to be able to translocate the plasma membrane at 4°C, *i.e.* when energy requiring uptake mechanisms are shut down. Depleting the membrane of cholesterol and has also shown to affect the uptake mechanism of octaarginine and there are also differences in uptake dynamics between cells from different tissues (Watkins *et al.*, 2009a) (Mueller *et al.*, 2008). One suggested mechanism of uptake of CPPs is through macropinocytosis (Snyder and Dowdy, 2004), which differs from endocytosis in a variety of

ways. Macropinosomes are not coated, they are larger (typically  $>1\mu\text{m}$  compared to 100nm for endosomes) and are formed by ruffling extrusions (Swanson and Watts, 1995). Ruffling has been shown in a variety of cell lines and can be induced using growth factors such as EGF, which is known to have an effect within 30 seconds and at concentration as low as 80nM (Meier *et al.*, 2002). To support a role for macropinocytosis in CPP uptake actin rearrangement was shown to occur when oligoarginines are added to cells (Futaki *et al.*, 2007). The uptake of dextran, was also shown to be enhanced by HIV-TAT (Kaplan *et al.*, 2005). Additionally, the use of inhibitors of macropinocytosis, such as amiloride and Wortmannin, reduced uptake of octaarginine in HeLa cells (Nakase *et al.*, 2004). Both TAT and octaarginine can induce Rac and F-actin rearrangement in lamellipodia (Nakase *et al.*, 2007). Rac activation was shown to occur five minutes following peptide addition with lamellipodia formation occurring within three minutes. There is however some controversy regarding the role of this pathway in CPP uptake and this may relate to the fact that drugs used to study macropinocytosis can have other effects on cells (Fretz *et al.*, 2006) (Jones, 2007). For example the amiloride analogue EIPA is also a powerful macropinocytosis inhibitor but the drug also inhibits albumin uptake (known to be internalised by endocytosis)

CPPs have now been studied for a number of years as delivery vectors for bioactive peptides and this falls under the remit of peptide therapeutics (Bidwell and Raucher, 2009, Mason, 2010). These include peptides that act inside cells to promote apoptosis and these are mainly studied as potential

anti-cancer drugs. A number of proapoptotic peptides have now been described and based on their sequence, some appear to be CPP in their own right. One example is the Proapoptotic Domain Peptide PAD (also known as KLA). This has the sequence (KLAKLAK)<sub>2</sub> and was originally discovered as an antimicrobial peptide (Javadpour *et al.*, 1996). It has relatively low toxicity in mammalian cells but inside cells the Lysines exposed in an  $\alpha$ -helix arrangement are predicted to interact with and damage mitochondrial membranes (Marks *et al.*, 2005) and thus promote apoptosis. This study also demonstrated this *in vivo* when targeted to different cell types in mouse models (Mai *et al.*, 2001).

Peptides used in this study are described below:

Unlabelled peptides	Sequence
r8	rrrrrrrrGC
R8	RRRRRRRRGC
gS <sub>4</sub>	gsgsgsgsGC
PAD	klaklakklaklakGC
r8-PAD	rrrrrrrr-GG-klaklakklaklakGC
fsr-l-r8	fsrslhslIG-X-rrrrrrrrGC
asr-a-r8	asrslhslaG-X-rrrrrrrrGC
asr-l-r8	asrslhslIG-X-rrrrrrrrGC
Fluorescent peptides	Sequence
r8-Alexa488	rrrrrrrrGC-Alexa488
r8-PAD-Alexa488	rrrrrrrr-GG-klaklakklaklakGC-Alexa488

### 5.1.3 Cell Death and Associated Cell Blebbing

Membrane blebbing can occur in different ways and for different reasons. Blebs can form as a way of helping cells move by releasing the plasma membrane to form a bleb and redistributing the actin internally (Fackler and Grosse, 2008). Similarly, blebs occur during cell division as a way of increasing the membrane surface area of the cell before division (Laster and Mackenzie, 1996). As such these blebs have been shown to contain filamentous actin and

have internal contents not dissimilar to the cytosol. Blebs can also form during apoptosis and different intracellular structures and macromolecules are compartmentalised into blebs before they can be released for safe phagocytic uptake by phagocytes (Utani *et al.*, 2011). During cell necrosis, large blebs form on the surface as the membrane dissociates from the cytoskeleton beneath it. Often these blebs can rupture leading to the uncontrolled release of intracellular contents and cell death (Laster and Mackenzie, 1996).

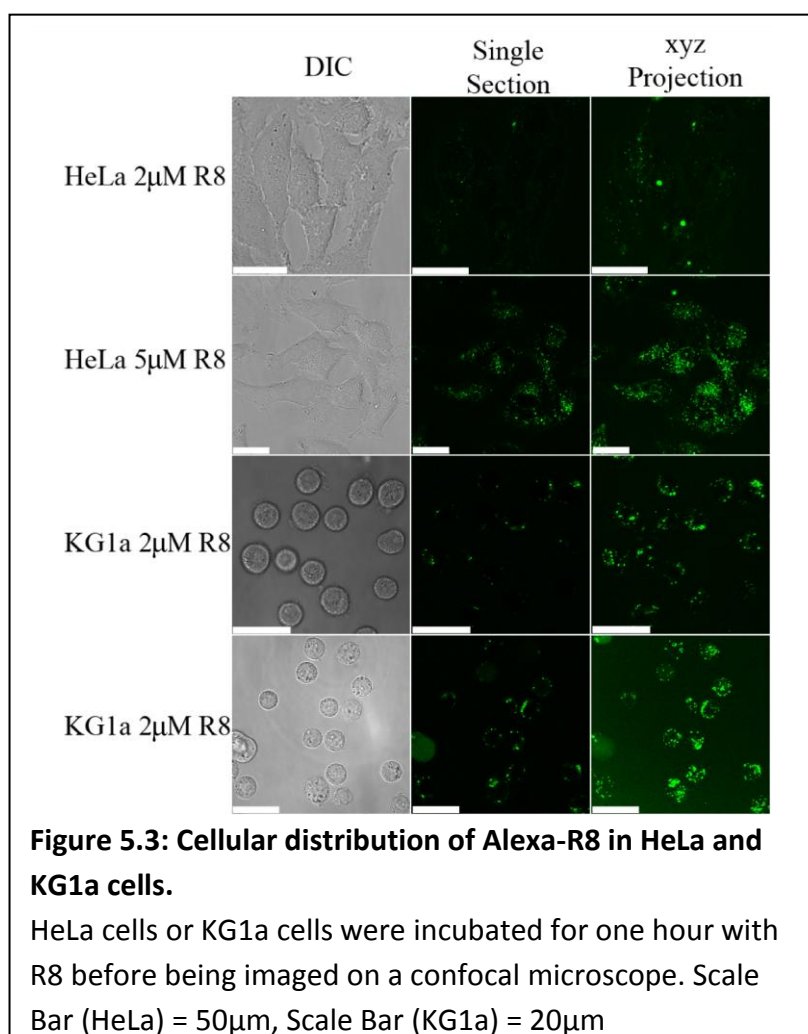
#### 5.1.4 Aims

The aim of this chapter is to further investigate the role of macropinocytosis in the uptake of octaarginine and to extend this to studies using this peptide extended with the PAD sequence. This chapter will also look at two different pro-apoptotic peptides, r8-PAD and the Bcl-2 targeting peptide fsr-l-r8. Focus will be on investigating the effects of these peptides on the plasma membrane with a view to elucidating their mechanism of uptake. To aid these studies use will be made of the microwells described in Chapter 3 to image and retain acute myeloid leukaemia KG1a cells during exposure to the Bcl-2 targeting peptide and its control.

## 5.2 Results

### 5.2.1 Uptake of Octaarginine

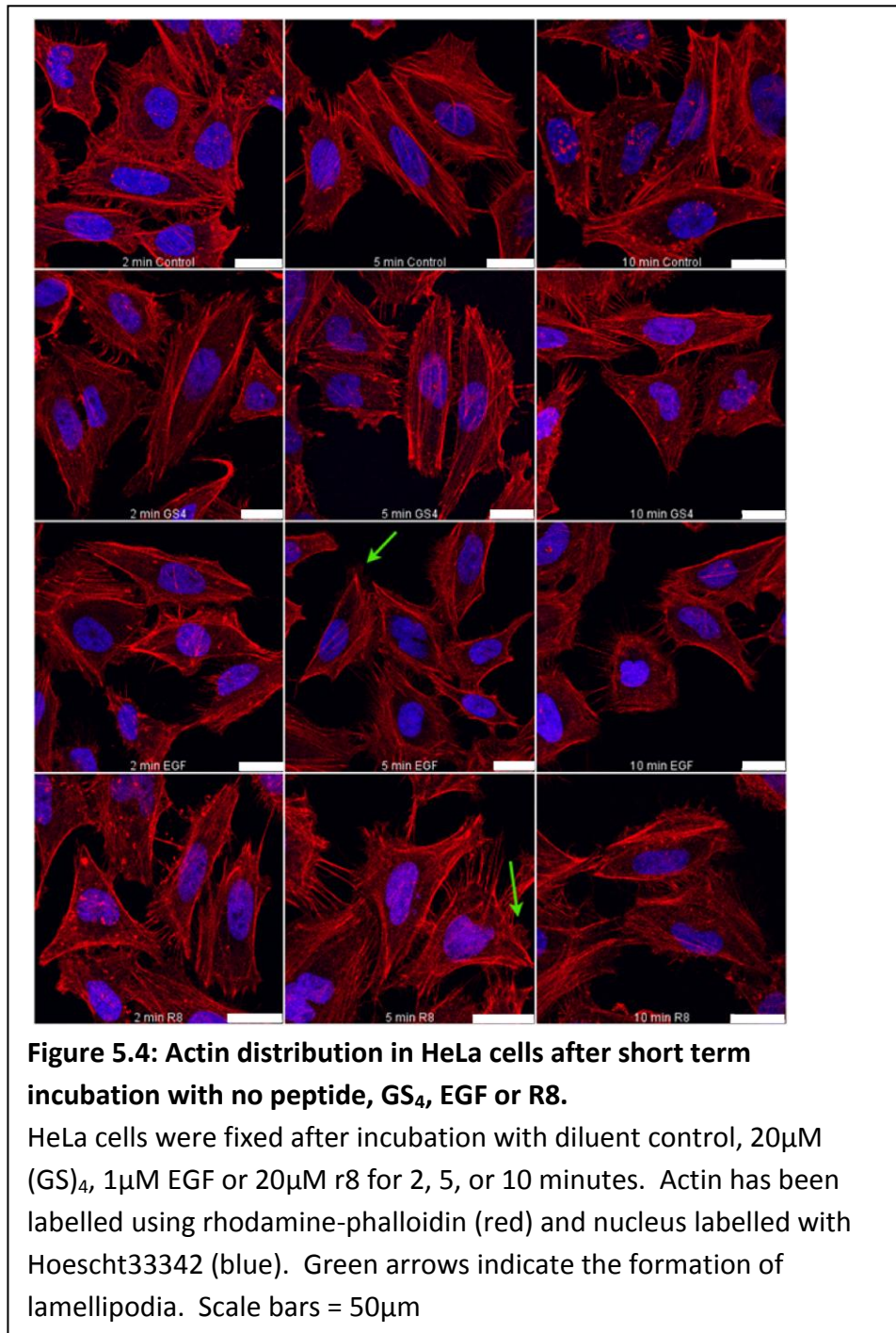
Octaarginine is a commonly used CPP and it has been suggested that there is a possible role of macropinocytosis in the uptake of this peptide. Macropinocytosis requires actin polymerisation to extend ruffles of membrane that envelope extracellular content which can be subsequently taken up by the cell. Uptake has shown to be reduced with macropinocytosis inhibitors EIPA and wortmannin (Nakase *et al.*, 2004). EIPA inhibits Na<sup>+</sup>/H<sup>+</sup> exchange protein of the plasma membrane, this lowers cytoplasmic pH which



reduces ruffling (Swanson and Watts, 1995). Wortmannin on the other hand, inhibits phosphoinositide-5-kinase, inhibition of PI-5-kinase prevents the closure of surface ruffles preventing the formation of macropinosomes (Araki *et al.*, 1996). The data in Figure 5.3 shows that fluorescently labelled octaarginine localised to tight punctate structures in adherent and non-adherent cell types following incubation at 37°C. This profile is typical of endosomal labelling and has been previously described in these two cell types (Watkins *et al.*, 2009b). Endosomal labelling indicates endocytosis had occurred, although distinguishing between the different endocytic routes by imaging fluorescent R8 alone was not possible. Co internalisation studies of R8 and the clathrin-mediated endocytosis marker transferrin showed little colocalisation indicating another form of endocytosis is used by the cell to internalise this peptide (Nakase *et al.*, 2004).

#### 5.2.2 Stimulation of Macropinocytosis by EGF and Octaarginine

Growth factors such as PDGF and EGF have been shown to stimulate macropinocytosis in cell lines such as A431, a human squamous carcinoma cell line, showing increases in surface ruffling when exposed to these growth factors. Actin remodelling has also been demonstrated in HeLa cells in response to EGF and octaarginine (Nakase *et al.*, 2004). Actin remodelling, along with inhibition studies, would give a strong argument for the role of macropinocytosis in uptake of octaarginine.



HeLa cells were therefore incubated with r8, EGF or a control peptide GS4

prior to fixing and labelling of the actin cytoskeleton with rhodamine phalloidin. Figure 5.4 shows that HeLa cells fixed after incubation with 20 $\mu$ M r8 or 1 $\mu$ M EGF showed a slight increase in the recruitment of f-actin to the periphery of the cell (figure 5.4) when compared with untreated cells or cells treated with GS<sub>4</sub>. The effect was most pronounced in EGF stimulated cells that had been incubated with the growth factor for five minutes. In control cells actin filaments formed a web around the edge of the cell with occasional extrusions of filopodia in localised regions of the cell and in between cells. In EGF and r8 incubated cells there were some lamellipodia formations with a

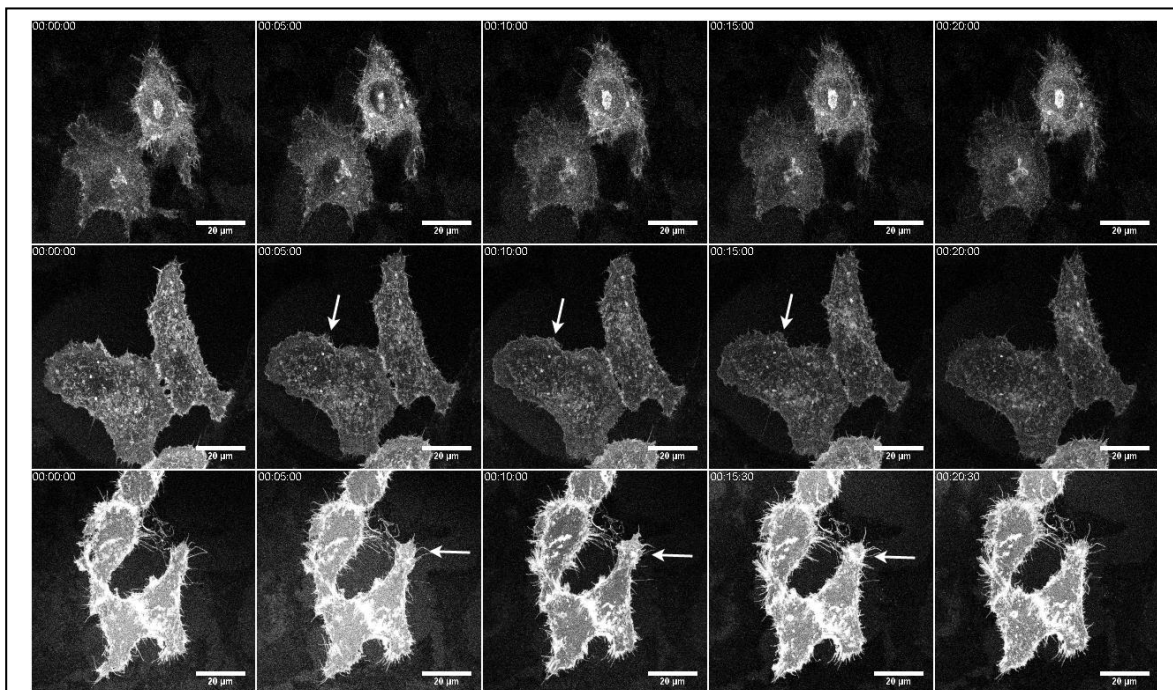


**Figure 5.5: GPI-GFP transfected HeLa cells incubated with GS<sub>4</sub>, r8 or EGF.**

HeLa cells have been transfected with a plasmid encoding GPI-GFP, which labels the plasma membrane before being exposed to 20 $\mu$ M GS<sub>4</sub> (top), 1 $\mu$ M EGF (middle) or 20 $\mu$ M r8 (bottom). Images represent an xyz projection taken on a confocal microscope using a resonant scanner with a new projection being taken every 30 seconds over half an hour. Arrow indicates lamellipodial extrusions. Scale bar = 20 $\mu$ m

greater amount of filopodia-like extrusions. With r8, however, this could be due to the shrinking of the cell in response to the large positive charge present due to the high concentration of this peptide.

Live cell imaging of plasma membrane ruffles was seen using HeLa cells transfected with the plasmid encoding the fluorescently labelled membrane

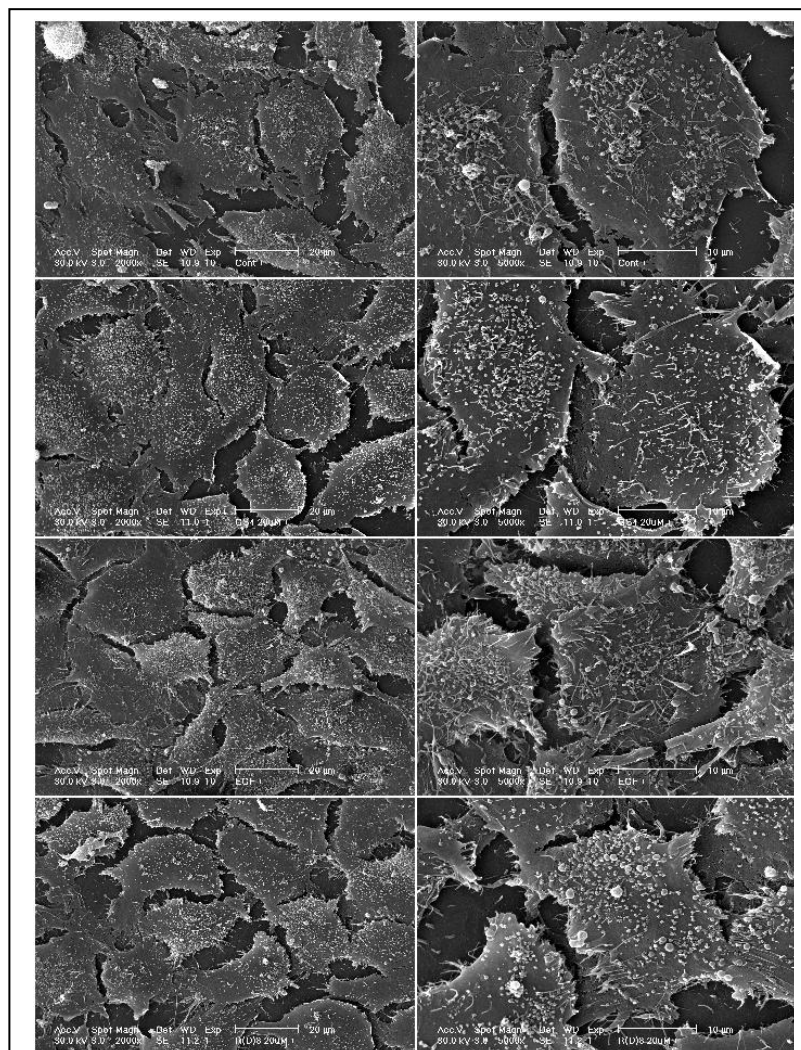


**Figure 5.6: Scanning electron micrographs of HeLa cells after short incubation with no peptide, GS<sub>4</sub>, r8 or EGF.** Cells were incubated for 10 mins with no peptide (top), 20 μM GS<sub>4</sub> (top-middle), 1 μM EGF (lower-middle) or 20 μM r8 (bottom) before fixation and preparation for SEM. Scale bars on left column = 20 μm, scale bars in right column = 10 μm

protein GPI-GFP (figure 5.5). When exposed to 1 $\mu$ M EGF, lamellipodia were seen extruding from the edges of the cells during the first 15 to 20 minutes after which the peripheral membrane reduces in activity. Exposure to 20 $\mu$ M r8 also produces localised lamellipodial activity at the cell periphery. There was less activity than that present during exposure to EGF but there was still an increase in this activity over the control peptide GS<sub>4</sub>. Interestingly there was little in the way of pseudopodia extensions in either EGF or r8 incubated cells, however pseudopodia are not strong evidence of macropinocytosis. Cells incubated with the control peptide showed these motile extensions moving around despite observations that this peptide does not internalise into HeLa cells (Fretz *et al.*, 2007). The reduction in these motile extensions after exposure to EGF or r8 could be due to a suppression of pseudopodia to enable better ruffling of the cell surface.

Fixed and live cell fluorescence imaging showed some evidence of membrane ruffling in both r8 and EGF exposed cells over the course of the first 15 minutes. Scanning electron micrographs of HeLa cells incubated with GS<sub>4</sub>, r8, EGF or without a stimulus for five minutes before fixation showed mixed results (figure 5.6). Overall cells that had not been incubated with any peptide showed a smooth surface whilst cells incubated with the control peptide showed small blebs on the surface. These effects were not consistent across the sample making it difficult to obtain an accurate impression. There was also little evidence of ruffling in the cells exposed to EGF, like the cells transfected with GPI-GFP; the effects were small but localised whilst visible

ruffling consisted of short, wide and sharp undulations on the surface of the cell. The CPP r8, however, showed little visible evidence of this ruffling with small blebs visible on the surface. During transfected cell experiments the ruffling was localised to only a couple of regions of the cell, this effect may make it harder to spot ruffling in the scanning electron micrographs of these cells. GPI-GFP was used here as a general marker of the plasma membrane but GPI linked proteins are most often associated with domains of the plasma membranes called lipid rafts (Lakhan *et al.*, 2009). The lack of major effects seen here may reflect that rafts are not as sensitive to the effects of CPPs and EGF as other areas of the plasma membrane.

### 5.2.3 Pro-apoptotic peptides and cell blebbing

#### *5.2.3.1 Plasma Membrane Blebbing*

Studies have shown that the treatment of cells with low levels of hydrogen peroxide induces the formation of different types of blebs, known as apoptotic and necrotic blebs (Barros *et al.*, 2003). At low hydrogen peroxide concentrations the majority of blebbing in HeLa and Clone 9 cells is apoptotic, whilst at higher concentrations (32mM) it was noticed necrotic blebs also forming (Sprague Dawley rat liver). There was also a time difference noted between the different types of blebbing, with apoptotic blebbing occurring during the first 20 minutes and necrotic blebbing occurring after one hour.

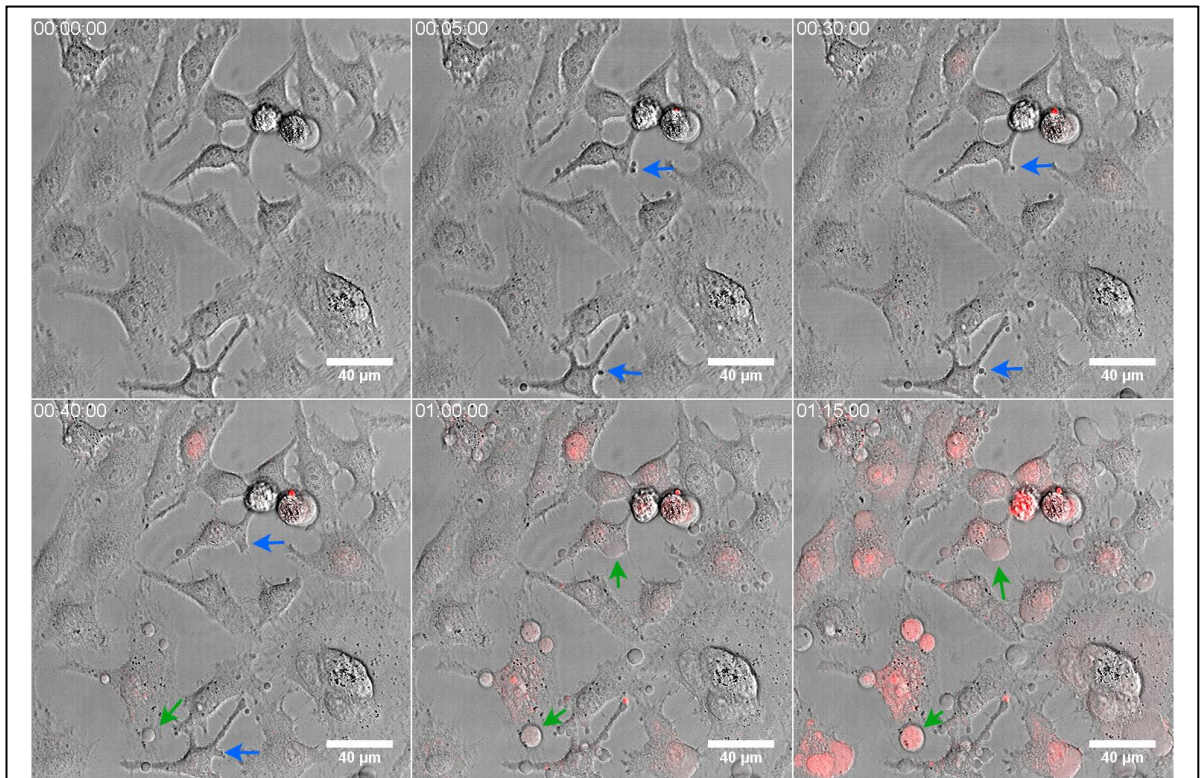


**Figure 5.7: Apoptotic and necrotic bleb formation in HeLa cells in response to hydrogen peroxide.**

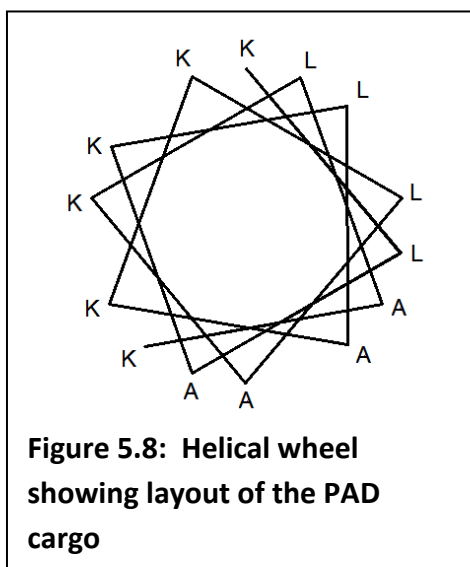
HeLa cells were continuously incubated with 32mM  $\text{H}_2\text{O}_2$  for 80 minutes with single section images taken on a confocal microscope every 30 seconds. Blue arrows show formation of apoptotic blebs whilst green arrows indicate necrotic blebs. Propidium iodide has been added as a marker of membrane integrity. All scale bars = 40µm.

Experiments were performed to investigate whether these blebs could be observed. For this, cells were treated with 32mM hydrogen peroxide to image the formation of both the apoptotic and necrotic blebs (figure 5.7). During the first five minutes, small 1-5µm blebs formed on the surface of a few cells, most of which later retracted. After an hour, cells started to become PI positive (indicative of membrane permeability) and larger necrotic blebs formed on the surface of these cells. The necrotic blebs become PI positive

along with the cell indicating permeabilisation of the plasma membrane had occurred.

#### 5.2.2.2 R8-PAD

The peptide sequence PAD is amphiphilic consisting of three different



residues (leucine, lysine and alanine) arranged in an  $\alpha$ -helix (figure 5.8), where the positively charged lysine line up opposite the hydrophobic leucine. Amphiphilic peptides have been shown to be strong antimicrobial agents, and were first discovered as such (Henriques *et al.*, 2006). However, it was noticed that these peptides can also produce apoptosis in cancer cells if the peptide can be effectively delivered into the cell. Attaching CPPs such as r8 and TAT, PAD has been shown to cause apoptosis in cancer cells (Ellerby *et al.*, 1999).

Cells incubated with 10  $\mu$ M r8-PAD-Alexa488 showed diffuse cytoplasmic labelling and strong labelling in the nucleolus after just 12 minutes (figure 5.9). Peptide uptake originated in specific regions on the plasma membrane

of the cell where the peptide accumulated before it flooded across the whole cell. This is immediately followed by the formation of large blebs (zeiosis) and these continued to grow in a uniform manner. After 45 minutes the cells become PI positive indicating membrane leakage.

If the cells were to become leaky as the peptide interacted with the plasma membrane, it would be expected that the cells would become PI positive at a much earlier stage. This did not seem to be the case and with no vesicular

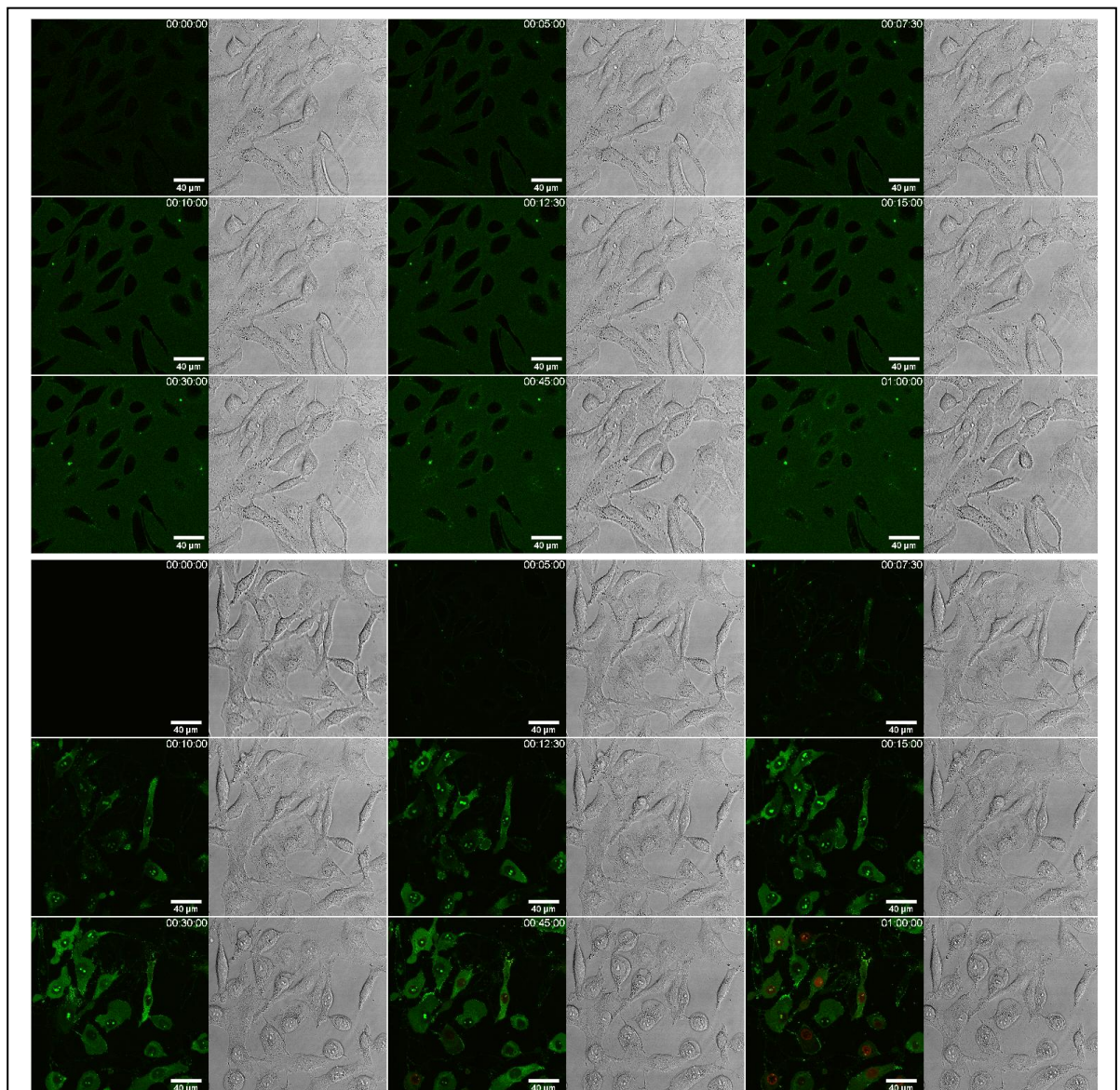


**Figure 5.9: HeLa cells incubated with 10 μM r8-Alexa488 or r8-pad-Alexa488**

Uptake of 10 μM Alexa488 labelled r8 (top) and r8-PAD (bottom) in HeLa cells over one hour. Propidium iodide (red) has been added as a marker for membrane integrity. All scale bars = 40 μm

labelling this peptide may have translocated directly across the membrane at this higher concentration. The zeiosis induced by the peptide also carried the hallmarks of necrosis. The blebs formed were large and grew at a constant rate, half an hour later the cells become PI positive as the membrane was breached and extracellular fluid flowed into the cell. Cells with the most peptide become PI positive first, whilst the surviving cells showed less uptake of the peptide.

Fixed cell imaging of HeLa cells allowed visualisation of actin distribution in cells exposed to different concentrations of r8-PAD after twenty minutes (figure 5.10). Cells incubated with 16 $\mu$ M r8 showed some recruitment of actin to the periphery of the cell when compared to those cells incubated with PAD, the (klaklak)<sub>2</sub> cargo alone. There was also some evidence of lamellipodia like extrusions emanating from the edge of the cell. PAD showed little actin recruitment to the periphery of the cell but showed some lamellipodia extrusions. Actin was strongly distributed around the edge of the cell at high concentrations of r8-PAD, although there was little evidence of lamellipodial extrusions. Whilst actin was recruited to the periphery of the cell, at higher concentrations of peptide the interior of the cell had fewer actin bundles resulting in more diffuse actin throughout.

The volume of nucleus was also measured in cells using ImageJ to calculate the cross-sectional area of each nucleus on each slice (see Section 2.28). This was performed because 3D reconstruction from confocal sections, of cells treated with this peptide seemed to indicate a possible increased nucleus volume in response to increasing r8-PAD concentrations. Measuring nucleus

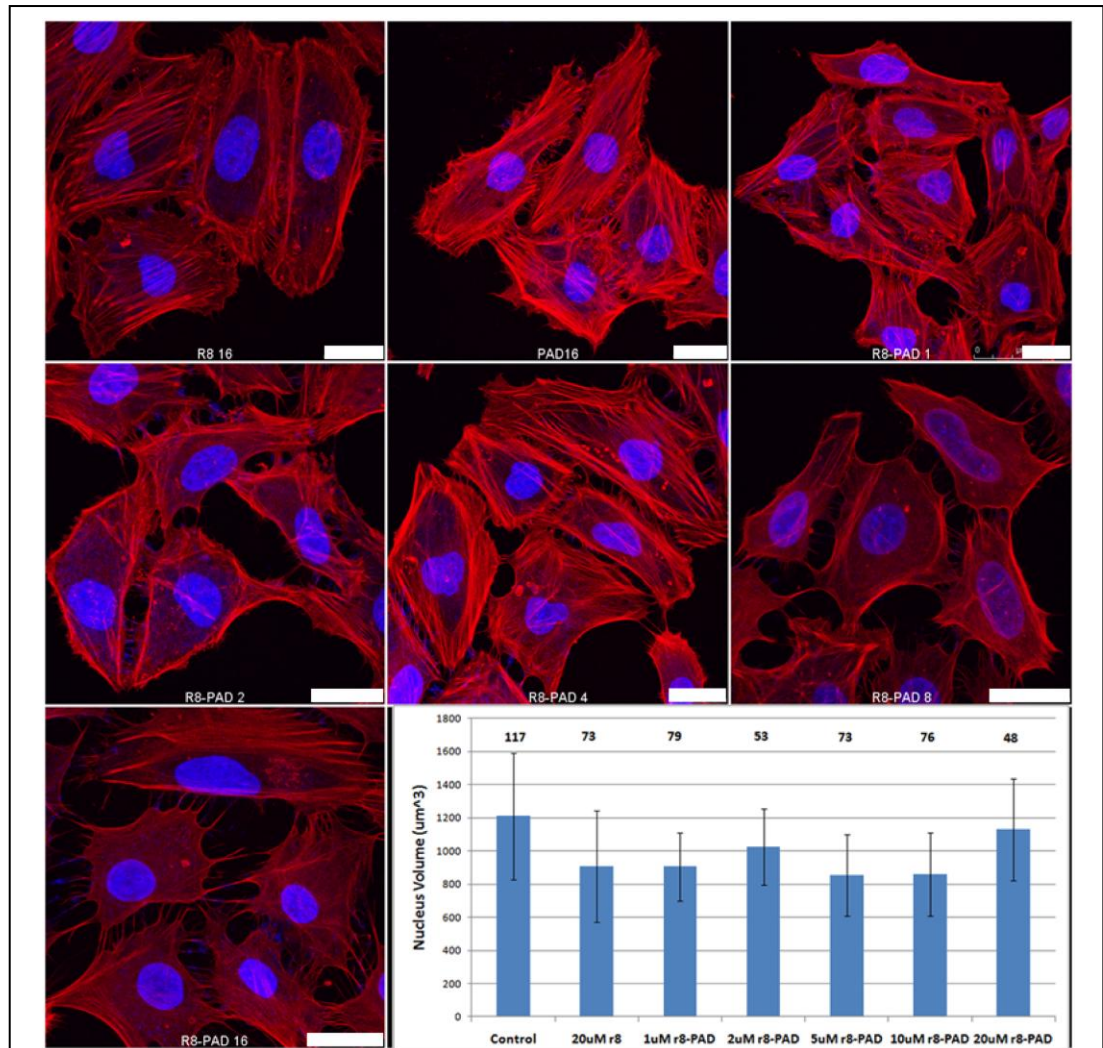


**Figure 5.10: HeLa cells after incubation with different concentrations of r8-PAD stained for actin and nucleus**

Confocal xyz projections (a) of HeLa cells fixed after incubation for 10 minutes with 16µM r8, 16µM PAD or 1, 2, 4, 8, 16µM R8-PAD with actin (red) and nucleus (blue) labelled. Nucleus volume (b) calculated from confocal xyz-projections using ImageJ. Error bars represent one standard deviation; numbers represent number of cells used in calculation. All scale bars = 25µm

volume showed no overall change in nucleus volume. This could be due to the nucleus looking more spherical at higher levels of r8-PAD from the normal nucleus shape in control cells (figure 5.10).

As previously described, using transfected HeLa cells we can monitor actin (using actin-GFP) and plasma membrane (GPI-GFP) movement during incubation with r8-PAD and compare this with r8 and PAD controls. GFP-actin and GFP-GPI cells were then used to further investigate the effects of PAD sequences on cells. Large blebs formed at the periphery of r8-PAD incubated cells, not present during incubation with the other peptides (figure 5.11). The blebs formed within the first ten minutes of the cell being exposed to the peptide and grew in size until the cell became PI positive. GPI-GFP transfected cells showed many blebs forming on the surface on the HeLa cells with some blebs merging together as they swelled. Actin-GFP transfected cells showed the large blebs forming with diffuse actin inside the blebs. After 20 minutes the actin depolymerised into a disordered state with propidium iodide positive particles later appearing after the nucleus became PI positive.

Pak-1 protein is involved in a range of cell activities including macropinocytosis and cell surface ruffling and many of these are linked with the cell cytoskeleton (Arias-Romero and Chernoff, 2008). It is activated by members of the Rho family of GTPases Rac and cdc42 that lie downstream of

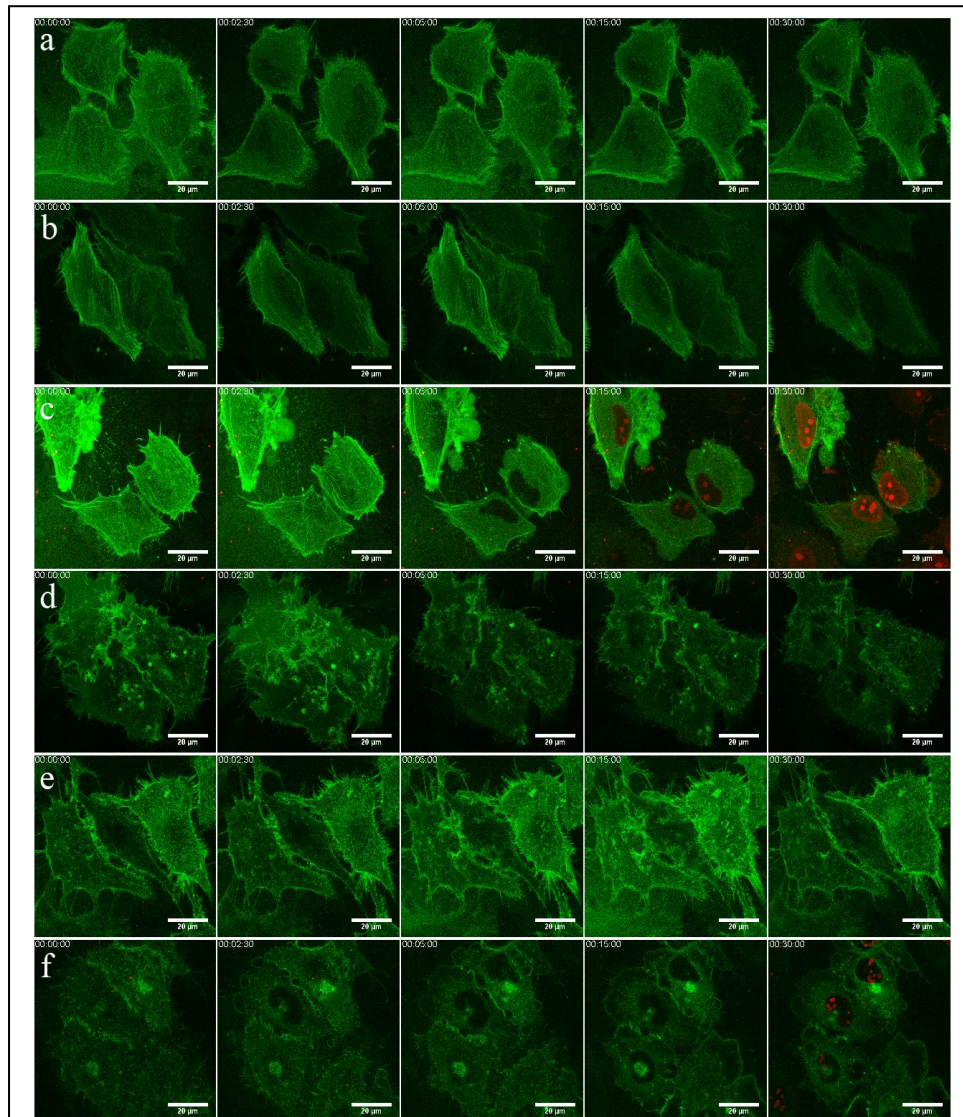


**Figure 5.11: HeLa cells transfected with actin-GFP or GPI-GFP expressing plasmid incubated with r8, PAD or r8-PAD.**

HeLa cells were transfected with actin GFP (a-c) or GPI-GFP (d-f) prior to incubation with 20µM r8 (a and d), PAD (b and e) or R8-PAD (c and f). Cells were immediately imaged on a confocal obtaining xyz images, with a new frame every 30 seconds. Propidium iodide (red) has been added as a marker for membrane integrity. All scale bars =

activation of receptors such as EGFR. Ligand binding to EGFR results in dramatic surface ruffling and macropinocytosis and this in part is regulated by Pak-1 (Dharmawardhane *et al.*, 2000). Pak-1 is involved in the phosphorylation of a variety of proteins including ROCK (Rho-associated protein kinase), which itself, via actin assembly, controls actin remodelling and apoptotic blebbing. Depleting Pak-1 with siRNA, or expression of a Pak-1 mutant in cells has been shown to inhibit macropinocytosis (Karjalainen *et al.*, 2008). If macropinocytosis is essential for uptake of CPPs in cells then Pak-1 depletion could inhibit CPP uptake. Equally the shown effects of CPP chimeras on actin dynamics such as the formation of ruffles and apoptotic bodies could also be regulated by Pak-1.

Methods for depleting Pak-1 from cells were fully characterised by another PhD student and this work is now in press (Al-Soraj *et al.*, 2012). HeLa Cells were then incubated with siRNA targeting Pak-1 or GFP (control) and 48 hrs later incubated with 20 $\mu$ M R8-PAD. Comparing Pak-1 and GFP (control) depleted cells with a sample just treated with oligofectamine showed little difference in blebbing or rate of cell death (figure 5.12). In all three of the samples microblebs formed in the first couple of minutes before large necrotic blebs also formed and the cells became quickly PI positive.. Thus based on these studies it does not seem that Pak-1 is involved in R8-PAD induced blebbing.

A more direct contributor to apoptotic blebbing is actin. During apoptotic blebbing, the membrane becomes dissociated from the underlying cytoskeleton, actin then repolymerises in the bleb to stop the bleb swelling and to later reduce the size of the bleb (Barros *et al.*, 2003). Actin also has a

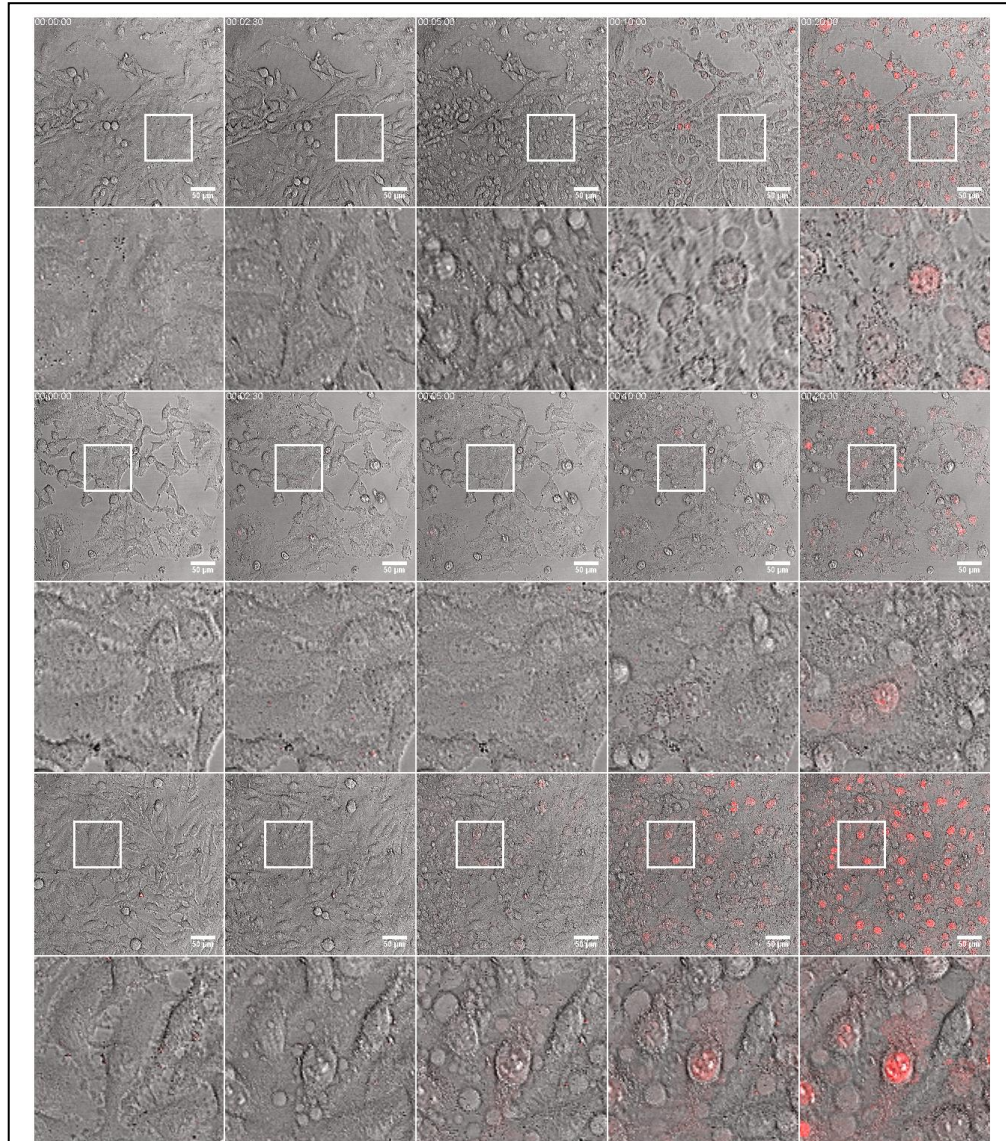


**Figure 5.12: HeLa cells treated with Pak-1 siRNA**

HeLa cells treated with oligofectamine (top), anti-GFP (middle) and anti-Pak-1 (bottom) have been exposed to 20 $\mu$ M R8-PAD over 30 minutes. Propidium iodide has been added as a marker for membrane porosity. Scale bars = 50 $\mu$ m

defined role in the formation of ruffling during macropinocytosis, actin polymerises within the ruffles and allow the ruffles to engulf extracellular fluids. Another important component of the cytoskeleton that has a role in macropinocytosis is myosin; this protein also has a small role in apoptotic blebbing (Bao *et al.*, 2010). During macropinocytosis, myosin IIB localises to areas of high activity where it has a role in cell surface ruffling. Depletion of myosin IIA has shown to increase macropinocytosis whilst depletion of myosin IIB or both myosin IIA and IIB shows a decrease in macropinocytosis. Myosin has also been shown to have a role in the contraction of membrane blebs. To provide further roles for myosin and actin in the observed cytoskeletal rearrangements, two cytoskeletal disrupting chemicals were used, cytochalasin D and blebbistatin. Cytochalasin D inhibits actin polymerisation (Goddette and Frieden, 1986) by allowing actin to form dimers. This removes actin monomers from the cell and increases the critical concentration at which actin filaments can form. Blebbistatin inhibits myosin II, by blocking actin-myosin crosslinking preventing the formation of the actomyosin cytoskeletal component (Sellers *et al.*, 2004). Both have been shown to inhibit macropinocytosis (Mercer and Helenius, 2009).

HeLa cells were therefore pretreated with using cytochalasin D or blebbistatin before being imaged during incubation with r8-PAD. With macropinocytosis and apoptotic blebbing relying on actin polymerisation, we should expect to see a reduction of these events taking place. Treating cells with either inhibitor, however, failed to prevent cell death and cell blebbing (figure 5.13).

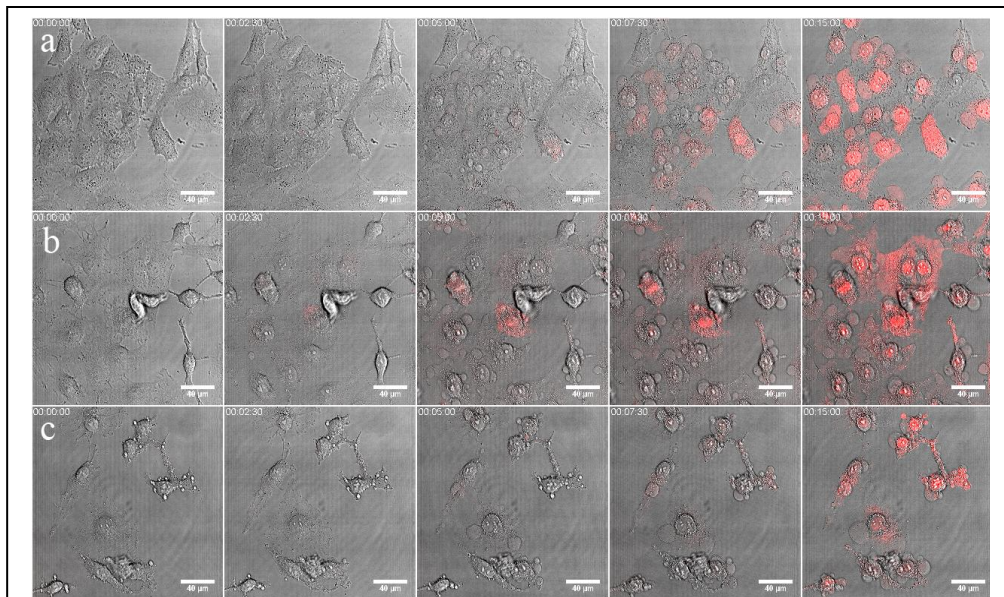


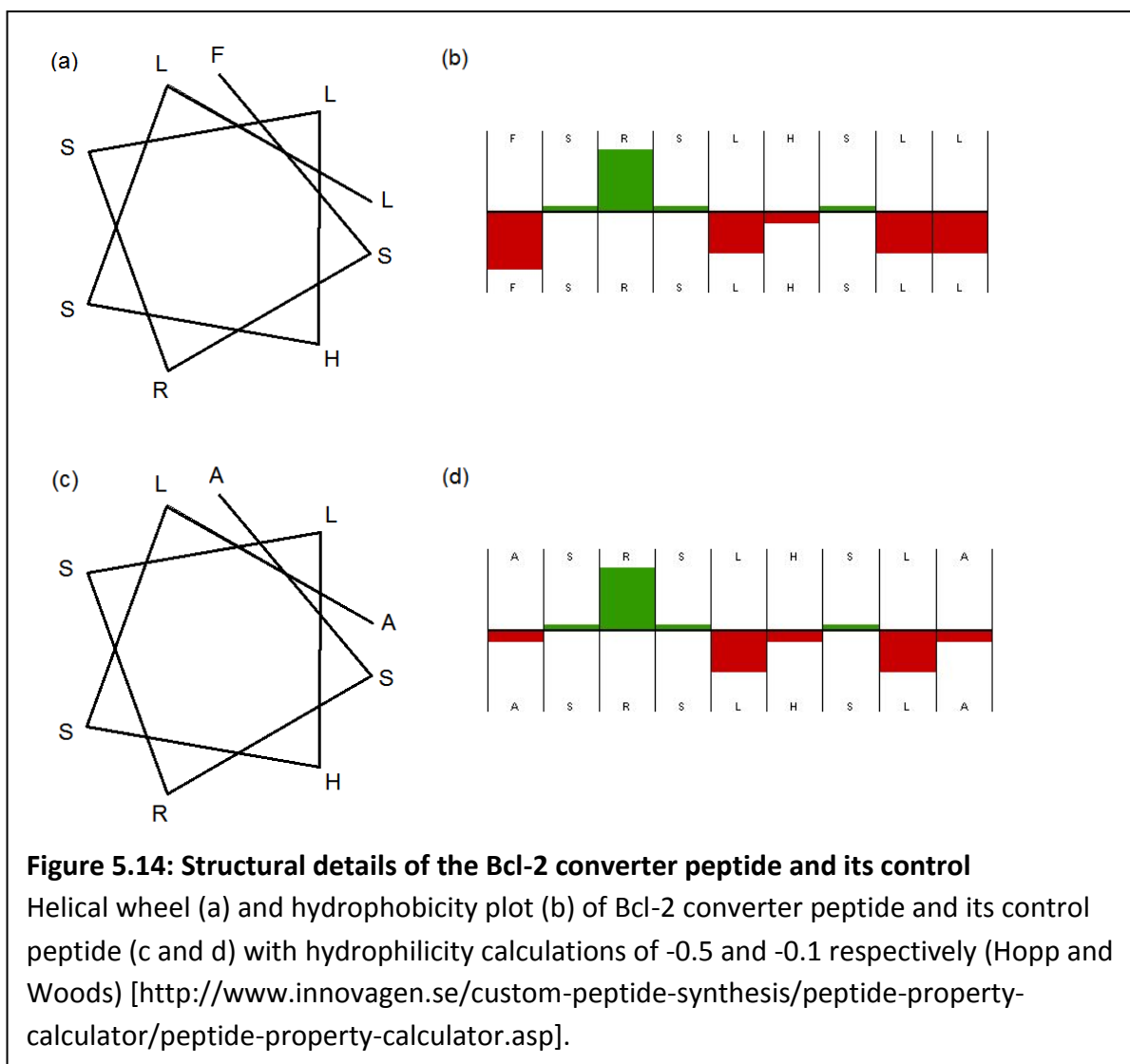
**Figure 5.13: HeLa cells incubated with r8-PAD after inhibition with cytochalasin D or Blebbistatin.**

HeLa cells were incubated with 20 $\mu$ M r8-PAD after pre-incubation with diluent control (a), cytochalasin D (b) or blebbistatin (c) and imaged every 30 seconds for 30 minutes on a confocal microscope. Propidium iodide has been added as a marker of membrane integrity. Scale bars = 40 $\mu$ m

Delivery of PAD by r8 caused the cells to undergo zebiosis and die. It is clear from this data that r8-PAD has a very high capacity to cause membrane rearrangements and cell death. The transfection and inhibitor studies suggest that this may not be due to a specific process but rather the arrangement of actin is a result of the general conformational changes that occur in cells when they are treated with r8-PAD.

### 5.2.2.3 Bcl-2 targeting peptide

Bcl-2 is an anti-apoptotic protein commonly up-regulated in several different cancers (Gogvadze *et al.*, 2008, Cory *et al.*, 2003). The proapoptotic



nuclear receptor family member Nur77 translocated from the nucleus and on to the mitochondria where it interacts with Bcl-2 to promote apoptosis (Li *et al.*, 2000). The interaction between these two proteins, in part, is via the short sequence FSRSLHSL located in Nur77. It was demonstrated that this Bcl-2

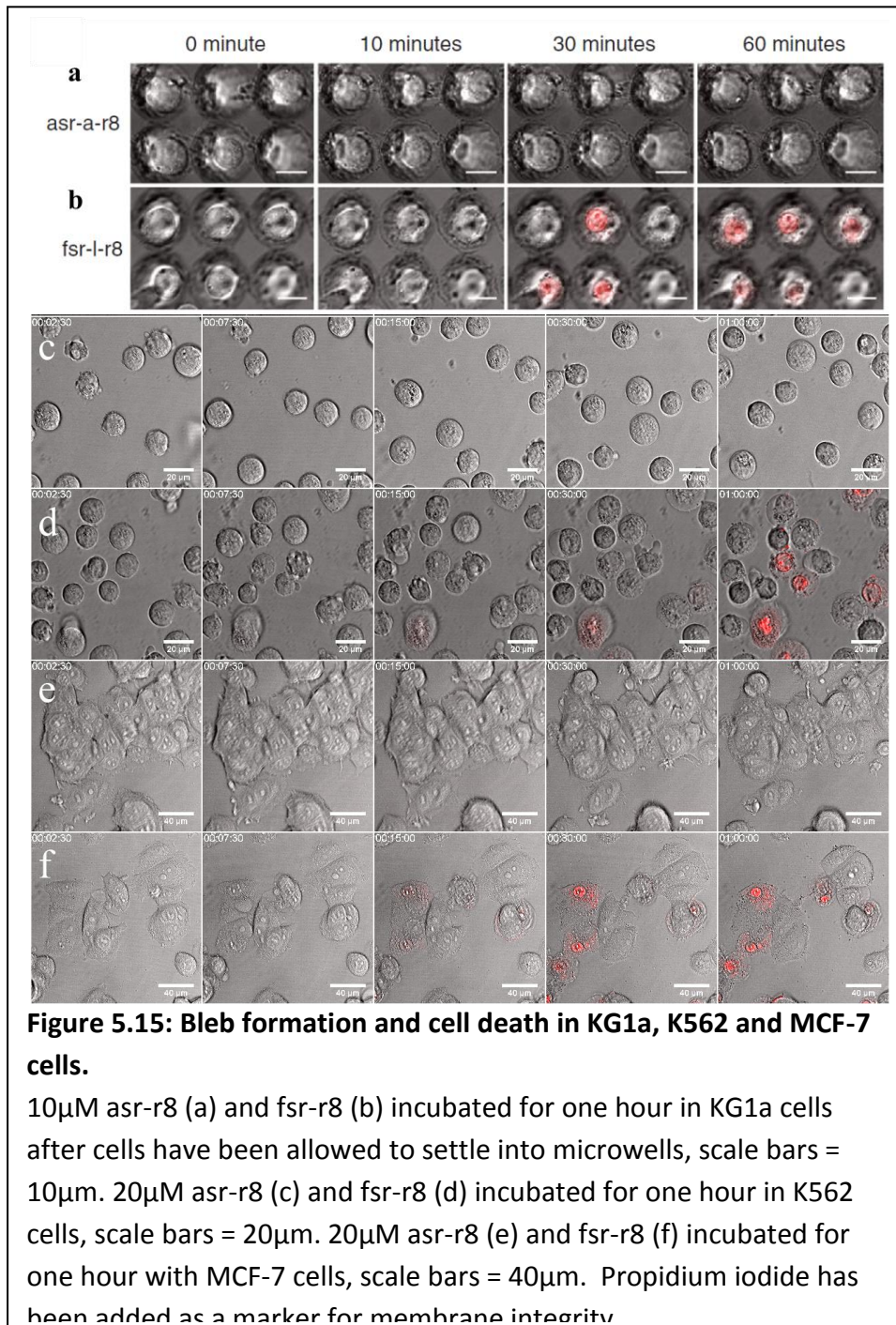
targeting peptide (as a L or D isomer) attached to the CPP r8, (the chimera is now sold commercially as D-NuBCP-9-r8 table 5.1) interacts with Bcl-2 to increase apoptosis in cells expressing this protein. Substitution of the N-terminal phenylalanine and the C-terminal leucine with alanine abrogated this effect, thus the effects were deemed to be specific. Studies performed in collaboration with another student in our laboratory suggested that the N-terminal phenylalanine of fsrslhslI was having a major synergistic effect with the r8 to influence cell uptake. Helical wheel plots (figure 5.14) of this peptide show the potential of this peptide to be amphiphilic with one side of the peptide exposing hydrophobic residues whilst the other exposing mainly neutral and hydrophilic residues. The overall hydrophilicity shows a decrease between the almost neutrally charged control (asrslhslaG-X-rrrrrrrrGC) and the more hydrophobic D-NuBCP-9 (fsrslhslIG-X-rrrrrrrrGC).

Western blot analysis in our laboratory had previously been carried out to show that leukaemia cell lines K562 and KG1a show different expression levels of Bcl-2. KG1a have strong Bcl-2 expression and K562 showing relatively weak expression of this protein.

Incubation of these two cell lines and the breast cancer cell line MCF-7 (Bcl-2 positive) (Perillo *et al.*, 2000) with fsr-l-r8 and asr-a-r8 at values similar to IC<sub>50</sub> values fsr-l-r8 showed similar morphological responses and PI permeability (figure 5.15). Cells incubated with fsr-l-r8 formed surface blebs and this was followed by propidium iodide flooding into the cell. Cells incubated with the control peptide showed no bleb formation and no propidium iodide uptake.

Bleb formation, as observed in cells incubated with r8-PAD is similar to necrotic bleb formation. That is, there are large continuously growing blebs on the surface. This would indicate any pro-apoptotic affect of the peptide is masked by necrosis.

Microwells generated in Chapter 3 were used to image KG1a cells incubated with both the fsr-l-r8 and asr-a-r8 peptides. Here cells were incubated with either peptide along with propidium iodide and imaged over the course of one hour. Cells incubated with fsr-l-r8 underwent blebbing after twenty minutes and after one hour were positive for PI indicating membrane leakage. Results using the microwells were consistant with images taken without the microwells indicating the microwells had no additional effects. The use of the microwells allowed imaging the cells at a higher magnification than would be possible without due to the movement of cells across the surface during imaging and addition of the peptide.



### **5.3 Discussion**

#### **5.3.1 Macropinocytosis and uptake of r8**

In this chapter the effects of adding agents that are well described to induce macropinocytosis was compared with cell penetrating peptides that are thought to induce this process. Whilst in most cases there was evidence of ruffling or lamellipodial extrusions in response to either r8 or EGF, the effects were small. Cell lines such as HeLa have been shown to ruffle in response to growth factors such as PDGF, however, the most common cell line to test these effects is A431, as this cell line has shown the ability to form strong ruffles in the past.

One major reason for this is that it expresses very high levels of EGFR and thus is highly responsive to EGF (Araki *et al.*, 2007).

At 4°C, or at high concentrations, cellular distribution of R8 is predominantly cytosolic in leukaemia cells within one hour of exposure to the peptide (Jones *et al.*, 2009b). This indicates there is an energy independent process in the uptake of octaarginine, however at 37°C uptake can still occur through an energy dependent uptake mechanism. It is likely that r8 has multiple uptake mechanisms. It is known that when some pathways are artificially down-regulated other pathways can up-regulate to maintain uptake of macromolecules. Down-regulation of macropinocytosis with pharmacological inhibitors can reduce internalisation of r8 but uptake of r8 is not fully eliminated. Indeed at 4°C, when macropinocytosis cannot function properly

due to the inhibition of actin polymerisation and regulation, r8 still enters the cell and this most likely occurs by direct translocation.

Internalisation of CPPs directly across the plasma membrane and into the cytosol shows little membrane damage raising the question of how translocation occurs (Herce and Garcia, 2007). Recently, however, studies in synthetic giant unilaminar vesicles (GUVs) indicate a subtle role of small modifications to a CPP can have on membrane interactivity (Mishra *et al.*, 2011). When GUVs are exposed to the CPP R<sub>6</sub> rapid membrane damage occurs releasing the intravesicular contents, however, with the addition of a tryptophan or FITC to the sequence, intravesicular contents is released through small pores in the membrane surface.

### 5.3.2 Cell dynamics of r8-PAD

The uptake of r8-PAD, like r8, may occur in multiple ways. At low concentrations (<5 $\mu$ M), r8-PAD localises in vesicles, whilst at higher concentrations (>5 $\mu$ M), the peptide starts to diffuse throughout the cell with strong labelling in the nucleolus (Jones *et al.*, 2009a). Work in this thesis suggests this is a non-specific event and independent of macropinocytosis. This is to be expected as at these concentrations the peptide has the ability to flood into the cell within minutes, bypassing any conventional uptake mechanism. At lower concentrations of 1-2 $\mu$ M, a better idea of whether this peptide enters the cell by macropinocytosis, using an inhibitor study would more likely produce a stronger result.

The almost identical peptide r7-kla (rrrrrrr-GG-klaklaklaklak) has been shown to efficiently kill both bacteria and cancer cells. The peptide interacts with the membrane of the mitochondria due to the charge across the surface. When this charge is reduced the effect of this peptide is subsequently also reduced. It is thought this interaction between the peptide and charged membrane causes the swelling and rupture of the mitochondria which releases the pro-apoptotic factor cytochrome *c*. *In vivo*, the PAD domain, attached to PTD-5, has been used to reduce the size of tumour in a mouse model (Mai *et al.*, 2001). Whilst PAD was also used to selectively kill HER-2 overexpressing cells when attached to an anti-HER-2 peptide (Law *et al.*, 2006). Apoptosis is generally considered to be cell death in a regulated manner, allowing a cell to die without releasing toxic components to neighbouring cells that can also be killed. Necrosis is, however, more unregulated and when cells die, their contents can be exposed to neighbouring cells posing a strong danger to these cells. It is possible that cells exposed to r8-PAD start to undergo apoptosis before the cell becomes more unstable and undergoes necrosis.

Inhibition of actin would affect apoptosis more than necrosis during bleb formation. Fluorescent-actin transfection shows actin to be present within the blebs, and in one of the cells filaments form within these blebs. This would support the case that apoptosis is happening. However, these blebs are not constrained in size and continue to grow, eventually becoming PI positive themselves. This would indicate necrosis is occurring, although it is not inconceivable that apoptosis can be induced before necrosis takes over.

Using different inhibitors to inhibit actin filaments there is no discernible difference in cell morphology between uninhibited cells and cells that have been inhibited. In all cases cells rapidly form large blebs on their surface before becoming PI positive. Again, this may be due to the concentration used on the cells. At 20 $\mu$ M r8-PAD, any apoptotic effects may be masked by proceeding necrosis. Apoptosis is an energy dependent process (Elmore, 2007), necrotic blebs form when there is a lack of ATP available, preventing the plasma membrane adequately binding to the cytoskeleton. It would be interesting to determine how the amount of ATP fluctuates when exposed to r8-PAD. If at high concentrations mitochondria are being damaged, then ATP is likely to be quickly used up helping necrotic blebs form in place of apoptotic blebs.

Zeiosis occurs when the plasma membrane becomes dissociated from the actinomyosin cytoskeleton. Membrane-actinomyosin interaction is an active mechanism requiring ATP. A reduction of ATP leads to the membrane becoming disassociated from the cytoskeleton leading to the formation of blebs. During apoptosis the cell shrinks, overall volume however remains the same thus putting excess pressure on the plasma membrane. Rapid shrinking leads to rapid formation of these small blebs, when this shrinking ceases the round uniform blebs start to shrivel and eventually retract back to the cell. During necrosis, cells start to uptake large amounts of fluid; this puts pressure on the membrane allowing the blebs to form. As the volume of the cells increases, so do the necrotic blebs, leading to large uniform blebs emanating

from the cell surface. The membrane becomes permeable allowing the efflux of extracellular content and the eventual expulsion of intracellular material.

### 5.3.3 Cell death from fsr-l-r8

The peptide fsr-l-r8 has was originally shown to cause cell death in a Bcl-2 dependent manner. Evidence presented here that is now published and available as an appendix to this thesis. The terminal phenylalanine residue was clearly having major effects on the dynamic of this peptide with cell membranes. A simple Phe-Ala substitution at this position completely changed the capacity of this peptide to cause membrane disruption. There is evidence in the literature that addition of hydrophobic groups at the end of CPPs effect their cellular dynamics (Elmquist *et al.*, 2006, Pham *et al.*, 2004). Of equal significance is the fact that our studies strongly suggest that the effects of fsr-r8 are initially independent of Bcl-2 expression and cause necrotic rather than apoptotic cell death. Finally the generation of microwells allowed for unprecedented opportunities to study the plasma membrane dynamics of leukaemia cells in the presence of these peptides. The wells will be useful for a host of other studies that require similar microscopic analysis of these types of cells at the single cell level.

### 5.3.4 Conclusions

The studies here suggest that many of the effects of CPPs on the actin cytoskeleton occur via a process distinct from macropinocytosis. Based on new information on the effects of CPPs on actin it will be important to study

whether this direct CPP-interaction is the cause of membrane rearrangements.

The data presented here clearly highlight that octaarginine linked to pro-apoptotic peptides r8-PAD and fsr-l-r8 have necrotic effects on different cell types. Whilst the research could not rule out apoptosis occurring, it is likely that this was masked by necrosis. The availability of the microwells was advantageous for the studies with leukaemia cells and these can now be utilised for other microscopy based applications.

#### **5.4 References**

AL-SORAJ, M., HE, L., PEYNSHAERT, K., COUSART, J., VERCAUTEREN, D.,  
BRAECKMANS, K., SMEDT, S. C. D. & JONES, A. T. (2012) siRNA and  
pharmacological inhibition of endocytic pathways to characterize  
the  
2 differential role of macropinocytosis and the actin cytoskeleton on  
cellular uptake of  
3 dextran and cationic cell penetrating peptides octaarginine (R8) and  
HIV-Tat. *Journal of Controlled Release, In Press.*

- ARAKI, N., EGAMI, Y., WATANABE, Y. & HATAE, T. (2007) Phosphoinositide metabolism during membrane ruffling and macropinosome formation in EGF-stimulated A431 cells. *Exp Cell Res*, 313, 1496-507.
- ARAKI, N., JOHNSON, M. T. & SWANSON, J. A. (1996) A role for phosphoinositide 3-kinase in the completion of macropinocytosis and phagocytosis by macrophages. *Journal of Cell Biology*, 135, 1249-1260.
- ARIAS-ROMERO, L. E. & CHERNOFF, J. (2008) A tale of two Paks. *Biol Cell*, 100, 97-108.
- BAO, Z. Z., JIANG, J. & KOLPAK, A. L. (2010) Myosin IIB Isoform Plays an Essential Role in the Formation of Two Distinct Types of Macropinosomes. *Cytoskeleton*, 67, 32-42.
- BARROS, L. F., KANASEKI, T., SABIROV, R., MORISHIMA, S., CASTRO, J., BITTNER, C. X., MAENO, E., ANDO-AKATSUKA, Y. & OKADA, Y. (2003) Apoptotic and necrotic blebs in epithelial cells display similar neck diameters but different kinase dependency. *Cell Death Differ*, 10, 687-97.
- BIDWELL, G. L., 3RD & RAUCHER, D. (2009) Therapeutic peptides for cancer therapy. Part I - peptide inhibitors of signal transduction cascades. *Expert Opin Drug Deliv*, 6, 1033-47.
- CORY, S., HUANG, D. C. & ADAMS, J. M. (2003) The Bcl-2 family: roles in cell survival and oncogenesis. *Oncogene*, 22, 8590-607.
- DHARMAWARDHANE, S., SCHURMANN, A., SELLS, M. A., CHERNOFF, J., SCHMID, S. L. & BOKOCH, G. M. (2000) Regulation of macropinocytosis by p21-activated kinase-1. *Mol Biol Cell*, 11, 3341-52.
- DIETZ, G. P. H. & BAHR, M. (2004) Delivery of bioactive molecules into the cell: The Trojan horse approach. *Molecular and Cellular Neuroscience*, 27, 85-131.

- DOHERTY, G. J. & MCMAHON, H. T. (2009) Mechanisms of endocytosis. *Annu Rev Biochem*, 78, 857-902.
- ELLERBY, H. M., ARAP, W., ELLERBY, L. M., KAIN, R., ANDRUSIAK, R., RIO, G. D., KRAJEWSKI, S., LOMBARDO, C. R., RAO, R., RUOSLAHTI, E., BREDESEN, D. E. & PASQUALINI, R. (1999) Anti-cancer activity of targeted pro-apoptotic peptides. *Nat Med*, 5, 1032-8.
- ELMORE, S. (2007) Apoptosis: a review of programmed cell death. *Toxicol Pathol*, 35, 495-516.
- ELMQUIST, A., HANSEN, M. & LANGEL, U. (2006) Structure-activity relationship study of the cell-penetrating peptide pVEC. *Biochim Biophys Acta*, 1758, 721-9.
- FACKLER, O. T. & GROSSE, R. (2008) Cell motility through plasma membrane blebbing. *J Cell Biol*, 181, 879-84.
- FAWELL, S., SEERY, J., DAIKH, Y., MOORE, C., CHEN, L. L., PEPINSKY, B. & BARSOUM, J. (1994) Tat-mediated delivery of heterologous proteins into cells. *Proc Natl Acad Sci U S A*, 91, 664-8.
- FRETZ, M., JIN, J., CONIBERE, R., PENNING, N. A., AL-TAEI, S., STORM, G., FUTAKI, S., TAKEUCHI, T., NAKASE, I. & JONES, A. T. (2006) Effects of Na<sup>+</sup>/H<sup>+</sup> exchanger inhibitors on subcellular localisation of endocytic organelles and intracellular dynamics of protein transduction domains HIV-TAT peptide and octaarginine. *J Control Release*, 116, 247-54.
- FRETZ, M. M., PENNING, N. A., AL-TAEI, S., FUTAKI, S., TAKEUCHI, T., NAKASE, I., STORM, G. & JONES, A. T. (2007) Temperature-, concentration- and cholesterol-dependent translocation of L- and D-octa-arginine across the plasma and nuclear membrane of CD34(+) leukaemia cells. *Biochemical Journal*, 403, 335-342.

- FUTAKI, S., NAKASE, I., TADOKORO, A., TAKEUCHI, T. & JONES, A. T. (2007) Arginine-rich peptides and their internalization mechanisms. *Biochem Soc Trans*, 35, 784-7.
- GODDETTE, D. W. & FRIEDEN, C. (1986) Actin Polymerization - the Mechanism of Action of Cytochalasin-D. *Journal of Biological Chemistry*, 261, 5974-5980.
- GOGVADZE, V., ORRENIUS, S. & ZHIVOTOVSKY, B. (2008) Mitochondria in cancer cells: what is so special about them? *Trends Cell Biol*, 18, 165-73.
- HEITZ, F., MORRIS, M. C. & DIVITA, G. (2009) Twenty years of cell-penetrating peptides: from molecular mechanisms to therapeutics. *Br J Pharmacol*.
- HENRIQUES, S. T., MELO, M. N. & CASTANHO, M. A. (2006) Cell-penetrating peptides and antimicrobial peptides: how different are they? *Biochem J*, 399, 1-7.
- HERCE, H. D. & GARCIA, A. E. (2007) Cell penetrating peptides: how do they do it? *J Biol Phys*, 33, 345-56.
- JAVADPOUR, M. M., JUBAN, M. M., LO, W. C., BISHOP, S. M., ALBERTY, J. B., COWELL, S. M., BECKER, C. L. & MCLAUGHLIN, M. L. (1996) De novo antimicrobial peptides with low mammalian cell toxicity. *J Med Chem*, 39, 3107-13.
- JONES, A. T. (2007) Macropinocytosis: searching for an endocytic identity and role in the uptake of cell penetrating peptides. *J Cell Mol Med*, 11, 670-84.
- JONES, A. T., WATKINS, C. L., BRENNAN, P., FEGAN, C., TAKAYAMA, K., NAKASE, I. & FUTAKI, S. (2009a) Cellular uptake, distribution and cytotoxicity of the hydrophobic cell penetrating peptide sequence PFVYLI linked to the proapoptotic domain peptide PAD. *Journal of Controlled Release*, 140, 237-244.
- JONES, A. T., WATKINS, C. L., SCHMALJOHANN, D. & FUTAKI, S. (2009b) Low concentration thresholds of plasma membranes for rapid energy-

independent translocation of a cell-penetrating peptide. *Biochemical Journal*, 420, 179-189.

KAPLAN, I. M., WADIA, J. S. & DOWDY, S. F. (2005) Cationic TAT peptide transduction domain enters cells by macropinocytosis. *J Control Release*, 102, 247-53.

KARJALAINEN, M., KAKKONEN, E., UPLA, P., PALORANTA, H., KANKAANPAA, P., LIBERALI, P., RENKEMA, G. H., HYYPIA, T., HEINO, J. & MARJOMAKI, V. (2008) A Raft-derived, Pak1-regulated entry participates in alpha2beta1 integrin-dependent sorting to caveosomes. *Mol Biol Cell*, 19, 2857-69.

LAKHAN, S. E., SABHARANJAK, S. & DE, A. (2009) Endocytosis of glycosylphosphatidylinositol-anchored proteins. *J Biomed Sci*, 16, 93.

LASTER, S. M. & MACKENZIE, J. M. (1996) Bleb formation and F-actin distribution during mitosis and tumor necrosis factor-induced apoptosis. *Microscopy Research and Technique*, 34, 272-280.

LAW, B., QUINTI, L., CHOI, Y., WEISSLEDER, R. & TUNG, C. H. (2006) A mitochondrial targeted fusion peptide exhibits remarkable cytotoxicity. *Mol Cancer Ther*, 5, 1944-9.

LEE, E. & KNECHT, D. A. (2002) Visualization of actin dynamics during macropinocytosis and exocytosis. *Traffic*, 3, 186-92.

LI, H., KOLLURI, S. K., GU, J., DAWSON, M. I., CAO, X., HOBBS, P. D., LIN, B., CHEN, G., LU, J., LIN, F., XIE, Z., FONTANA, J. A., REED, J. C. & ZHANG, X. (2000) Cytochrome c release and apoptosis induced by mitochondrial targeting of nuclear orphan receptor TR3. *Science*, 289, 1159-64.

LIBERALI, P., KAKKONEN, E., TURACCHIO, G., VALENTE, C., SPAAR, A., PERINETTI, G., BOCKMANN, R. A., CORDA, D., COLANZI, A., MARJOMAKI, V. & LUINI, A.

- (2008) The closure of Pak1-dependent macropinosomes requires the phosphorylation of CtBP1/BARS. *EMBO J*, 27, 970-81.
- LUZIO, J. P., PRYOR, P. R. & BRIGHT, N. A. (2007) Lysosomes: fusion and function. *Nat Rev Mol Cell Biol*, 8, 622-32.
- MAI, J. C., MI, Z., KIM, S. H., NG, B. & ROBBINS, P. D. (2001) A proapoptotic peptide for the treatment of solid tumors. *Cancer Res*, 61, 7709-12.
- MARKS, A. J., COOPER, M. S., ANDERSON, R. J., ORCHARD, K. H., HALE, G., NORTH, J. M., GANESHAGURU, K., STEELE, A. J., MEHTA, A. B., LOWDELL, M. W. & WICKREMASINGHE, R. G. (2005) Selective apoptotic killing of malignant hemopoietic cells by antibody-targeted delivery of an amphipathic peptide. *Cancer Res*, 65, 2373-7.
- MASON, J. M. (2010) Design and development of peptides and peptide mimetics as antagonists for therapeutic intervention. *Future Med Chem*, 2, 1813-22.
- MEADE, B. R. & DOWDY, S. F. (2007) Exogenous siRNA delivery using peptide transduction domains/cell penetrating peptides. *Adv Drug Deliv Rev*, 59, 134-40.
- MEIER, O., BOUCKE, K., HAMMER, S. V., KELLER, S., STIDWILL, R. P., HEMMI, S. & GREBER, U. F. (2002) Adenovirus triggers macropinocytosis and endosomal leakage together with its clathrin-mediated uptake. *J Cell Biol*, 158, 1119-31.
- MERCER, J. & HELENIUS, A. (2009) Virus entry by macropinocytosis. *Nat Cell Biol*, 11, 510-20.
- MISHRA, A., LAI, G. H., SCHMIDT, N. W., SUN, V. Z., RODRIGUEZ, A. R., TONG, R., TANG, L., CHENG, J., DEMING, T. J., KAMEI, D. T. & WONG, G. C. (2011) Translocation of HIV TAT peptide and analogues induced by multiplexed

membrane and cytoskeletal interactions. *Proc Natl Acad Sci U S A*, 108, 16883-8.

MUELLER, J., KRETZSCHMAR, I., VOLKMER, R. & BOISGUERIN, P. (2008) Comparison of cellular uptake using 22 CPPs in 4 different cell lines. *Bioconjug Chem*, 19, 2363-74.

NAKASE, I., NIWA, M., TAKEUCHI, T., SONOMURA, K., KAWABATA, N., KOIKE, Y., TAKEHASHI, M., TANAKA, S., UEDA, K., SIMPSON, J. C., JONES, A. T., SUGIURA, Y. & FUTAKI, S. (2004) Cellular uptake of arginine-rich peptides: Roles for macropinocytosis and actin rearrangement. *Molecular Therapy*, 10, 1011-1022.

NAKASE, I., TADOKORO, A., KAWABATA, N., TAKEUCHI, T., KATOH, H., HIRAMOTO, K., NEGISHI, M., NOMIZU, M., SUGIURA, Y. & FUTAKI, S. (2007) Interaction of arginine-rich peptides with membrane-associated proteoglycans is crucial for induction of actin organization and macropinocytosis. *Biochemistry*, 46, 492-501.

PERILLO, B., SASSO, A., ABBONDANZA, C. & PALUMBO, G. (2000) 17beta-estradiol inhibits apoptosis in MCF-7 cells, inducing bcl-2 expression via two estrogen-responsive elements present in the coding sequence. *Mol Cell Biol*, 20, 2890-901.

PHAM, W., KIRCHER, M. F., WEISSLEDER, R. & TUNG, C. H. (2004) Enhancing membrane permeability by fatty acylation of oligoarginine peptides. *Chembiochem*, 5, 1148-51.

SELLERS, J. R., KOVACS, M., TOTH, J., HETENYI, C. & MALNASI-CSIZMADIA, A. (2004) Mechanism of blebbistatin inhibition of myosin II. *Journal of Biological Chemistry*, 279, 35557-35563.

- SNYDER, E. L. & DOWDY, S. F. (2004) Cell penetrating peptides in drug delivery. *Pharm Res*, 21, 389-93.
- SWANSON, J. A. & WATTS, C. (1995) Macropinocytosis. *Trends Cell Biol*, 5, 424-8.
- UTANI, K., OKAMOTO, A. & SHIMIZU, N. (2011) Generation of micronuclei during interphase by coupling between cytoplasmic membrane blebbing and nuclear budding. *PLoS One*, 6, e27233.
- WATKINS, C. L., SCHMALJOHANN, D., FUTAKI, S. & JONES, A. T. (2009a) Direct translocation of the cell penetrating peptide octaarginine across the plasma membrane. *Journal of Controlled Release*, In Press.
- WATKINS, C. L., SCHMALJOHANN, D., FUTAKI, S. & JONES, A. T. (2009b) Low concentration thresholds of plasma membranes for rapid energy-independent translocation of a cell-penetrating peptide. *Biochem J*, 420, 179-89.

## **6. General Discussion**

Correlative microscopy is an important tool for cell biology research. Until now, it has been difficult to obtain correlative images of non-adherent cell types due to the cells moving around. Different methods could be used to retain cells from surface patterning to the physical retention of a microwell. Microwells were used in this study for their ability to be made easily locatable.

A simple circular microwell array was shown to be able to correlatively image between live cell imaging and imaging under a scanning electron microscope. The microwells used held the cells in place during the fixation, washing and dehydration steps involved in preparing the sample for SEM. Ouyangs group have shown that microwell dimensions can affect the retention of cells within a microwell array (Luo *et al.*, 2007) and the microwells we produced held the cells in place. This is most likely a factor of both the size and well produced, leukocytes are typically 10.1  $\mu\text{m}$  in diameter and the wells produced were 15  $\mu\text{m}$  in diameter and 10  $\mu\text{m}$  deep. Fluid flow would have also played a role as the fixative was gently added reducing the likely hood of flow forcing the cell out of the microwell.

The production of an encoded microwell is an important step to allow for correlative microscopy. Using this method it is possible to track a well under light microscopy and SEM. The code was made, however, to run through the height of the well. This would allow the code to be seen after the microwells have been sectioned, although we were not able to fully demonstrate this. To make the wells fully visible under TEM a contrast would need to be made between the wells and the resin used to back fill. Table 6.1 discusses various

methods which could be used to make the coded array visible under a variety of different microscopy techniques. It is hoped that by using encoded microwells, correlative microscopy between multiple types of microscope, beyond correlative light-electron microscopy techniques currently used. This however, needs to be validated and at the time of writing is just a hypothesis.

The method used to generate the encoded microwells was originally laser ablation. This would not be the most optimal method to use to generate the wells due to the detail required during sectioning. Alternative methods such as deep ion reactive etching would better generate the tidy vertical walls required of the code. One of the levels of encoding missing in the design is a method for marking depth into the well. One way to solve this would be to use sloping walls, so the array reduces slightly in diameter as the sections cut deeper into the well. Whilst it is possible to read the well, optimally a computer method could be generated to recognise a microwell shape and determine its value.

The use of a clear epoxy resin is important to the correlative microscopy design. Although PDMS was originally researched to fill this role, it proved to be too flexible. It may be possible to produce a suitable polymer out of PDMS, using techniques such as an interpenetrating network to strengthen the polymer. Although it would be important to maintain the non-fluorescent properties of the elastomer. Surface modification of PDMS proved successful in changing the surface to better suit cell adhesion. Silanisation of the surface produced the most successful method of modifying the surface and this would allow further modifications to take place.

Cell penetrating peptides were researched along with pro-apoptotic peptides. The CPP r8 had previously been shown to be internalised by macropinocytosis. This was disputed although not altogether ruled out. The pro-apoptotic peptides r8-PAD and fsr-1-r8 were also shown to produce necrotic effects at the high concentrations used. Again, apoptosis cannot be ruled out at the lower concentrations but it is highly likely that necrosis plays a role in cell death in response to these peptides.

	<b>Imaging Method<sup>2 3</sup></b>	<b>Biological Specimen</b>	<b>Visible unit</b>	<b>Alterations needed to microwell</b>
<b>Visible and UV Light</b>	Epifluorescent microscopy	Cells / tissue	Fluorescent probes	Surface features visible under bright field element
	Confocal microscopy	Cells / tissue	Fluorescent probes	Surface features visible under bright field element
	Total internal reflection fluorescence (TIRF) microscopy	Cells / tissue	Fluorescent probes	Surface features visible under bright field element
	Stochastic optical reconstruction microscopy (STORM)	Cells / tissue	FRET (Förster radiation emission transfer) of fluorescent probes	Surface features visible under bright field element
	Two photon fluorescence microscopy (2-Pi)	Cells / tissue	Fluorescent probes	Surface features visible under bright field element
	Stimulated emission depletion microscopy (STED)	Cells / tissue	Fluorescent probes	Surface features visible under bright field element
	Ellipsometry	Cells	Change in polarisation	Surface features visible
	Digital holographic microscopy	Cells	Holographic reconstruction	Surface features visible
	Saturated structured illumination microscopy (SSIM)	Cells / tissue	Fluorescent probes	Surface features visible under bright field element
	Photo-activated localization microscopy (PALM)	Cells	Fluorescent probes	Surface features visible under bright field element
White light nanoscope <sup>1</sup>	Cells / bacteria / viruses	Visible light	Surface features visible	

	<b>Imaging Method<sup>2 3</sup></b>	<b>Biological Specimen</b>	<b>Visible unit</b>	<b>Alterations needed to microwell</b>
<b>Electron</b>	Scanning electron microscopy (SEM)	Cells / tissue	Electron scattering	Surface features visible
	Transmission electron microscopy (TEM)	Cells	Electron transmission/absorption	Contrasting agent needed (uranyl acetate or other electron dense compound)
	Scanning electron tomography	Cells / tissue	Electron transmission/absorption	Contrasting agent needed (uranyl acetate or other electron dense compound)
<b>Physical</b>	Atomic force microscopy (AFM)	Cells / bacteria / viruses	Physical scanning of surface	Surface features visible, wells must be small and shallow
	Scanning tunnelling microscopy (STM)	Surfaces / membranes	Electrical conductance	Surface needs to be electrically conductive, electrical resistance contrast may need to be used.
<b>Infra-red</b>	Coherent anti-Stokes Raman spectroscopy (CARS)	Cells/ lipids	Chemical bonds	Contrasting agent (lipid or gold coating)
	Surface-enhanced Raman spectroscopy (SERS)	Cells	Chemical bonds	Contrasting agent (nanoparticle, carbon nano-tube or graphene coating)
	Fourier-transform infrared (FTIR) microscopy	Cells	Chemical bond	Contrast agent with unique chemical signature
	Scanning near-field optical microscopy (SNOM)	Cells	Phase contrast and chemical bond	Contrasting agent with unique chemical signature

	<b>Imaging Method<sup>2 3</sup></b>	<b>Biological Specimen</b>	<b>Visible unit</b>	<b>Alterations needed to microwell</b>
<b>X-ray</b>	X-ray phase contrast	Cells	Carbon – oxygen contrast	Contrasting agent needed
	X-ray fluorescence microscopy	Cells	Fluorescence of heavy metals	Contrasting agent needed (heavy metals)
	Particle induced x-ray emission (PIXE)	Cells	Fluorescence of elements heavier than fluorine	Contrasting agent needed (metals)
<b>Ion</b>	Secondary ion mass spectrometry microscopy ( $\mu$ SIMS)	Cells	Particle scatter from ion beam	Contrasting agent needed

1. Wang, Z., *et al.* Optical virtual imaging at 50 nm lateral resolution with a white-light nanoscope. *Nat Commun* **2**, 218 (2011).
2. Petibois, C. Imaging methods for elemental, chemical, molecular, and morphological analyses of single cells. *Analytical and Bioanalytical Chemistry* **397**, 2051-2065 (2010).
3. Bullen, A. Microscopic imaging techniques for drug discovery. *Nature Reviews Drug Discovery* **7**, 54-67 (2008)

**Table 6.1: How the coded microwell array may be modified for use with alternative microscopes**

## 7 Appendix

© The American Society of Gene &amp; Cell Therapy

original article

### Co-operative Membrane Disruption Between Cell-penetrating Peptide and Cargo: Implications for the Therapeutic Use of the Bcl-2 Converter Peptide D-NuBCP-9-r8

Catherine L Watkins<sup>1</sup>, Edward J Sayers<sup>1,2</sup>, Chris Allender<sup>1</sup>, David Barrow<sup>2</sup>, Christopher Fegan<sup>3</sup>, Paul Brennan<sup>4</sup> and Arwyn T Jones<sup>1</sup><sup>1</sup>Welsh School of Pharmacy, Cardiff University, Cardiff, UK; <sup>2</sup>Institute of Green Electronic Systems - Communications, Sensors and Materials, Cardiff School of Engineering, Queens Buildings, The Parade, Cardiff University, Cardiff, UK; <sup>3</sup>Department of Hematology, University Hospital of Wales, Cardiff, UK; <sup>4</sup>Infection, Immunity and Biochemistry, School of Medicine, Cardiff University, Heath Park, Cardiff, UK

Delivering apoptosis inducing peptides to cells is an emerging area in cancer and molecular therapeutics. Here, we have identified an alternative mechanism of action for the proapoptotic chimeric peptide D-NuBCP-9-r8. Integral to D-NuBCP-9-r8 is the Nur-77-derived D-isofom sequence frrslhsl that targets Bcl-2, and the cell-penetrating peptide (CPP) octaarginine (r8) that is required for intracellular delivery. We find that the N-terminal phenylalanine of frrslhsl acts in synergy with the cell-penetrating moiety to enhance peptide uptake at low nontoxic levels and cause rapid membrane blebbing and cell necrosis at higher ( $IC_{50}$ ) concentrations. These effects were not observed when a single phenylalanine-alanine mutation was introduced at the N-terminus of D-NuBCP-9-r8. Using primary samples from chronic lymphocytic leukemia (CLL) patients and cancer cell lines, we show that NuBCP-9-r8 induced toxicity, via membrane disruption, is independent of Bcl-2 expression. Overall, this study demonstrates a new mechanism of action for this peptide and cautions its use as a highly specific entity for targeting Bcl-2. For delivery of therapeutic peptides the work emphasizes that key amino acids in cargo, located several residues away from the cell-penetrating sequence, can significantly influence their cellular uptake and mode of action.

Received 28 April 2011; accepted 25 July 2011; advance online publication 20 September 2011. doi:10.1038/mt.2011.175

#### INTRODUCTION

Important regulators of apoptotic mechanisms are the Bcl-2 family of proteins including antiapoptotic variants Bcl-2 and Bcl-X<sub>L</sub> and proapoptotic Bax and Bak.<sup>1</sup> The correct balance of activities, interaction, and expression of these proteins is critical for cell survival and central to the induction of apoptosis. Cancer cells are noted for having dysregulated apoptosis and this is often due to increased expression and thus activity of Bcl-2.<sup>1-3</sup> The increase in Bcl-2 expression confers a survival advantage especially when the cells are challenged with chemotherapy during anticancer

treatments. Thus targeting Bcl-2 is an active area of research in cancer, including lymphomas and leukemias, and a number of anti-Bcl-2 drugs are now in clinical trials.<sup>1,5,6</sup>

Most of these drugs are small-molecule entities that freely diffuse through the plasma membrane to interact with Bcl-2.<sup>1</sup> Targeted peptides are also promising therapeutic entities but a major hurdle to their efficacy lies in the fact that they are generally membrane impermeable and additional components or vectors are required to allow them access to the cell interior.<sup>7</sup> These include cell-penetrating peptides (CPP) or protein transduction domains that are typically <30 residues in length. Hundreds of different CPP sequences have now been described but all have a universal capacity to breach biological membranes and enter cells, either alone or associated with cargo.<sup>8,9</sup> The best characterized are those with sequences enriched in cationic residues lysine and arginine; notable examples include the HIV-TAT peptide and synthetic oligoarginines R6-20. The mechanism by which CPPs enter cells is still largely unresolved despite intense studies over the past two decades.<sup>10,11</sup> There is strong evidence for both uptake through endocytic pathways and directly across the plasma membrane; this is especially the case where the cargo is small, for example a fluorophore or short peptide.

Using CPPs to deliver apoptotic peptides is an active area of research and recently a short peptide sequence, FRSRLHSL, as the D isomer frrslhsl was found to be cytotoxic when delivered to cells by the CPP octaarginine, whilst a mutated control peptide with an alanine inserted in place of the N-terminal phenylalanine and the C-terminal leucine asrslhsla-r8 chimera was nontoxic.<sup>12</sup> The targeting sequence is derived from Nur77, a member of the orphan receptor superfamily that interacts with Bcl-2 to tether it and its effector and effector proteins as antiapoptotic complexes. The CPP-linked Nur77-derived peptide, now commercially available as the Bcl-2 converter peptide D-NuBCP-9-r8, was shown to interact with Bcl-2 to expose a BH3 domain that ultimately activates and releases proapoptotic factors such as Bax.

Here, we initially investigated the capacity of this peptide to affect the viability of leukemia cell lines and primary tissue from patients with chronic lymphocytic leukemia (CLL). Using a combination of live cell confocal microscopy and viability assays we

Correspondence: Arwyn T Jones, Welsh School of Pharmacy, Redwood Building, Cardiff University, Cardiff, CF10 3NB, Wales, UK. E-mail: jonesat@cardiff.ac.uk

Molecular Therapy

1

find that the presence of the N-terminal phenylalanine of the Nur77-derived sequence significantly enhances the ability of the peptide to interact with the plasma membrane, to gain access to cells and also mediate rapid cell death through a mechanism that is independent of Bcl-2 expression. These studies were confirmed in adherent cells highlighting the strong membrane interacting synergy between phenylalanine and octaarginine even when they are located 10 residues away from each other. These studies have important implications for the use of CPP as vectors for therapeutic peptides but also for the applicability of D-NuBCP-9-r8 as a Bcl-2 targeting entity.

## RESULTS

### Viability of KG1a cells following incubation with r8-, asr-a-r8, and fsr-l-r8

Incubation of FSRSLHSLI- or fsrslhslI, attached to the CPP octaarginine-induced cytotoxicity in Bcl-2-transfected Jurkat cells, over parental cells, but a control L and D sequence ASRSLHSLA attached to the same CPP was relatively nontoxic.<sup>12</sup> We initially investigated the viability of acute myeloid leukemia KG1a cells following 24-hour exposure to increasing concentrations of r8 alone or of r8 conjugated to fsrslhslI (fsr-l-r8) or asrslhsla (asr-a-r8, Table 1). These sequences, including the presence of the aminohexanoic acid bridge were as previously described<sup>12</sup> with the exception that here the N-terminus was not acetylated and the C-terminal was further extended with GC to allow subsequent attachment of a fluorescent probe. The results (Figure 1a) show that r8 or asr-a-r8-treated cells are viable up to 20  $\mu\text{mol/l}$  but fsr-l-r8 was toxic to KG1a cells ( $\text{IC}_{50}$  12  $\mu\text{mol/l}$ ); this is comparable to values observed in the previous study.<sup>12</sup>

Incubation of cells for only 10 minutes with either of two proliferating cell nuclear antigen-binding domain peptides fused to the CPP HIV-TAT was sufficient to inhibit cell cycle progression of mouse myoblasts by 30% for up to 8 hours after peptide incubation.<sup>13</sup> To investigate whether the toxicity of the fsr-l-r8 peptide was dependent on incubation time, peptide incubations were performed at 37°C for 1 hour before removal of the extracellular peptide and further incubating the KG1a cells in peptide-free

complete medium for a further 23 hours. The viability of the cells was compared with those incubated in the continued presence of the peptide for 24 hours. Incubation with the peptide for just 1 hour was sufficient to give similar  $\text{IC}_{50}$  values to those observed when the peptide was left on the cells for 24 hours (Figure 1b).

We also performed the initial 1-hour peptide incubation in medium lacking serum; CPPs such as R8 have been shown to bind strongly to serum proteins thus reducing their effective extracellular peptide concentration for cellular interaction and penetration.<sup>14</sup> Cells were incubated with fsr-l-r8 for 1 hour in serum-free medium, washed of peptide and further incubated for 23 hours in complete medium. The  $\text{IC}_{50}$  for fsr-l-r8 decreased from 12 to 2  $\mu\text{mol/l}$  in these experiments thus highlighting the effect of protein binding to peptide activity (Figure 1b). Comparative viability assays were also performed between peptide fsr-l-r8 and an identical sequence, lacking the terminal GC that we use for linking the fluorophore (fsr-l-r8 $\Delta\text{GC}$ , Table 1) and the same cytotoxicity profiles were observed demonstrating no effect of addition of these two residues (Supplementary Figure S1). The cellular morphology of the cells after this 24-hour incubation was then assessed and cells incubated with fsr-l-r8 showed extensive morphological changes or were completely destroyed (Figure 1c).

### Uptake and subcellular distribution of r8-, asr-a-r8, and fsr-l-r8-Alexa488 in KG1a cells

We investigated the subcellular distribution of Alexa488-labeled r8, asr-a-r8 and fsr-l-r8 following incubations with these cells. These were initially determined following 1-hour incubation at 2  $\mu\text{mol/l}$  extracellular peptide concentration with KG1a cells at 37°C. Both r8- and asr-a-r8-Alexa488 were endocytosed to label intracellular vesicles (Figure 1d). Unexpectedly, the subcellular distribution of fsr-l-r8 was very different showing diffuse cytoplasmic labeling and in most cases the nucleolus was also labeled. Cells incubated with 10  $\mu\text{mol/l}$  Alexa488-labeled r8, asr-a-r8 or fsr-l-r8 displayed diffuse but strong cytoplasmic labelling.

We previously monitored the immediate cellular uptake of R8-Alexa488 in leukemia cells using time-lapse microscopy;<sup>15</sup> these experiments were performed in the continued presence of the peptide thus excluding the requirement for the washing steps. The uptake of these peptides was similarly continuously monitored from the time of peptide addition for a 10-minute period. In cells incubated with either 2  $\mu\text{mol/l}$  r8-Alexa488 or asr-a-r8-Alexa488 (Figure 1e, Supplementary Videos S1 and S2) the intracellular fluorescence was low throughout the incubation period and the peptides were predominantly located on the plasma membrane. Peptide fsr-l-r8-Alexa488 very rapidly localized to the periphery of cells and after 5 minutes most of the cells were diffusely labeled with peptide and the intensity increased further to the end of the incubation period (Figure 1e and Supplementary Video S3). When identical 2  $\mu\text{mol/l}$  peptide experiments were performed at 4°C, thus inhibiting endocytosis, all three peptides labeled the cytoplasm and nucleolus and this was more obvious when the peptide concentration was increased to 10  $\mu\text{mol/l}$  (Supplementary Figure S2a). Quantification of uptake at 4°C showed comparable fluorescence for all peptides (Supplementary Figure S2b).

Table 1 Name and sequence of peptides used in this study

Unlabeled peptides	Sequence
r8	$\text{NH}_2$ -rrrrrrrrGC-COOH
fsr-l-r8	$\text{NH}_2$ -fsrslhslG-Ahx-rrrrrrrrGC-COOH
fsr-l-r8 $\Delta\text{GC}$	$\text{NH}_2$ -fsrslhslG-Ahx-rrrrrrrr-COOH
L-NuBCP-9-R8	Ac-FSRSLHSLIG-Ahx-RRRRRRRR-NH <sub>2</sub>
D-NuBCP-9-r8	Ac-fsrslhslG-Ahx-rrrrrrrr-NH <sub>2</sub>
asr-a-r8	$\text{NH}_2$ -asrslhslaG-Ahx-rrrrrrrrGC-COOH
asr-l-r8	$\text{NH}_2$ -asrslhslG-Ahx-rrrrrrrrGC-COOH
Fluorescent peptides	Sequence
r8-Alexa488	$\text{NH}_2$ -rrrrrrrrGC-Alexa488
fsr-l-r8-Alexa488	$\text{NH}_2$ -fsrslhslG-Ahx-rrrrrrrrGC-Alexa488
asr-l-r8-Alexa488	$\text{NH}_2$ -asrslhslG-Ahx-rrrrrrrrGC-Alexa488
asr-a-r8-Alexa488	$\text{NH}_2$ -asrslhslaG-Ahx-rrrrrrrrGC-Alexa488

lower case letters denotes D amino acids, Ahx denotes aminohexanoic acid.

### Membrane activity of *fsr-l-r8* is dependent on the N-terminal phenylalanine of the Nur77-derived sequence

Despite there being only two residue differences between the Bcl-2 targeting peptide and the control peptide they show major differences in their capacities to gain access to cells. To further investigate the link between peptide sequence and affect, *asr-l-r8* was synthesized and evaluated; this differs from *fsr-l-r8* by a single

amino acid at the N-terminus which has been changed from *f* in *fsr-l-r8* to a in *asr-l-r8* (Table 1). This peptide did not reduce cell viability and had a cellular uptake profile that was the same as the previous control variant *asr-a-r8* (Figure 2a,b). This demonstrated the significant influence of the N-terminal phenylalanine on the cellular dynamics of *fsr-l-r8*. We quantified the uptake of these peptides at 37°C after 1-hour incubation at 2 µmol/l extracellular peptide concentration. Peptides *asr-l-r8* and *asr-a-r8*-Alexa488

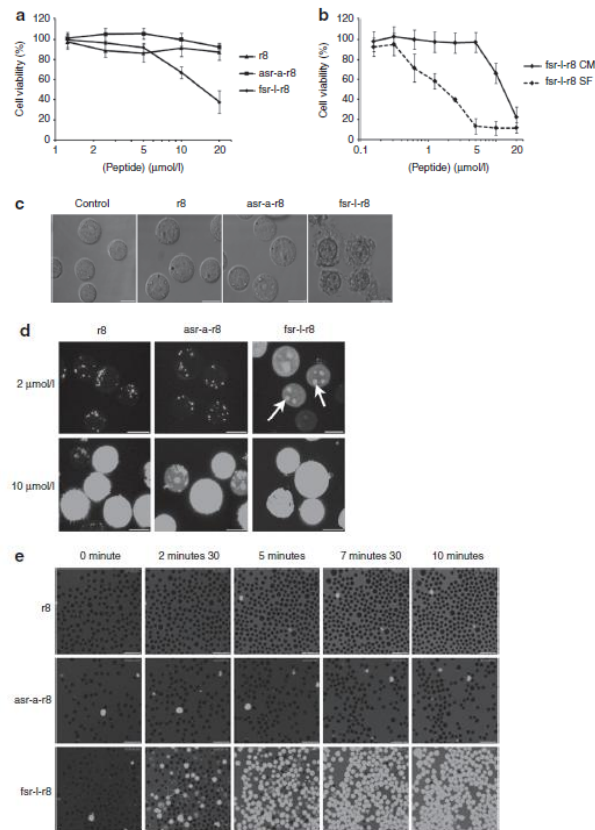
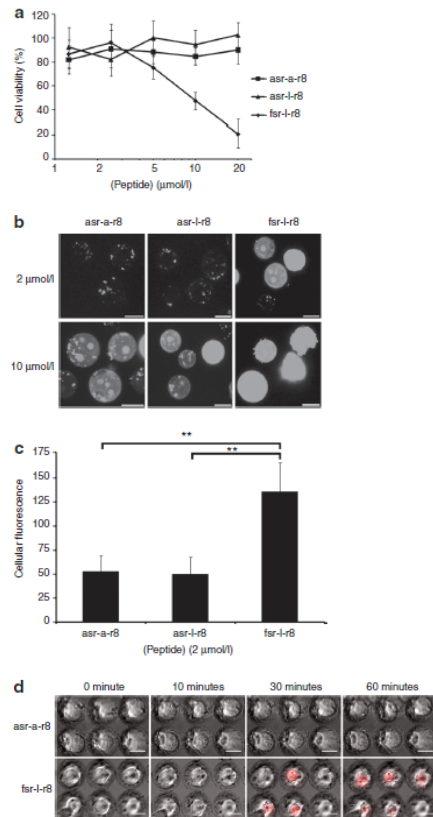


Figure 1 Cell uptake and cytotoxicity of Bcl-2 targeted peptides in KG1a leukemia cells. (a) Viability of cells following 24-hour incubation with 0–20 µmol/l unlabeled r8, asr-a-r8, and fsr-l-r8, results represent means ± SD for three separate experiments performed in triplicate. (b) Viability of cells incubated with peptides for 1 hour in either complete medium (CM) or serum-free medium (SF) and then for 23 hours in the absence of peptides. Results represent means ± SD for two separate experiments performed in triplicate. (c) Morphological analysis of cells incubated in the absence (control) or presence of 20 µmol/l r8-, asr-a-r8, or fsr-l-r8 for 24 hours. (d) Cells were incubated at 37°C with 2 or 10 µmol/l r8-, asr-a-r8-, or fsr-l-r8-Alexa488 for 1 hour before washing and analysis by confocal microscopy. Results shown represent maximum projection images of Alexa488 fluorescence, arrows show peptide enrichment in the nucleolus. (e) Media-containing 2 µmol/l r8-, asr-a-r8-, or fsr-l-r8-Alexa488 was added to cells before analyzing peptide uptake by time-lapse microscopy at 37°C for 10 minutes. Bar = 10 µm. Available as **Supplementary Videos S1–S3**.

New Bcl-2 Independent Mechanism of Action for the Bcl-2 Converter Peptide

© The American Society of Gene & Cell Therapy



**Figure 2** Contribution of the N-terminal phenylalanine residue to cellular uptake and rapid cytotoxicity of fsr-l-r8. **(a)** Viability of KG1a cells following incubations with 0–20 µmol/l unlabeled asr-a-r8, asr-l-r8, or fsr-l-r8 for 24 hours. Results represent means ± SD for three separate experiments performed in triplicate. **(b)** Cells were incubated at 37°C with 2 or 10 µmol/l asr-a-r8-, asr-l-r8-, or fsr-l-r8-Alexa488 for 1 hour before washing and analysis by confocal microscopy. Results shown represent maximum projection images of Alexa488 fluorescence. **(c)** Cells were incubated at 37°C with 2 µmol/l asr-a-r8-, asr-l-r8-, or fsr-l-r8-Alexa488 for 1 hour before processing for flow cytometry and quantification of peptide uptake. Results represent the geometric means ± SD from three separate experiments performed in duplicate, \*\**P* < 0.01. **(d)** Unlabeled asr-a-r8 or fsr-l-r8 and propidium iodide (PI) were added to KG1a cells (nested in microwells) that were then immediately imaged by confocal microscopy at 37°C for 1 hour. Results represent single-section images of morphology and PI fluorescence. Bar = 10 µm. Full-time lapse series available as **Supplementary Videos S4 and S5**.

gave similar fluorescence values (**Figure 2c**) but fluorescence values of cells incubated with fsr-l-r8 were much higher thus confirming the earlier microscopy analysis.

4

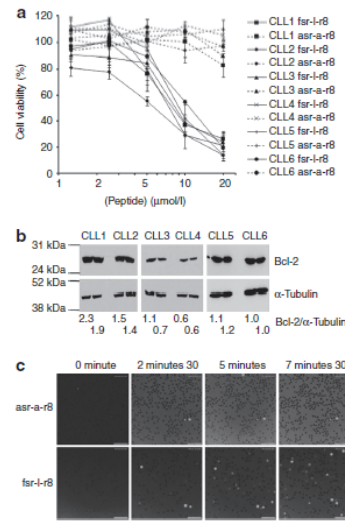


**Figure 3** Viability and uptake of Bcl-2 targeting peptides in chronic lymphocytic leukemia (CLL) cells. **(a)** CLL cells from six individual patients were incubated with 0–20 µmol/l peptides for 24 hours, results are means ± SD for one experiment performed in triplicate. **(b)** Bcl-2 expression in samples analyzed in **(a)**. Results are expressed as Bcl-2/α-tubulin ratios for each set of bands and samples were loaded in duplicate. **(c)** Complete media-containing 2 µmol/l asr-a-r8- or fsr-l-r8-Alexa488 was added to cells before analysis of peptide uptake by time-lapse microscopy at 37°C for 10 minutes. Results represent single-section images of Alexa488 fluorescence. Bar = 10 µm. Full-time lapse series available as **Supplementary Videos S6 and S7**.

**Manufacture of microwells for time lapse imaging of leukemia cells with fsr-l-r8**

The use of time-lapse microscopy allowed us to analyze the immediate effects of apoptotic peptide-CPP chimeras on morphology and membrane integrity of adherent cells.<sup>16</sup> Peptides in imaging medium-containing serum, and propidium iodide (PI) as a marker of plasma membrane integrity were placed on cells that were then sequentially imaged to allow real-time analysis of cell morphology and, via PI leakage, plasma membrane integrity. This is normally difficult with nonadherent cells settled on similar plane surfaces as they move from the field of view or focus following addition of solutions. Using laser ablation, we therefore designed and manufactured custom microwells to retain the cells in one position. A scanning electron micrograph of a manufactured microwell array is shown (**Supplementary Figure S3**). This technique allows for the design of wells of multiple shapes and volumes and for KG1a cells, having a mean diameter of 10.1 µm, wells of 15 µm diameter were manufactured. This allowed us to settle the cells into wells before addition of the peptides. For experiments shown in (**Figure 2d**) cells were incubated with 10 µmol/l asr-a-r8 or fsr-l-r8 and cellular morphology and PI fluorescence was monitored for 1 hour.

www.moleculartherapy.org

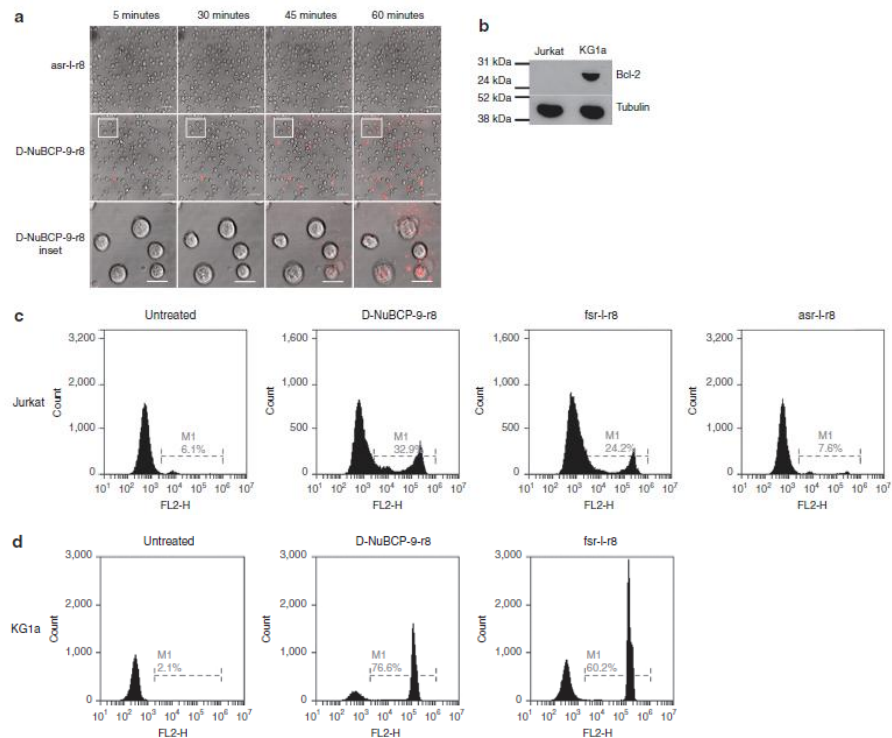


**Figure 4** Membrane activity of Bcl-2 targeted peptides in Jurkat cells. **(a)** Time-lapse images of Jurkat cells incubated with propidium iodide (PI) and 10  $\mu\text{mol/l}$  asr-l-r8 or D-NuBCP-9-r8 for 1 hour at 37°C. Insert represent magnified image of five cells showing rapid cellular destruction. Results represent single-section images of morphology and PI fluorescence. Full-time lapse series available as **Supplementary Videos S8 and S9**. **(b)** Bcl-2 expression in KG1a and Jurkat cells. **(c)** Jurkat or **(d)** KG1a cells were incubated for 1 hour in the presence of unlabeled peptides and propidium iodide (PI) for 1 hour at 37°C. Results show flow cytometry histograms (PI uptake and percentage PI positive) in untreated (control) and peptide-treated cells.

Those incubated with asr-a-r8 retained their normal morphology and were PI negative after 1 hour (**Figure 2d** and **Supplementary Video S4**) whereas cells incubated with fsr-l-r8 showed initial (<10 minutes) evidence of microblebbing and then extensive blebbing terminating in swelling and PI intake (**Supplementary Video S5**). There was a degree of variation regarding the time at which these effects were observed with some cells leaking PI within 20 minutes and others taking longer to reveal themselves as PI positive. Identical results were obtained with fsr-l-r8 $\Delta\text{GC}$  (data not shown). This confirms that this peptide causes rapid membrane blebbing and eventual loss of plasma membrane integrity.

#### Uptake, subcellular distribution, and cytotoxicity of fsr-l-r8 in primary cells

We then investigated the degree of cytotoxicity of this peptide relative to the control (asr-a-r8) peptide in six fresh primary

samples from patients with CLL. Human peripheral blood mononuclear cells were isolated from blood and then incubated for 24 hours with 0–20  $\mu\text{mol/l}$  peptide. There was no loss of viability in cells treated with the control peptide and a similar dose response profile was observed for all patient samples treated with fsr-l-r8, giving a  $\text{IC}_{50}$  range of 6–10  $\mu\text{mol/l}$  (**Figure 3a**). Immunolabeling following sodium dodecyl sulfate-polyacrylamide gel electrophoresis confirmed Bcl-2 expression in all six samples and the ratio of Bcl-2 intensity against internal  $\alpha$ -tubulin control revealed a range for between 0.6 and 2.3 (**Figure 3b**). There was no evidence of a correlation between Bcl-2 expression and fsr-l-r8-mediated cytotoxicity. As previously described for KG1a cells, peptide uptake was then investigated by monitoring CLL cells for 10 minutes immediately (from 30 seconds) after peptide addition. In cells incubated with 2  $\mu\text{mol/l}$  asr-a-r8-Alexa488 no significant cellular fluorescence was observed within this timeframe (**Figure 3c** and

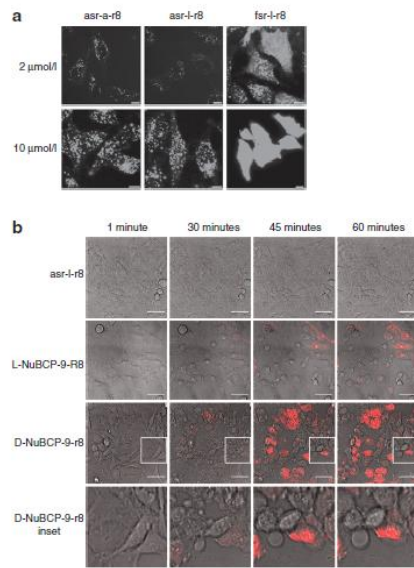


**Figure 5** Cellular uptake and membrane activity of Bcl-2-targeted peptides in HeLa cells. **(a)** Cells were incubated at 37°C for 1 hour with 2 or 10 μmol/l Alexa488-labeled asr-a-r8, asr-l-r8 or fsr-l-r8 before analysis by confocal microscopy. Results shown represent maximum projection images of Alexa488 fluorescence. Bar = 10 μm. **(b)** Time-lapse images of HeLa cells incubated with propidium iodide (PI) and 20 μmol/l asr-l-r8, L-NuBCP-9-r8, or D-NuBCP-9-r8 for 1 hour at 37°C. Inset represent magnified image highlighting extensive blebbing before PI intake. Results represent single-section images of morphology and PI fluorescence. Bar = 50 μm. Full-time lapse series available as **Supplementary Videos S10–S12**.

**Supplementary Video S6**). In cells incubated with 2 μmol/l fsr-l-r8-Alexa488, cellular fluorescence was observed after only 2.5 minutes (**Figure 3c** and **Supplementary Video S7**) and the number of labeled cells increased throughout the 10-minute period, however, the proportion of cells displaying diffuse cytosolic labeling was much lower compared with KG1a cells under the same experimental setup.

#### Effects of D-NuBCP-9-r8 is independent of Bcl-2 expression

Initial characterization of D-NuBCP-9-r8 was performed in Bcl-2-Jurkat cells that were found to be less sensitive to the peptide compared with cells transfected with Bcl-2.<sup>12</sup> As we had shown that fsr-l-r8 causes PI leakage within 1 hour in KG1a cells we incubated Jurkat cells with 10 μmol/l of unlabeled asr-l-r8 or D-NuBCP-9-r8 which is now commercially available as the Bcl-2 converter peptide. Cells incubated with asr-l-r8 retained normal morphology throughout the experimental period and were PI negative (**Figure 4a** and **Supplementary Video S8**). For D-NuBCP-9-r8

there was differential sensitivity within the cell population with some cells seeming to be unaffected while others underwent rapid membrane disruption (**Figure 4a** and **Supplementary Video S9**). This resulted in the expulsion of cellular contents that became PI positive as they were ejected from the cell; often these cells were PI negative just before this event took place. Immunolabeling of cell lysates confirmed that the Jurkat cells used here were Bcl-2<sup>-</sup> in contrast to KG1a<sup>+</sup> cells (**Figure 4b**).

The effects of the peptides were quantified by flow cytometric analysis of PI uptake in Jurkat cells incubated with the peptides at 37°C for 1 hour. D-NuBCP-9-r8 and fsr-l-r8 increased the number of dead cells to 20–30% of the cell culture within 1 hour while the viability of the cells treated with asr-l-r8 peptide was the same as untreated cells (**Figure 4c**). When the same experiments were performed in KG1a cells, the PI positive fraction was much larger, representing up to 75% of the analyzed cell population (**Figure 4d**).

#### Effects of fsr-l-r8 on adherent cell lines

To further investigate the cellular effects of these peptides we performed experiments in adherent epithelial HeLa cells that we have previously used to investigate CPP uptake.<sup>15,16</sup> Comparative cellular uptake of Alexa488-conjugated peptides asr-a-r8, asr-l-r8, and fsr-l-r8 at 2 and 10 μmol/l extracellular concentration confirmed the results obtained in nonadherent cells as fsr-l-r8-Alexa488-treated cells had much stronger labeling and even at 2 μmol/l some peptide was located in the cytosol in addition to punctate structures (**Figure 5a**). Thus for this peptide the effects of the terminal phenylalanine on cell uptake were not limited to nonadherent cells.

We then performed similar time-lapse microscopy in HeLa cells incubated with 20 μmol/l of either asr-l-r8, D-NuBCP-9-r8, or the L-isomer of this peptide (L-NuBCP-9-r8) in serum containing medium-containing PI. Cells incubated with asr-l-r8 (**Figure 5b** and **Supplementary Video S10**) and r8 (data not shown) had normal morphologies and were PI negative after 1 hour. Cells incubated with D-NuBCP-9-r8, showed signs of blebbing after ~30 minutes and for the remainder of the incubation period some extensive membrane reorganization and swelling on distinct parts of the plasma membrane of cells was observed before leakage of PI (**Figure 5b** and **Supplementary Video S11**). Within the same population of cells, there was again a large variation in the response to the effects of the peptides with some remaining PI negative throughout the experiment. The effects of L-NuBCP-9-r8 on the cells (**Supplementary Video S12**) were less rapid than those observed with D-NuBCP-9-r8 and also fsr-l-r8 (data not shown), but extensive membrane reorganization was observed.

#### DISCUSSION

CPP have in the last two decades received widespread attention as potential delivery vectors for macromolecular therapeutics.<sup>17</sup> This includes a number of targeted peptides that by a variety of mechanisms are designed to influence apoptosis.<sup>18</sup> We and others have highlighted that the plasma membrane of cells have distinct thresholds for excluding CPPs such as R8 and HIV-TAT from direct entry rather than through endocytosis.<sup>15,19,20</sup> We initially extended on these studies here by analyzing the cellular dynamics

and effects of the Nur77-derived sequence attached to r8. The specificity of the Nur77 targeting sequence was initially shown by simultaneously replacing respectively the N- and C-terminal phenylalanine and leucine residues for alanine.<sup>12</sup>

Confocal microscopy experiments highlighted large and unexpected differences in the extent of uptake and subcellular distribution of asr-a-r8- and fsr-l-r8-Alexa488 that was later pinpointed, via synthesis of another peptide differing in only one amino acid, to be a result of the NH<sub>2</sub> phenylalanine residue. Addition of FF at the C-terminus of R9 (R9FFC) showed an enhanced capacity over other CPPs to deliver antisense morpholino oligomers to cells,<sup>21</sup> but later studies suggested that the peptide also had some membrane disrupting effects.<sup>22</sup> A recent study in HeLa and glioma cells found that addition of a penetration accelerating sequence FFLIPKG upstream of R8 increased uptake significantly compared to R8 alone.<sup>23</sup> FFLIPKG-R8 was observed to diffusely label the cytoplasm within five minutes of addition to cells whereas R8 only labeled vesicles. This is similar to our comparative observations in adherent and nonadherent cell types incubated with relatively low concentrations of fsr-l-r8 and asr-a-r8. The presence of two phenylalanines at the NH<sub>2</sub> terminus of histidine-containing amphipathic cationic peptides also significantly enhanced toxicity of these entities against mammalian cells and bacteria.<sup>24</sup> A common feature of antimicrobial peptides and also CPPs such as penetratin is that they are either amphipathic throughout the sequence and helical, or that they contain a cationic sequence and a hydrophobic cluster that may be only two residues in length.<sup>9</sup> The cationic residues are thought to locate the peptide, via electrostatic interactions, to the plasma membrane and hydrophobic residues allow for immersion into the hydrocarbon portion of the membrane.<sup>25</sup> It is likely that the NH<sub>2</sub> terminal phenylalanine, unlike alanine in the control peptide, was sufficient to promote the former and change the dynamics of the peptide with cells. By performing similar cell uptake experiments on ice we show that this effect is temperature-dependent, suggesting a requirement for a more fluidic membrane.

At higher concentrations (10 μmol/l) the plasma membrane was permeable to all peptides studied here but in the case of fsr-l-r8 there was also additional dramatic morphological damage. By continuous visualization of cells from the point of addition of the peptide, we observed extensive cell blebbing in HeLa cells and in KG1a cells. In the case of nonadherent cells, these observations were made possible by the generation of engineered grids to hold the cells in position. A proportion of these cells was also permeable to PI within 60 minutes suggesting strongly that here it is acting as a necrotic rather than an apoptotic factor. Currently we do not know why some cells in a single population are more sensitive than others.

Cells were equally sensitive to fsr-l-r8 when the peptide incubations were performed for 24 hours or 1 hour followed by washing and further incubation in peptide-free medium for 23 hours. Two cell cycle targeting peptides attached to the CPP Tat had bioactivity in mouse myoblasts for over 6 hours after only 10-minute incubation indicating that a biological response to CPP:peptide fusions is mediated within minutes and can last long after the peptides are washed away.<sup>13</sup> The IC<sub>50</sub> could also be reduced significantly by omitting serum from the incubation medium and our previous studies have shown extensive binding of R8 to serum

proteins.<sup>14</sup> In serum containing medium a large fraction of the peptide is sequestered by serum proteins thus the active concentration required for membrane penetration and/or perturbation is increased. Serum also contains proteases that can further reduce the potency of CPPs and cargo especially if they are of the L-form. This may have caused the much delayed morphological effects in HeLa cells when they were incubated with L-NuBCP-9-R8 compared with D-NuBCP-9-r8. It agrees with the previous demonstration of diminished activity of D-NuBCP-9-r8 when fsrslhll as cargo was substituted with FSRSLHSL.<sup>12</sup>

Regarding a requirement for Bcl-2, three separate lines of evidence suggest that this protein does not play a role in the membrane blebbing caused by fsr-l-r8 and D-NuBCP-9-r8. Most importantly, we can clearly observe significant peptide-induced blebbing in Jurkat cells that are Bcl-2<sup>-</sup>. Secondly membrane damage and leakage in all cell lines occurs within 1 hour; a time scale that is faster than that typically observed for cellular apoptosis. Thirdly, in primary human cells from CLL patients, the cell death observed did not correlate with the level of expression of Bcl-2 found in these patients. Our data does not exclude that possibility that the presence of Bcl-2 could further increase the potency of peptide-induced cell death as KG1a cells, which are Bcl-2 positive, were more susceptible than Jurkat cells and the lack of correlation in primary cells could be due to a requirement for just low levels of Bcl-2 for this effect. However, our data cautions the use of D-NuBCP-9-r8 as a highly specific entity for targeting Bcl-2; the peptide is clearly membrane active thus giving it dual potency as a cytotoxic agent.

Overall the data questions the specificity of D-NuBCP-9-r8 and illustrates how a single amino acid residue in the cargo sequence can significantly alter the membrane activity of r8, highlighting, as previously described for another apoptotic peptide,<sup>16</sup> that relatively small cargo can have large effects on the dynamics of CPPs with cells.

#### MATERIALS AND METHODS

Alexa Fluor 488-C5-maleimide and all tissue culture reagents were from Invitrogen (Paisley, UK). Glass-bottomed culture dishes (35 mm) for microscopy were from MatTek (Ashland, MA). 3-[4,5-Dimethylthiazol-2-yl]-2,5-diphenyl tetrazolium bromide, PI and antibodies against Bcl-2 and  $\alpha$ -tubulin were from Sigma (Gillingham, UK). Complete miniprotease inhibitor cocktail were from Roche (Mannheim, Germany). Horseradish peroxidase-conjugated anti-mouse antibody was from Pierce (Northumberland, UK). Menzel-Glazer cover slips (no. 0) were from Fisher Scientific (Loughborough, UK).

**Peptide synthesis and conjugation.** Sequences of the peptides used in this study are shown in Table 1; lower case letters denote D isoforms, Ahx denotes aminohexanoic acid. L-NuBCP-9-R8 was from Thermo Fisher Scientific (Ulm, Germany), D-NuBCP-9-r8 (Bcl-2 Converter) was from Merck KGaA (Darmstadt, Germany) and all other peptides were from Severn Biotech (Worcester, UK). Labeling of peptides with Alexa488 was performed through a C-terminal cysteine as previously described.<sup>15,20</sup> All peptides were purified and characterized using reversed phase high-performance liquid chromatography on a C18 Luna 100 Å 5-μm semipreparative column (Phenomenex, Macclesfield, UK) and peptide masses were confirmed using matrix-assisted laser-desorption ionization-time-of-flight spectrometry.

**Cell lines and primary tissue.** Human acute myeloid leukemia KG1a cells and acute T-cell lymphocytic Jurkat cells were cultured in a humidified 5%

CO<sub>2</sub> incubator at 37°C and maintained at a confluency of 0.5–2 × 10<sup>6</sup> cells/ml in RPMI 1640 medium, supplemented with 10% (vol/vol) fetal bovine serum, 100 IU/ml penicillin, and 100 µg/ml streptomycin. Human cervical carcinoma, HeLa cells were maintained as a subconfluent monolayer in D-MEM supplemented with 10% (vol/vol) fetal bovine serum, 100 IU/ml penicillin, and 100 µg/ml streptomycin. Peripheral blood was collected from CLL patients with their informed consent in accordance with the Declaration of Helsinki and in keeping with the ethical approval obtained from South East Wales Research Ethics Committee (02/4806). Cells were isolated from freshly collected blood samples by density centrifugation and maintained for in RPMI 1640 medium, supplemented with 10% (vol/vol) fetal bovine serum, 100 IU/ml penicillin, and 100 µg/ml streptomycin.<sup>26</sup>

**Cellular localization of Alexa488-labeled peptides in KG1a and HeLa cells.** KG1a (5 × 10<sup>5</sup>) cells were washed by centrifugation (800g for 2 minutes) in complete medium and equilibrated in this medium at 37°C (or on ice) for 15 minutes. The medium was replaced with fresh temperature equilibrated (4 or 37°C) medium-containing 2 or 10 µmol/l r8, asr-a-r8-, or fsr-l-r8-Alexa488 and incubated under tissue-culture conditions for 1 hour. Cells were then washed twice in serum-free RPMI 1640 medium (serum-free medium), once in imaging medium (serum-free medium without phenol red) and finally resuspended in 500 µl of imaging medium. A fraction of the cell suspension (100 µl) was transferred to the centre of glass-bottomed 35-mm culture dishes and the cells were allowed to settle for 30 seconds–1 minute. They were then analyzed on a Leica SP5 confocal laser-scanning microscope equipped with an Ar laser and a 63 × oil immersion objective. Cells were imaged through the z-axis to generate maximum projection profiles which were finally arranged using Adobe Photoshop. HeLa cells (1.8 × 10<sup>5</sup>) were seeded into glass-bottomed, 35-mm culture dishes and allowed to adhere for 24 hours. The cells were then incubated in complete medium-containing 2 or 10 µmol/l Alexa488-labeled peptides for 1 hour at 37°C before washing once in imaging medium and then analyzed by confocal microscopy as described above but using a 40 × oil immersion objective.

**Time-lapse microscopy of KG1a and CLL cells incubated with Alexa488-labeled peptides.** The experiments were performed as previously described.<sup>19</sup> Briefly, KG1a (1 × 10<sup>5</sup>) and CLL (2 × 10<sup>5</sup>) cells were washed in complete medium, resuspended in imaging medium-containing 10% fetal bovine serum and transferred to 35-mm imaging dishes that were then placed on an imaging platform on the confocal microscope, equilibrated at 37°C. Fluorescently labeled peptides were added to final concentrations of 2 or 10 µmol/l and the cells were allowed to settle for 30 seconds. Images were then acquired using the ×63 oil immersion objective every 30 seconds for 10 minutes using a laser exposure of 1.3 seconds to capture each frame. Images showing fluorescent profiles were selected at different time points and **Supplementary Videos** show Direct Interference Contrast bright field and fluorescence frames processed as side-by-side animations using NIH [ImageJ] software.

**Time-lapse microscopy of unlabeled peptides in HeLa and Jurkat cells.** HeLa cells (1.8 × 10<sup>5</sup>) were seeded into glass-bottomed, 35-mm culture dishes and allowed to adhere for 24 hours. The cells were washed and replaced with 1.0 ml Dulbecco's modified Eagle's medium (no phenol red) containing 10% fetal bovine serum, 10 mmol/l Na-HEPES pH 7.4, 1.0 µg/ml PI, and peptides at 20 µmol/l. Jurkat cells (4 × 10<sup>5</sup> ml) were washed 2× in phenol red-free RPMI medium-containing 10 mmol/l Na-HEPES pH 7.4, and then incubated in 1.0 ml of this medium-containing 1.0 µg/ml PI and peptides at 10 µmol/l. Cells were imaged every 30 seconds (laser exposure 1.5 seconds) for 1 hour at 37°C by confocal microscopy capturing bright field and PI frames with a HeNe 543 laser.

**Microwell manufacture and time-lapse microscopy in KG1a cells.** The microwells were fabricated into glass cover slips using laser ablation. For this, Menzel-Glazer cover slips were first coated with a layer of liquid ink blackboard maker (Pentel easyflo) to provide a sacrificial layer before

ablation.<sup>27</sup> Microwells (15 µmol/l diameter, 18 µm pitch) in a 10 by 10 array were ablated individually into the cover slip using a 157 nm F<sub>2</sub> excimer laser. Radiation of 157 nm was delivered from a coherent LPPF220i laser source and coupled through an enclosed, N<sub>2</sub>-perfused, 3-m long beamline, to a 25× Schwarzschild projection lens. Beam shaping was achieved through a pair of 25 element spherical arrays manufactured from CaF<sub>2</sub>. Microwells were ablated with exposures of 200 shots per microwell and pulse energy of 24 mJ. Substrates were held on a precision vacuum chuck supported by X-Y-Z-θ, stage set with a resolution of 50 nm (MetaFAB, Cardiff, UK). Laser debris was removed from the surface by sonicating the surfaces for 20 minutes in each of ethanol, 1 mol/l HCl/H<sub>2</sub>O and water. Surfaces were further etched by treating in 7 mol/l KOH/H<sub>2</sub>O at 70°C for 1 hour followed by sonication for 20 minutes in water. For experimentation, KG1a cells (1 × 10<sup>5</sup>) were washed and resuspended in 600 µl imaging medium before being pipetted slowly on to the microwells and allowed to settle for 10 minutes under tissue-culture conditions. Imaging medium-containing 10% fetal bovine serum, Na-HEPES (pH 7.4), 1 µg/ml PI, and fsr-l-r8 or asr-a-r8 (final concentration 10 µmol/l) were added to the cells and these were imaged as described above.

**Quantification of the cellular uptake of r8-, asr-a-r8-, asr-l-r8- and fsr-l-r8-Alexa488.** KG1a cells (5 × 10<sup>5</sup>) were washed once in complete medium and equilibrated at 4 or 37°C for 15 minutes, before centrifugation and incubation for 1 hour with fresh temperature equilibrated medium (4°C, 37°C) containing 2 µmol/l Alexa488 peptides; incubations were performed at either 4 or 37°C. Cells were washed once with ice-cold phosphate-buffered saline (PBS), incubated with 0.25 mg/ml trypsin/EDTA solution at 37°C for 5 minutes and then placed as a suspension in 1.5-ml centrifuge tubes. The cells were washed once in ice-cold PBS, twice with PBS-containing 14 µg/ml heparin and finally resuspended in 200 µl ice-cold PBS. Trypsinization and heparin washes are required to remove surface bound peptides. Cellular fluorescence was then immediately quantified using the 488 nm excitation laser on a Becton Dickinson FACSCalibur analyzer. Live cells were gated on a forward and side scatter basis, and 10,000 viable cells were assayed.

**Cell viability assays.** KG1a (4 × 10<sup>4</sup> cells/well in a total volume of 200 µl) and CLL cells (3 × 10<sup>5</sup>/well in a total volume of 200 µl) were seeded in 96-well plates and incubated with 0–20 µmol/l unlabeled peptides for 20 hours under tissue-culture conditions. Cell viability was then assessed using the MTT assays as previously described.<sup>20</sup> For all experiments, viability is expressed as the percentage of viable cells relative to untreated controls. Cell viability was also measured using an Accuri C6 flow cytometer following incubation of the cells with 10 µmol/l peptide and 0.5 µg/ml PI at 37°C for 1 hour. Changes in forward scatter and exclusion of PI were used to determine the death of cells.

**Influence of incubation time, and serum on peptide cytotoxicity.** KG1a cells were incubated with 0–20 µmol/l unlabeled peptides for 1 hour at 37°C in complete medium or serum-free medium, washed and then further incubated in complete medium for 19 hours. MTT viability assays were then performed.

**Bcl-2 expression in cell lines and primary samples.** Cells were washed and harvested by centrifugation and an equal volume of cell pellet and ice-cold lysis buffer (50 mmol/l Tris-HCl, pH 8.0, 150 mmol/l NaCl, 0.02% sodium azide, 1% Triton X-100, 1 mmol/l DTT) containing protease inhibitor cocktail was added. These were mixed and incubated on ice for 10 minutes before centrifugation at 13,000g (4°C) for 10 minutes. Supernatants corresponding to 15-µg protein were then mixed with SDS sample buffer and loaded on 12% sodium dodecyl sulfate-polyacrylamide gel electrophoresis gels. Following electrophoresis the proteins were transferred to nitrocellulose papers, probed with anti-Bcl-2 and α-tubulin antibodies, washed and incubated with horseradish peroxidase-conjugated antibodies. Subsequently bands were visualized using enhanced chemiluminescence. [ImageJ] was

used to perform densitometric analysis and the Bcl-2 signal was divided by the tubulin signal to allow comparison between the different CLL samples. In order to facilitate quantitation, samples were run in duplicate.

**Statistical methods.** Statistical analysis was performed using one-way ANOVA followed by a Tukey–Kramer *post hoc* test.

#### SUPPLEMENTARY MATERIAL

**Figure S1.** Viability of cells following 24-hour incubation with 0–20  $\mu\text{mol/l}$  fsr-I-r8 or fsr-I-r8 $\Delta\text{GC}$ .

**Figure S2.** Cellular distribution and uptake of Alexa488-labeled peptides in KG1a cells at 4°C.

**Figure S3.** Scanning electron micrograph of an array of circular microwells.

**Video S1.** Uptake of 2  $\mu\text{mol/l}$  Alexa488-labeled r8 in KG1a cells, supplement to **Figure 1e**.

**Video S2.** Uptake of 2  $\mu\text{mol/l}$  Alexa488-labeled asr-a-r8 in KG1a cells, supplement to **Figure 1e**.

**Video S3.** Uptake of 2  $\mu\text{mol/l}$  Alexa488-labeled fsr-I-r8 in KG1a cells, supplement to **Figure 1e**.

**Video S4.** KG1a cells incubated with 10  $\mu\text{mol/l}$  asr-a-r8 while resting in microwells, supplement to **Figure 2d**.

**Video S5.** KG1a cells incubated with 10  $\mu\text{mol/l}$  fsr-I-r8 while resting in microwells, supplement to **Figure 2d**.

**Video S6.** Uptake of 2  $\mu\text{mol/l}$  Alexa488-labeled asr-a-r8 in CLL cells, supplement to **Figure 3c**.

**Video S7.** Uptake of 2  $\mu\text{mol/l}$  Alexa488-labeled fsr-I-r8 in CLL cells, supplement to **Figure 3c**.

**Video S8.** Jurkat cells incubated with 10  $\mu\text{mol/l}$  asr-I-r8, PI added as a marker for membrane integrity, supplement to **Figure 4a**.

**Video S9.** Jurkat cells incubated with 10  $\mu\text{mol/l}$  D-NuBCP-9-r8, PI has been added as a marker for membrane integrity, supplement to **Figure 4a**.

**Video S10.** HeLa cells incubated with 10  $\mu\text{mol/l}$  20  $\mu\text{mol/l}$  asr-I-r8, PI has been added as a marker for membrane integrity, supplement to **Figure 5b**.

**Video S11.** HeLa cells incubated with 20  $\mu\text{mol/l}$  D-NuBCP-9-r8, PI has been added as a marker for membrane integrity, supplement to **Figure 5b**.

**Video S12.** HeLa cells incubated with 20  $\mu\text{mol/l}$  L-NuBCP-9-r8, PI has been added as a marker for membrane integrity, supplement to **Figure 5b**.

**Video S13.** HeLa cells incubated with 20  $\mu\text{mol/l}$  L-NuBCP-9-r8, PI has been added as a marker for membrane integrity, supplement to **Figure 5b**.

**Video S14.** HeLa cells incubated with 20  $\mu\text{mol/l}$  L-NuBCP-9-r8, PI has been added as a marker for membrane integrity, supplement to **Figure 5b**.

**Video S15.** HeLa cells incubated with 20  $\mu\text{mol/l}$  L-NuBCP-9-r8, PI has been added as a marker for membrane integrity, supplement to **Figure 5b**.

**Video S16.** HeLa cells incubated with 20  $\mu\text{mol/l}$  L-NuBCP-9-r8, PI has been added as a marker for membrane integrity, supplement to **Figure 5b**.

**Video S17.** HeLa cells incubated with 20  $\mu\text{mol/l}$  L-NuBCP-9-r8, PI has been added as a marker for membrane integrity, supplement to **Figure 5b**.

**Video S18.** HeLa cells incubated with 20  $\mu\text{mol/l}$  L-NuBCP-9-r8, PI has been added as a marker for membrane integrity, supplement to **Figure 5b**.

**Video S19.** HeLa cells incubated with 20  $\mu\text{mol/l}$  L-NuBCP-9-r8, PI has been added as a marker for membrane integrity, supplement to **Figure 5b**.

**Video S20.** HeLa cells incubated with 20  $\mu\text{mol/l}$  L-NuBCP-9-r8, PI has been added as a marker for membrane integrity, supplement to **Figure 5b**.

**Video S21.** HeLa cells incubated with 20  $\mu\text{mol/l}$  L-NuBCP-9-r8, PI has been added as a marker for membrane integrity, supplement to **Figure 5b**.

**Video S22.** HeLa cells incubated with 20  $\mu\text{mol/l}$  L-NuBCP-9-r8, PI has been added as a marker for membrane integrity, supplement to **Figure 5b**.

**Video S23.** HeLa cells incubated with 20  $\mu\text{mol/l}$  L-NuBCP-9-r8, PI has been added as a marker for membrane integrity, supplement to **Figure 5b**.

**Video S24.** HeLa cells incubated with 20  $\mu\text{mol/l}$  L-NuBCP-9-r8, PI has been added as a marker for membrane integrity, supplement to **Figure 5b**.

**Video S25.** HeLa cells incubated with 20  $\mu\text{mol/l}$  L-NuBCP-9-r8, PI has been added as a marker for membrane integrity, supplement to **Figure 5b**.

**Video S26.** HeLa cells incubated with 20  $\mu\text{mol/l}$  L-NuBCP-9-r8, PI has been added as a marker for membrane integrity, supplement to **Figure 5b**.

**Video S27.** HeLa cells incubated with 20  $\mu\text{mol/l}$  L-NuBCP-9-r8, PI has been added as a marker for membrane integrity, supplement to **Figure 5b**.

**Video S28.** HeLa cells incubated with 20  $\mu\text{mol/l}$  L-NuBCP-9-r8, PI has been added as a marker for membrane integrity, supplement to **Figure 5b**.

**Video S29.** HeLa cells incubated with 20  $\mu\text{mol/l}$  L-NuBCP-9-r8, PI has been added as a marker for membrane integrity, supplement to **Figure 5b**.

**Video S30.** HeLa cells incubated with 20  $\mu\text{mol/l}$  L-NuBCP-9-r8, PI has been added as a marker for membrane integrity, supplement to **Figure 5b**.

**Video S31.** HeLa cells incubated with 20  $\mu\text{mol/l}$  L-NuBCP-9-r8, PI has been added as a marker for membrane integrity, supplement to **Figure 5b**.

**Video S32.** HeLa cells incubated with 20  $\mu\text{mol/l}$  L-NuBCP-9-r8, PI has been added as a marker for membrane integrity, supplement to **Figure 5b**.

**Video S33.** HeLa cells incubated with 20  $\mu\text{mol/l}$  L-NuBCP-9-r8, PI has been added as a marker for membrane integrity, supplement to **Figure 5b**.

**Video S34.** HeLa cells incubated with 20  $\mu\text{mol/l}$  L-NuBCP-9-r8, PI has been added as a marker for membrane integrity, supplement to **Figure 5b**.

**Video S35.** HeLa cells incubated with 20  $\mu\text{mol/l}$  L-NuBCP-9-r8, PI has been added as a marker for membrane integrity, supplement to **Figure 5b**.

**Video S36.** HeLa cells incubated with 20  $\mu\text{mol/l}$  L-NuBCP-9-r8, PI has been added as a marker for membrane integrity, supplement to **Figure 5b**.

**Video S37.** HeLa cells incubated with 20  $\mu\text{mol/l}$  L-NuBCP-9-r8, PI has been added as a marker for membrane integrity, supplement to **Figure 5b**.

**Video S38.** HeLa cells incubated with 20  $\mu\text{mol/l}$  L-NuBCP-9-r8, PI has been added as a marker for membrane integrity, supplement to **Figure 5b**.

**Video S39.** HeLa cells incubated with 20  $\mu\text{mol/l}$  L-NuBCP-9-r8, PI has been added as a marker for membrane integrity, supplement to **Figure 5b**.

**Video S40.** HeLa cells incubated with 20  $\mu\text{mol/l}$  L-NuBCP-9-r8, PI has been added as a marker for membrane integrity, supplement to **Figure 5b**.

**Video S41.** HeLa cells incubated with 20  $\mu\text{mol/l}$  L-NuBCP-9-r8, PI has been added as a marker for membrane integrity, supplement to **Figure 5b**.

**Video S42.** HeLa cells incubated with 20  $\mu\text{mol/l}$  L-NuBCP-9-r8, PI has been added as a marker for membrane integrity, supplement to **Figure 5b**.

**Video S43.** HeLa cells incubated with 20  $\mu\text{mol/l}$  L-NuBCP-9-r8, PI has been added as a marker for membrane integrity, supplement to **Figure 5b**.

**Video S44.** HeLa cells incubated with 20  $\mu\text{mol/l}$  L-NuBCP-9-r8, PI has been added as a marker for membrane integrity, supplement to **Figure 5b**.

**Video S45.** HeLa cells incubated with 20  $\mu\text{mol/l}$  L-NuBCP-9-r8, PI has been added as a marker for membrane integrity, supplement to **Figure 5b**.

**Video S46.** HeLa cells incubated with 20  $\mu\text{mol/l}$  L-NuBCP-9-r8, PI has been added as a marker for membrane integrity, supplement to **Figure 5b**.

**Video S47.** HeLa cells incubated with 20  $\mu\text{mol/l}$  L-NuBCP-9-r8, PI has been added as a marker for membrane integrity, supplement to **Figure 5b**.

- Cotter, TG (2009). Apoptosis and cancer: the genesis of a research field. *Nat Rev Cancer* **9**: 501–507.
- Reed, JC (2008). Bcl-2-family proteins and hematologic malignancies: history and future prospects. *Blood* **111**: 3322–3330.
- Yip, KW and Reed, JC (2008). Bcl-2 family proteins and cancer. *Oncogene* **27**: 6398–6406.
- Szakacs, G, Paterson, JK, Ludwig, JA, Booth-Genthe, C and Gottesman, MM (2006). Targeting multidrug resistance in cancer. *Nat Rev Drug Discov* **5**: 219–234.
- Jones, AT (2008). Gateways and tools for drug delivery: endocytic pathways and the cellular dynamics of cell penetrating peptides. *Int J Pharm* **354**: 34–38.
- Foged, C and Nielsen, HM (2008). Cell-penetrating peptides for drug delivery across membrane barriers. *Expert Opin Drug Deliv* **5**: 105–117.
- Henriques, ST, Melo, MN and Castanho, MA (2006). Cell-penetrating peptides and antimicrobial peptides: how different are they? *Biochem J* **399**: 1–7.
- Foerg, C and Merkle, HP (2008). On the biomedical promise of cell penetrating peptides: limits versus prospects. *J Pharm Sci* **97**: 144–162.
- Fonseca, SB, Pereira, MP and Kelley, SO (2009). Recent advances in the use of cell-penetrating peptides for medical and biological applications. *Adv Drug Deliv Rev* **61**: 953–964.
- Kolluri, SK, Zhu, X, Zhou, X, Lin, B, Chen, Y, Sun, K et al. (2008). A short Nur77-derived peptide converts Bcl-2 from a protector to a killer. *Cancer Cell* **14**: 285–298.
- Tunematsu, G, Martin, RM, Haupt, S, Patsch, C, Edenhofer, F and Cardoso, MC (2006). Cargo-dependent mode of uptake and bioavailability of TAT-containing proteins and peptides in living cells. *FASEB J* **20**: 1775–1784.
- Kosuge, M, Takeuchi, T, Nakase, I, Jones, AT and Futaki, S (2008). Cellular internalization and distribution of arginine-rich peptides as a function of extracellular peptide concentration, serum, and plasma membrane associated proteoglycans. *Bioconjug Chem* **19**: 656–664.
- Watkins, CL, Schmaljohann, D, Futaki, S and Jones, AT (2009). Low concentration thresholds of plasma membranes for rapid energy-independent translocation of a cell-penetrating peptide. *Biochem J* **420**: 179–189.
- Watkins, CL, Brennan, P, Fegan, C, Takayama, K, Nakase, I, Futaki, S et al. (2009). Cellular uptake, distribution and cytotoxicity of the hydrophobic cell penetrating peptide sequence RFWLL linked to the proapoptotic domain peptide PWD. *J Control Release* **140**: 237–244.
- Heitz, F, Morris, MC and Divita, G (2009). Twenty years of cell-penetrating peptides: from molecular mechanisms to therapeutics. *Br J Pharmacol* **157**: 195–206.
- Stewart, KM, Horton, KL and Kelley, SO (2008). Cell-penetrating peptides as delivery vehicles for biology and medicine. *Org Biomol Chem* **6**: 2242–2255.
- Duchardt, F, Fotin-Mleczek, M, Schwarz, H, Fischer, R and Brock, R (2007). A comprehensive model for the cellular uptake of cationic cell-penetrating peptides. *Traffic* **8**: 848–866.
- Fretz, MM, Penning, NA, Al-Taei, S, Futaki, S, Takeuchi, T, Nakase, I et al. (2007). Temperature-, concentration- and cholesterol-dependent translocation of L- and D-octyl-arginine across the plasma and nuclear membrane of CD34<sup>+</sup> leukaemia cells. *Biochem J* **403**: 335–342.
- Moulton, HM, Nelson, MH, Hatlevig, SA, Reddy, MT and Iversen, PL (2004). Cellular uptake of antisense morpholino oligomers conjugated to arginine-rich peptides. *Bioconjug Chem* **15**: 290–299.
- Abes, S, Moulton, HM, Clair, P, Prevot, P, Youngblood, DS, Wu, RP et al. (2006). Vectorization of morpholino oligomers by the (R-Ahx-R)<sub>4</sub> peptide allows efficient splicing correction in the absence of endosomal agents. *J Control Release* **116**: 304–313.
- Takayama, K, Nakase, I, Michiue, H, Takeuchi, T, Tomizawa, K, Matsui, H et al. (2009). Enhanced intracellular delivery using arginine-rich peptides by the addition of penetration accelerating sequences (Pas). *J Control Release* **138**: 128–133.
- Mason, AJ, Moussaoui, W, Abdelrahman, T, Boukhari, A, Bertani, P, Marquette, A et al. (2009). Structural determinants of antimicrobial and antiparasitic activity and selectivity in histidine-rich amphipathic cationic peptides. *J Biol Chem* **284**: 119–133.
- Sientak-Bechor, D, Haliloglu, T and Ben-Tal, N (2007). Interactions of cationic-hydrophobic peptides with lipid bilayers: a Monte Carlo simulation method. *Biophys J* **93**: 1858–1871.
- Pepper, C, Ward, R, Lin, TT, Brennan, P, Starczynski, J, Musson, M et al. (2007). Highly purified CD38<sup>+</sup> and CD38<sup>-</sup> sub-clones derived from the same chronic lymphocytic leukemia patient have distinct gene expression signatures despite their monoclonal origin. *Leukemia* **21**: 687–696.
- Shin, DS, Lee, JH, Suh, J and Kim, TH (2006). Elimination of surface debris generated by KrF excimer laser ablation of polyimide. *Materials Science and Engineering a-Structural Materials Properties Microstructure and Processing* **416**: 205–210.

#### ACKNOWLEDGMENTS

Funding for this work was obtained through BBSRC grant D013038 awarded to A.T.J. and EPSRC grant EP/P502381/1 awarded to D.B. Research in the Cardiff CLL Research group by P.B. and C.F. is funded by a leukemia and Lymphoma Research Specialist Programme. The authors declared no conflict of interest.

#### REFERENCES

- Borden, EC, Kluger, H and Crowley, J (2008). Apoptosis: a clinical perspective. *Nat Rev Drug Discov* **7**: 959.
- Ashkenazi, A (2008). Directing cancer cells to self-destruct with pro-apoptotic receptor agonists. *Nat Rev Drug Discov* **7**: 1001–1012.